Groundwater storage dynamics in the world's large aquifer systems from GRACE: uncertainty and role of extreme precipitation

Mohammad Shamsudduha[1,2,*] and Richard G. Taylor[1]

[1] Department of Geography, University College London, London, UK

[2] Department of Geography, University of Sussex, Falmer, Brighton, UK

[*] Corresponding author: M. Shamsudduha (M.Shamsudduha@sussex.ac.uk)

The Supplementary Material contains supplementary Tables S1–S4 and supplementary Figures S1–S80.

Supplementary Table S1. Characteristics of the world's 37 large aquifer systems according to the WHYMAP database including aquifer area, total number of population, proportion of groundwater (GW)-fed irrigation, mean aridity index, mean annual rainfall, variability in rainfall and total terrestrial water mass (ΔTWS), and correlation coefficients between monthly ΔTWS and precipitation with reported lags.

WHYMAP aquifer number	**Aquifer name**	**Continent**	**Population (million)**	**Aquifer area (km^2)**	**GW irrigation (%)**	**Climate zones based on Aridity indices**	**Mean (2002-16) annual precipitation (mm)**	**Rainfall variability (%)**	**TWS variance (cm^2)**	**Correlation between TWS and precipitation (lag in month)**
1	Nubian Sandstone Aquifer System	Africa	86.01	2,176,068	1.6	Hyper-arid	30	12.1	1.5	0.16 (13)
2	Northwestern Sahara Aquifer System	Africa	5.93	1,007,536	4.4	Arid	69	17.3	1.9	0.19 (8)
3	Murzuk-Djado Basin	Africa	0.35	483,817	2.3	Hyper-arid	8	36.6	1.3	0.20 (-8)
4	Taoudeni-Tanezrouft Basin	Africa	0.35	720,991	0.0	Hyper-arid	66	14.6	1.2	0.46 (1)
5	Senegal-Mauritanian Basin	Africa	17.77	294,613	1.0	Semi-arid	540	14.6	31.9	0.73 (2)
6	Iullemmeden-Irhazer Aquifer System	Africa	21.57	580,870	0.4	Arid	302	11.7	6.9	0.66 (2)
7	Lake Chad Basin	Africa	32.25	1,516,233	0.4	Arid	415	9.5	16.8	0.82 (2)
8	Umm Ruwaba Aquifer (Sudd Basin)	Africa	10.52	509,174	0.0	Semi-arid	789	10.7	44.4	0.86 (2)
9	Ogaden-Juba Basin	Africa	20.27	1,080,953	0.3	Arid	393	14.2	2.7	0.48 (1)
10	Congo Basin	Africa	34.74	1,487,858	0.0	Humid	1,566	5.6	33.0	0.66 (2)
11	Upper Kalahari-Cuvelai-Zambezi Basin	Africa	6.02	1,000,812	0.1	Semi-arid	819	10.0	145.1	0.66 (2)
12	Lower Kalahari-Stampriet Basin	Africa	0.76	426,487	0.6	Arid	297	24.1	5.3	0.47 (2)
13	Karoo Basin	Africa	14.53	568,213	2.1	Semi-arid	479	17.6	6.5	0.30 (2)
14	Northern Great Plains Aquifer	North America	6.62	1,507,325	14.5	Sub-humid	461	9.7	24.5	0.45 (10)
15	Cambro-Ordovician Aquifer System	North America	13.86	129,588	91.7	Humid	880	11.6	35.1	0.39 (10)
16	California Central Valley Aquifer System	North America	8.10	71,430	57.8	Semi-arid	515	32.0	176.5	0.53 (2)
17	Ogallala Aquifer (High Plains)	North America	2.44	501,374	86.8	Semi-arid	507	16.1	19.7	0.39 (9)

18	Atlantic and Gulf Coastal Plains Aquifer	North America	65.38	1,125,968	55.8	Humid	1,230	11.4	43.1	0.43 (8)
19	Amazon Basin	South America	8.93	2,279,522	1.0	Humid	2,505	8.3	347.2	0.84 (2)
20	Maranhao Basin	South America	10.81	592,680	32.6	Humid	1,502	15.7	217.2	0.82 (2)
21	Guarani Aquifer System (Parana Basin)	South America	47.84	1,834,681	20.5	Humid	1,450	10.6	40.5	0.61 (3)
22	Arabian Aquifer System	Asia	27.43	1,782,954	7.2	Arid	65	15.0	6.1	0.12 (0)
23	Indus River Basin	Asia	155.85	308,436	31.0	Semi-arid	375	16.2	13.0	0.56 (1)
24	Ganges-Brahmaputra Basin	Asia	596.44	616,422	55.8	Humid	1,391	12.1	255.6	0.73 (2)
25	West Siberian Artesian Basin	Asia	12.71	2,703,532	3.4	Humid	483	8.1	39.1	0.71 (8)
26	Tunguss Basin	Asia	0.43	1,241,981	0.1	Humid	432	9.8	38.1	0.66 (8)
27	Angara-Lena Basin	Asia	2.50	620,591	1.3	Humid	472	7.9	21.6	0.55 (8)
28	Yakut Basin	Asia	0.63	861,053	0.7	Humid	386	8.2	19.5	0.58 (-4)
29	North China Plains Aquifer System	Asia	336.70	438,954	37.1	Humid	826	10.0	32.8	0.32 (2)
30	Song-Liao Plain	Asia	54.49	279,044	53.5	Humid	514	17.0	19.5	0.20 (1)
31	Tarim Basin	Asia	7.69	454,288	2.8	Arid	90	23.6	1.9	0.50 (0)
32	Paris Basin	Europe	28.58	178,513	82.3	Humid	727	10.8	32.9	0.24 (6)
33	East European Aquifer System	Europe	100.22	2,859,962	16.6	Humid	606	6.2	35.3	0.54 (7)
34	North Caucasus Basin	Europe	13.30	294,821	4.2	Semi-arid	524	11.6	49.2	0.30 (10)
35	Pechora Basin	Europe	0.19	220,245	0.0	Humid	559	9.5	51.2	0.60 (7)
36	Great Artesian Basin	Australia	0.20	1,765,830	0.9	Semi-arid	444	28.9	20.2	0.55 (2)
37	Canning Basin	Australia	0.01	432,774	0.4	Arid	443	21.2	50.3	0.47 (2)

Supplementary Table S2. Characteristics of the world's 37 large aquifer systems according to the WHYMAP database including mean annual rainfall, mean aridity index, and variability in total terrestrial water mass (ΔTWS), and correlation coefficients between ΔTWS and annual precipitation. The variance (cm^2) in the ensemble GRACE ΔTWS and the proportion of variance explained by surface water and snow water equivalent combined (SWS+SNS), soil moisture storage (SMS) and groundwater storage (GWS) are tabulated.

WHYMAP aquifer number	Aquifer name	Mean (2002–2016) Annual precipitation (mm)	Climate zones based on Aridity indices	TWS variance (cm^2)	Correlation between annual changes in TWS and annual precipitation	TWS variance explained by SWS+SNS combined (%)	TWS variance explained by SMS (%)	TWS variance explained by GWS (%)
1	Nubian Sandstone Aquifer System	30	Hyper-arid	1.5	0.32	0.5	32.4	67.1
2	Northwestern Sahara Aquifer System	69	Arid	1.9	0.62	0.9	14.2	84.9
3	Murzuk-Djado Basin	8	Hyper-arid	1.3	0.08	1.6	1.5	96.9
4	Taoudeni-Tanezrouft Basin	66	Hyper-arid	1.2	0.21	6	14.3	79.6
5	Senegal-Mauritanian Basin	540	Semi-arid	31.9	0.65	14.6	56.6	28.8
6	Iullemmeden-Irhazer Aquifer System	302	Arid	6.9	0.36	12.4	55.7	32
7	Lake Chad Basin	415	Arid	16.8	0.50	14.8	66.6	18.6
8	Umm Ruwaba Aquifer (Sudd Basin)	789	Semi-arid	44.4	0.76	1.7	72.9	25.5
9	Ogaden-Juba Basin	393	Arid	2.7	0.14	1.7	35.9	62.3
10	Congo Basin	1,566	Humid	33.0	0.53	15.6	23.7	60.7
11	Upper Kalahari-Cuvelai-Zambezi Basin	819	Semi-arid	145.1	0.78	0.2	45.6	54.3
12	Lower Kalahari-Stampriet Basin	297	Arid	5.3	0.68	5.7	44.3	50
13	Karoo Basin	479	Semi-arid	6.5	0.72	3.3	1	95.7
14	Northern Great Plains Aquifer	461	Sub-humid	24.5	0.60	4.8	26.5	68.7
15	Cambro-Ordovician Aquifer System	880	Humid	35.1	0.75	1.5	60.1	38.3

16	California Central Valley Aquifer System	515	Semi-arid	176.5	0.46	2.8	56	41.2
17	Ogallala Aquifer (High Plains)	507	Semi-arid	19.7	0.80	2.6	14.6	82.8
18	Atlantic and Gulf Coastal Plains Aquifer	1,230	Humid	43.1	0.61	33.8	51.6	14.6
19	Amazon Basin	2,505	Humid	347.2	0.28	30.6	48.9	20.5
20	Maranhao Basin	1,502	Humid	217.2	0.92	27.5	64.2	8.3
21	Guarani Aquifer System (Parana Basin)	1,450	Humid	40.5	0.38	21	52.3	26.7
22	Arabian Aquifer System	65	Arid	6.1	0.57	5.2	56.7	38.1
23	Indus River Basin	375	Semi-arid	13.0	0.39	4	32.4	63.5
24	Ganges-Brahmaputra River Basin	1,391	Humid	255.6	0.69	17.7	62.7	19.5
25	West Siberian Artesian Basin	483	Humid	39.1	0.71	36.8	11.8	51.4
26	Tunguss Basin	432	Humid	38.1	0.71	57.2	1.9	40.9
27	Angara-Lena Basin	472	Humid	21.6	0.71	23.3	27.1	49.6
28	Yakut Basin	386	Humid	19.5	0.47	26	12	61.9
29	North China Plains Aquifer System	826	Humid	32.8	0.22	0.3	65.4	34.3
30	Song-Liao Plain	514	Humid	19.5	0.62	9.4	59.5	31.1
31	Tarim Basin	90	Arid	1.9	0.32	3	8.3	88.7
32	Paris Basin	727	Humid	32.9	0.86	8.9	57.4	33.7
33	East European Aquifer System	606	Humid	35.3	0.75	39.3	41.2	19.5
34	North Caucasus Basin	524	Semi-arid	49.2	0.86	2.7	59.1	38.2
35	Pechora Basin	559	Humid	51.2	0.56	70	1.8	28.1
36	Great Artesian Basin	444	Semi-arid	20.2	0.89	17.6	55	27.3
37	Canning Basin	443	Arid	50.3	0.85	3	49.1	47.9

Supplementary Table S3. Characteristics of the relationships between CRU precipitation and GRACE ΔGWS in the world's 37 large aquifer systems.

WHYMAP aquifer number	Aquifer name	Mean (1901 to 2016) annual (hydrological year) precipitation (mm)	90th percentile precipitation (period: 1901–2016)	Rainy season: calendar year (Jan–Dec) or hydrological year (Aug–Jul)	Extreme hydrological years (≥90th percentile) over GRACE period (2002–2016)	Positive change in non-linear trends in GRACE-ΔGWS over the period of 2002–2016 and reported values between two consecutive years (cm)
1	Nubian Sandstone Aquifer System	33	41	Jan–Dec	2014 (51st)	2014 (0.43) 2015 (0.63)
2	Northwestern Sahara Aquifer System	72	92	Aug–Jul	2003–2004 2005–2006	2005–2006 (0.25) 2015–2016 (0.41)
3	Murzuk-Djado Basin	8	11	Jan–Dec	2015 (78th)	2015 (0.83) 2016 (0.70)
4	Taoudeni-Tanezrouft Basin	63	75	Jan–Dec	2010	2014 (0.30) 2015 (0.31)
5	Senegal-Mauritanian Basin	548	703	Jan–Dec	2010	2010 (1.96) 2011 (1.53)
6	Iullemmeden-Irhazer Aquifer System	301	377	Jan–Dec	2010 (68th)	2010 (0.75) 2011 (0.86)
7	Lake Chad Basin	392	460	Jan–Dec	2012	2012 (0.45) 2013 (0.69)
8	Umm Ruwaba Aquifer (Sudd Basin)	788	889	Jan–Dec	2007 (87th) 2008 (78th) 2014 (60th)	2008 (0.83) 2013 (0.98) 2014 (1.27)
9	Ogaden-Juba Basin	376	465	Jan–Dec	2013	2006 (0.92) 2013 (0.69)
10	Congo Basin	1632	1740	Aug–Jul	2015–2016 (56th)	2013–2014 (5.15) 2015–2016 (2.93)
11	Upper Kalahari-Cuvelai-Zambezi Basin	800	935	Aug–Jul	2008-2009 (74th) 2010-2011 (70th)	2008–2009 (3.05) 2010–2011 (5.12)
12	Lower Kalahari-Stampriet Basin	286	386	Aug–Jul	2010–2011	2006–2007 (0.80) 2010–2011 (0.78)
13	Karoo Basin	500	623	Aug–Jul	2010–2011	2010–2011 (1.86) 2011–2012 (1.50)
14	Northern Great Plains Aquifer	429	487	Jan–Dec	2005, 2010, 2013	2005 (1.71) 2010 (2.70) 2011 (2.42)
15	Cambro-Ordovician Aquifer System	819	960	Jan–Dec	2010, 2013, 2015	2010 (2.70) 2011 (2.42)
16	California Central Valley Aquifer System	567	772	Aug–Jul	2005–2006	2004–2005 (3.92) 2005–2006 (4.15) 2010–2011 (2.05)
17	Ogallala Aquifer (High Plains)	489	578	Jan–Dec	2015	2008 (2.26) 2009 (1.83)
18	Atlantic and Gulf Coastal Plains Aquifer	1205	1356	Jan–Dec	2009, 2013, 2015	2009 (1.40) 2013 (0.80) 2015 (0.55)

19	Amazon Basin	2416	2627	Aug–Jul	2005–2006 2007–2008 2008–2009	2007–2008 (2.58) 2011–2012 (3.31)
20	Maranhao Basin	1470	1762	Aug–Jul	2008–2009 2010–2011	2003–2004 (2.45) 2009–2010 (1.83)
21	Guarani Aquifer System (Parana Basin)	1384	1573	Aug–Jul	2009–2010 2015–2016	2010–2011 (1.65) 2015–2016 (5.78)
22	Arabian Aquifer System	74	87	Jan–Dec	2004 (40th)	2003 (0.15) 2004 (0.12)
23	Indus River Basin	330	452	Jan–Dec	2010, 2015	2014 (0.93) 2015 (0.82)
24	Ganges-Brahmaputra Basin	1483	1663	Jan–Dec	2011 (59th)	2011 (1.44)
25	West Siberian Artesian Basin	452	505	Jan–Dec	2013, 2014, 2015	2013 (2.57) 2014 (3.08) 2015 (2.17)
26	Tunguss Basin	415	461	Jan–Dec	2007, 2008, 2015	2005 (3.25) 2006 (3.25) 2013 (4.49)
27	Angara-Lena Basin	456	512	Jan–Dec	2006, 2008, 2009	2006 (1.71) 2013 (1.80)
28	Yakut Basin	342	402	Jan–Dec	2005, 2006, 2007, 2008, 2013	2005 (1.89) 2006 (2.15)
29	North China Plains Aquifer System	793	916	Jan–Dec	2003	2003 (3.21) 2004 (3.73)
30	Song-Liao Plain	531	629	Jan–Dec	2012, 2013	2013 (2.14) 2014 (1.57)
31	Tarim Basin	78	105	Jan–Dec	2003, 2005, 2010, 2013	2015 (0.74) 2016 (1.04)
32	Paris Basin	724	862	Aug–Jul	2006–2007 2015–2016	2013–2014 (2.34) 2014-2015 (1.84) 2015–2016 (1.53)
33	East European Aquifer System	585	638	Jan–Dec	2004, 2012	2005 (1.84) 2006 (2.17)
34	North Caucasus Basin	514	602	Jan–Dec	2004	2004 (3.32) 2005 (3.21)
35	Pechora Basin	490	583	Jan–Dec	2003, 2007, 2014	2013 (3.37) 2014 (3.21)
36	Great Artesian Basin	438	584	Aug–Jul	2009–2010 2010–2011	2009–2010 (1.72) 2010–2011 (3.34)
37	Canning Basin	377	547	Aug–Jul	2005–2006 2010–2011 2013–2014	2010–2011 (1.46) 2011–2012 (2.37)

Supplementary Table S4. Characteristics of the relationships between GPCC precipitation and GRACE ΔGWS in the world's 37 large aquifer systems.

WHYMAP aquifer number	**Aquifer name**	**Mean (1901 to 2016) annual (hydrological year) precipitation (mm)**	**90th percentile precipitation (period: 1901–2016)**	**Rainy season: calendar year (Jan–Dec) or hydrological year (Aug–Jul)**	**Extreme hydrological years (≥90th percentile) over GRACE period (2002–2016)**	**Positive change in non-linear trends in GRACE-ΔGWS over the period of 2002–2016 and reported values between two consecutive years (cm)**
1	Nubian Sandstone Aquifer System	32	44	Jan–Dec	2014 (61st) 2015 (72nd)	2014 (0.43) 2015 (0.63)
2	Northwestern Sahara Aquifer System	68	94	Aug–Jul	2003–2004 2005–2006 2008–2009	2005–2006 (0.25) 2015–2016 (0.41)
3	Murzuk-Djado Basin	15	23	Jan–Dec	2013 (74th) 2015 (34th)	2015 (0.83) 2016 (0.70)
4	Taoudeni-Tanezrouft Basin	91	125	Jan–Dec	2010	2014 (0.30) 2015 (0.31)
5	Senegal-Mauritanian Basin	511	655	Jan–Dec	2010	2010 (1.96) 2011 (1.53)
6	Iullemmeden-Irhazer Aquifer System	275	350	Jan–Dec	2010 (75th)	2010 (0.75) 2011 (0.86)
7	Lake Chad Basin	385	452	Jan–Dec	2012	2012 (0.45) 2013 (0.69)
8	Umm Ruwaba Aquifer (Sudd Basin)	778	882	Jan–Dec	2006, 2007 (66th), 2008 (83rd), 2009 (87th), 2011 (84th) 2014 (81st)	2008 (0.83) 2013 (0.98) 2014 (1.27)
9	Ogaden-Juba Basin	393	481	Jan–Dec	2006	2006 (0.92) 2013 (0.69)
10	Congo Basin	1657	1750	Aug–Jul	2015–2016 (48th)	2013–2014 (5.15) 2015–2016 (2.93)
11	Upper Kalahari-Cuvelai-Zambezi Basin	840	952	Aug–Jul	2005–2006 2008–2009 (87th) 2010–2011 (84h)	2008–2009 (3.05) 2010–2011 (5.12)
12	Lower Kalahari-Stampriet Basin	303	409	Aug–Jul	2006–2007 2010–2011	2006–2007 (0.80) 2010–2011 (0.78)
13	Karoo Basin	500	620	Aug–Jul	2010–2011	2010–2011 (1.86) 2011–2012 (1.50)
14	Northern Great Plains Aquifer	427	484	Jan–Dec	2005, 2010	2005 (1.71) 2010 (2.70) 2011 (2.42)
15	Cambro-Ordovician Aquifer System	834	969	Jan–Dec	2008, 2010	2010 (2.70) 2011 (2.42)
16	California Central Valley Aquifer System	552	749	Aug–Jul	2005–2006	2004–2005 (3.92) 2005–2006 (4.15) 2010–2011 (2.05)
17	Ogallala Aquifer (High Plains)	501	602	Jan–Dec	2015	2008 (2.26) 2009 (1.83)

18	Atlantic and Gulf Coastal Plains Aquifer	1215	1372	Jan–Dec	2004, 2009, 2015	2009 (1.40) 2013 (0.80) 2015 (0.55)
19	Amazon Basin	2500	2661	Aug–Jul	2005–2006 2007–2008 2008–2009 2013–2014	2007–2008 (2.58) 2011–2012 (3.31)
20	Maranhao Basin	1421	1703	Aug–Jul	2008–2009	2003–2004 (2.45) 2009–2010 (1.83)
21	Guarani Aquifer System (Parana Basin)	1378	1535	Aug–Jul	2003–2004 2009–2010 2014–2015 2015–2016	2010–2011 (1.65) 2015–2016 (5.78)
22	Arabian Aquifer System	81	99	Jan–Dec	2003 (66^{th}) 2005 (52^{nd}) 2013 (88^{th})	2003 (0.15) 2004 (0.12)
23	Indus River Basin	336	466	Jan–Dec	2011, 2015	2014 (0.93) 2015 (0.82)
24	Ganges-Brahmaputra Basin	1490	1650	Jan–Dec	2007 (89^{th}) 2008 (78^{th}) 2011 (39^{th})	2011 (1.44)
25	West Siberian Artesian Basin	443	497	Jan–Dec	2002, 2007, 2014, 2015	2013 (2.57) 2014 (3.08) 2015 (2.17)
26	Tunguss Basin	389	434	Jan–Dec	2002, 2007, 2008, 2011, 2014, 2015	2005 (3.25) 2006 (3.25) 2013 (4.49)
27	Angara-Lena Basin	422	471	Jan–Dec	2004, 2005, 2006, 2008, 2009	2006 (1.71) 2013 (1.80)
28	Yakut Basin	316	363	Jan–Dec	2004, 2005, 2006, 2007, 2008, 2012 2013	2005 (1.89) 2006 (2.15)
29	North China Plains Aquifer System	795	933	Jan–Dec	2003	2003 (3.21) 2004 (3.73)
30	Song-Liao Plain	534	636	Jan–Dec	2012, 2013	2013 (2.14) 2014 (1.57)
31	Tarim Basin	48	66	Jan–Dec	2003, 2005, 2010, 2013, 2015	2015 (0.74) 2016 (1.04)
32	Paris Basin	750	914	Aug–Jul	2006–2007 2015–2016	2013–2014 (2.34) 2014-2015 (1.84) 2015–2016 (1.53)
33	East European Aquifer System	561	624	Jan–Dec	2004, 2012	2005 (1.84) 2006 (2.17)
34	North Caucasus Basin	488	584	Jan–Dec	2004	2004 (3.32) 2005 (3.21)
35	Pechora Basin	470	565	Jan–Dec	2002, 2003, 2005, 2006, 2007, 2012	2013 (3.37) 2014 (3.21)
36	Great Artesian Basin	429	568	Aug–Jul	2009–2010 2010–2011 2011–2012	2009–2010 (1.72) 2010–2011 (3.34)
37	Canning Basin	438	587	Aug–Jul	2004–2005 2010–2011	2010–2011 (1.46) 2011–2012 (2.37)

Supplementary Figure captions

Fig. S1-S36. Time-series data of terrestrial water storage anomaly (ΔTWS) from GRACE and individual water stores from GLDAS Land Surface Models (LSMs): (a) Ensemble monthly GRACE ΔTWS from three solutions (CSR, Mascons, GRGS), (b-c) ensemble monthly ΔSMS and ΔSWS + ΔSNS from four GLDAS LSMs (CLM, Noah, VIC, Mosaic), (d) computed monthly ΔGWS and (e) monthly precipitation from August 2002 to July 2016 for WHYMAP large aquifer systems from no. 1 to 37, except for the High Plains Aquifer System in the USA (no. 17) which is shown as Fig. 2. Values in the Y-axis of the top four panels show monthly water-storage anomalies (cm) and the bottom panel shows monthly precipitation (cm).

Fig. S37. Seasonal-trend decomposition (STL) of an ensemble monthly GRACE ΔTWS time-series data from three solutions (CSR, Mascons, GRGS) for the High Plains Aquifer System in the USA (no. 17)

Fig. S38. Comparison of ΔGWS time series datasets from GRACE and in situ piezometric observations. ΔGWS time-series records in the unconsolidated, alluvial aquifer within the humid Bengal Basin of Bangladesh (a), and a weathered crystalline rock aquifer in the semi-arid Limpopo Basin in South Africa (b). Shaded bands in light-pink and light-blue around ΔGWS lines denote the standard deviation of the estimated mean value. Monthly precipitation records are shown as stair-step lines in blue on both panels with a dashed blue line indicating the long-term monthly mean value.

Fig. S39. Time-series data of terrestrial water storage anomaly (ΔTWS) from GRACE and individual water stores from GLDAS Land Surface Models (LSMs): (a) Ensemble monthly GRACE ΔTWS from three solutions (CSR, Mascons, GRGS), (b-c) ensemble monthly ΔSMS and ΔSWS + ΔSNS from four GLDAS LSMs (CLM, Noah, VIC, Mosaic), (d) computed monthly ΔGWS and (e) monthly precipitation from August 2002 to July 2016 for the Bengal Basin of Bangladesh.

Fig. S40. Time-series data of terrestrial water storage anomaly (ΔTWS) from GRACE and individual water stores from GLDAS Land Surface Models (LSMs): (a) Ensemble monthly GRACE ΔTWS from three solutions (CSR, Mascons, GRGS), (b-c) ensemble monthly

ΔSMS and ΔSWS + ΔSNS from four GLDAS LSMs (CLM, Noah, VIC, Mosaic), (d) computed monthly ΔGWS and (e) monthly precipitation from August 2002 to July 2016 for the Limpopo Basin of South Africa.

Fig. S41-S77. Decomposition of time-series components of GRACE ΔGWS data for all 37 large aquifer systems using a non-parametric, Seasonal-Trend decomposition procedure based on Loess (STL) technique. The graph on the top shows monthly anomaly data and decomposed time-series components of the series into seasonal, trend and remainder components. The graph also shows monthly precipitation records from CRU data along with annual total precipitation values (cm) written next to each annual cycle. The pie chart at the bottom shows the proportion of variance (%) in GRACE ΔGWS explained by the time-series components (S=seasonal, T=trend, R=residual/remainder).

Fig. S78. Time series of ensemble mean GRACE ΔTWS (red), GLDAS ΔSMS (green), ΔSWS + ΔSNS (blue) and computed GRACE ΔGWS (black) showing the calculation of anomalously negative or positive values of GRACE ΔGWS that deviate substantially from underlying trends. Cases for the Upper Kalahari-Cuvelai-Zambezi Basin (11) under a semi-arid climate, the Congo Basin (10) under a tropical humid climate, and the Angara-Lena Basin (27) in given in Fig. 6.

Fig. S79. Uncertainty in the estimates of GRACE-derived GWS from 20 realisations using 3 GRACE (CSR, JPL-Mascons, GRGS) products and 4 LSMs (CLM, Noah, VIC, Mosaic) and their ensemble means for the WHYMAP large aquifer systems from no. 1 to 37, except for the High Plains Aquifer System in the USA (no. 17) which is shown as Fig. 2.

Fig. S80. Long-term in-situ groundwater-level records from Makutapora Wellfield in central Tanzania (*n*=5) and Limpopo Basin in South Africa (*n*=4). Groundwater levels of from Makutapora site are referenced to a fixed datum (mean sea level, msl) and thus indicate piezometric heads; records in Limpopo Basin are plotted below groundwater level (bgl), hence the negative sign. The frequency of these multi-decadal groundwater-level records varies from daily to monthly with irregular time intervals. Annual rainfall time-series records are shown below each graph with a dashed, grey line denoting the mean of the time series.

Supplementary Fig. S1–S80:

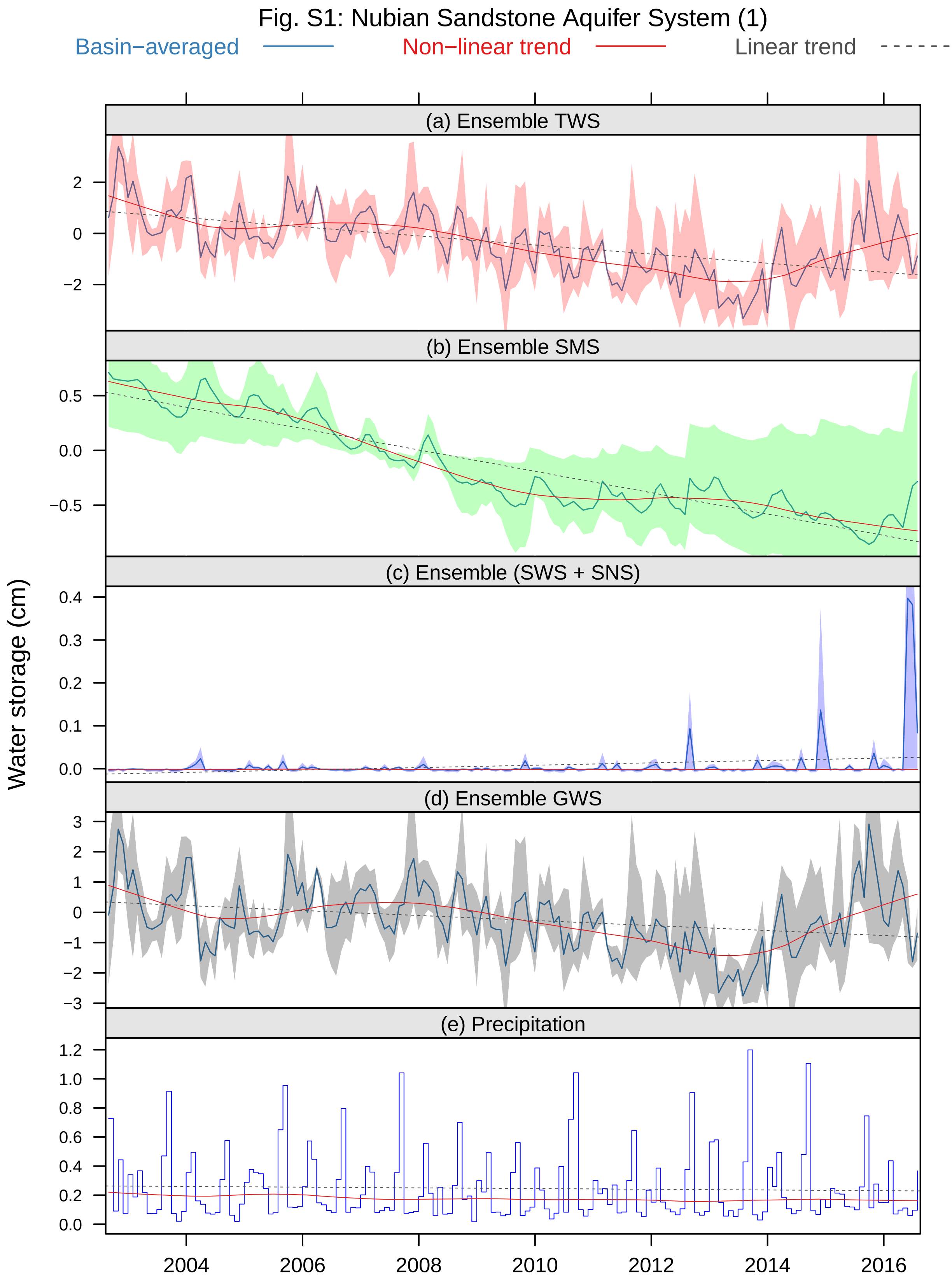
Fig. S1: Nubian Sandstone Aquifer System (1)
Basin−averaged
Non−linear trend
Linear trend
(a) Ensemble TWS
(b) Ensemble SMS
(c) Ensemble (SWS + SNS)
(d) Ensemble GWS
(e) Precipitation
Water storage (cm)
2004
2006
2008
2010
2012
2014
2016

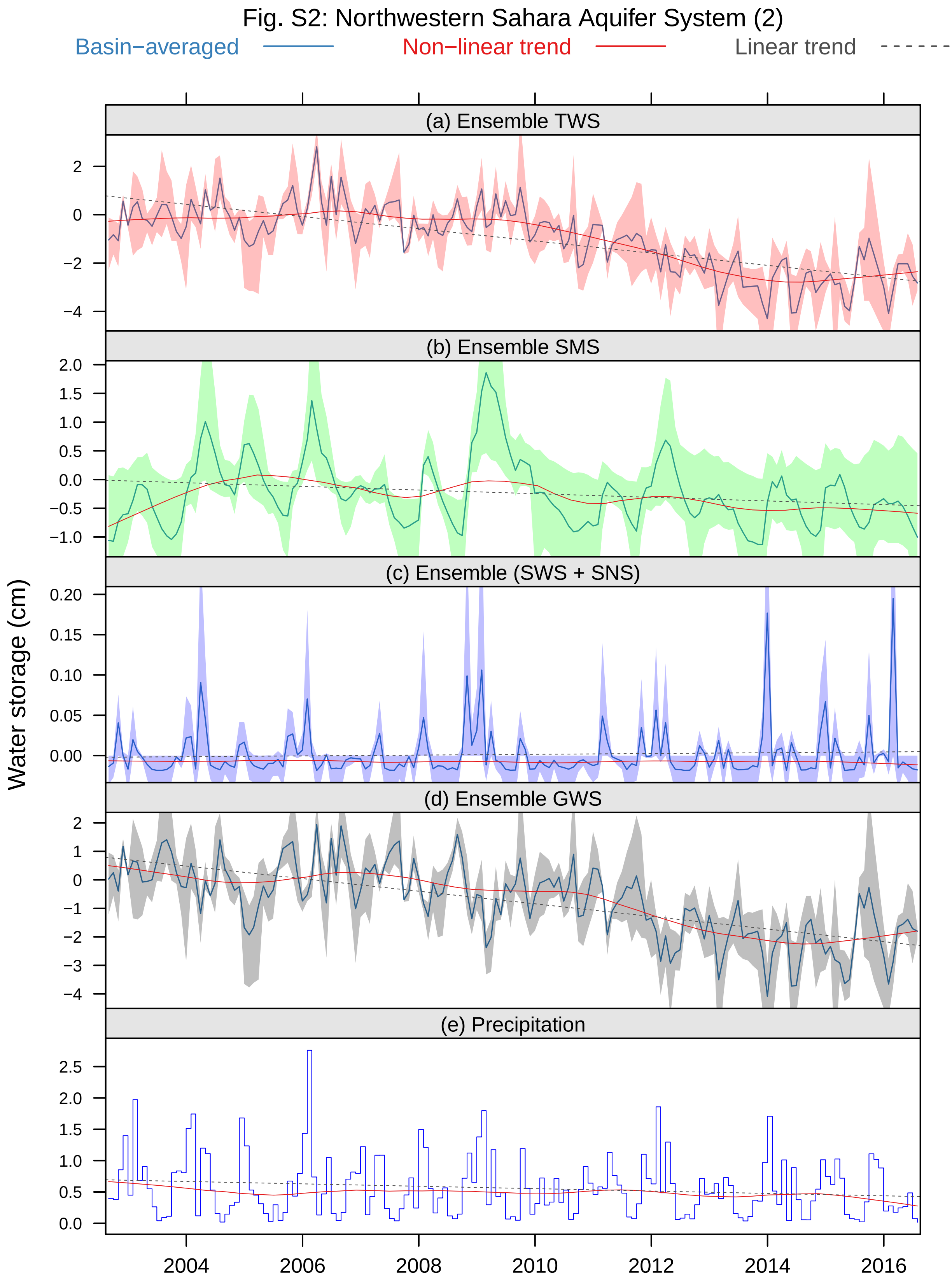
Fig. S2: Northwestern Sahara Aquifer System (2)
Basin−averaged
Non−linear trend
Linear trend
(a) Ensemble TWS
(b) Ensemble SMS
(c) Ensemble (SWS + SNS)
(d) Ensemble GWS
(e) Precipitation
Water storage (cm)
2004
2006
2008
2010
2012
2014
2016

Fig. S3: Murzuk−Djado Basin (3)

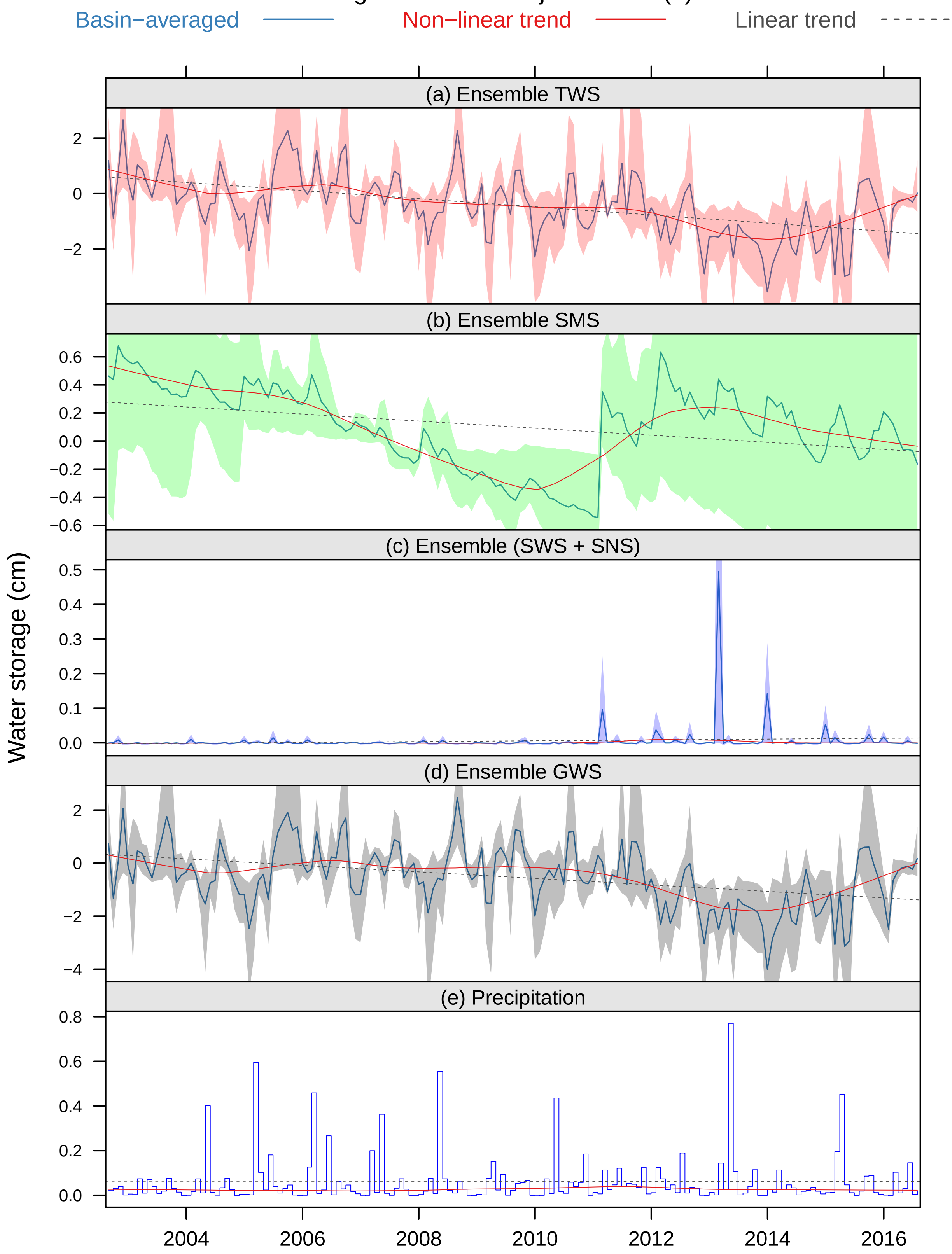

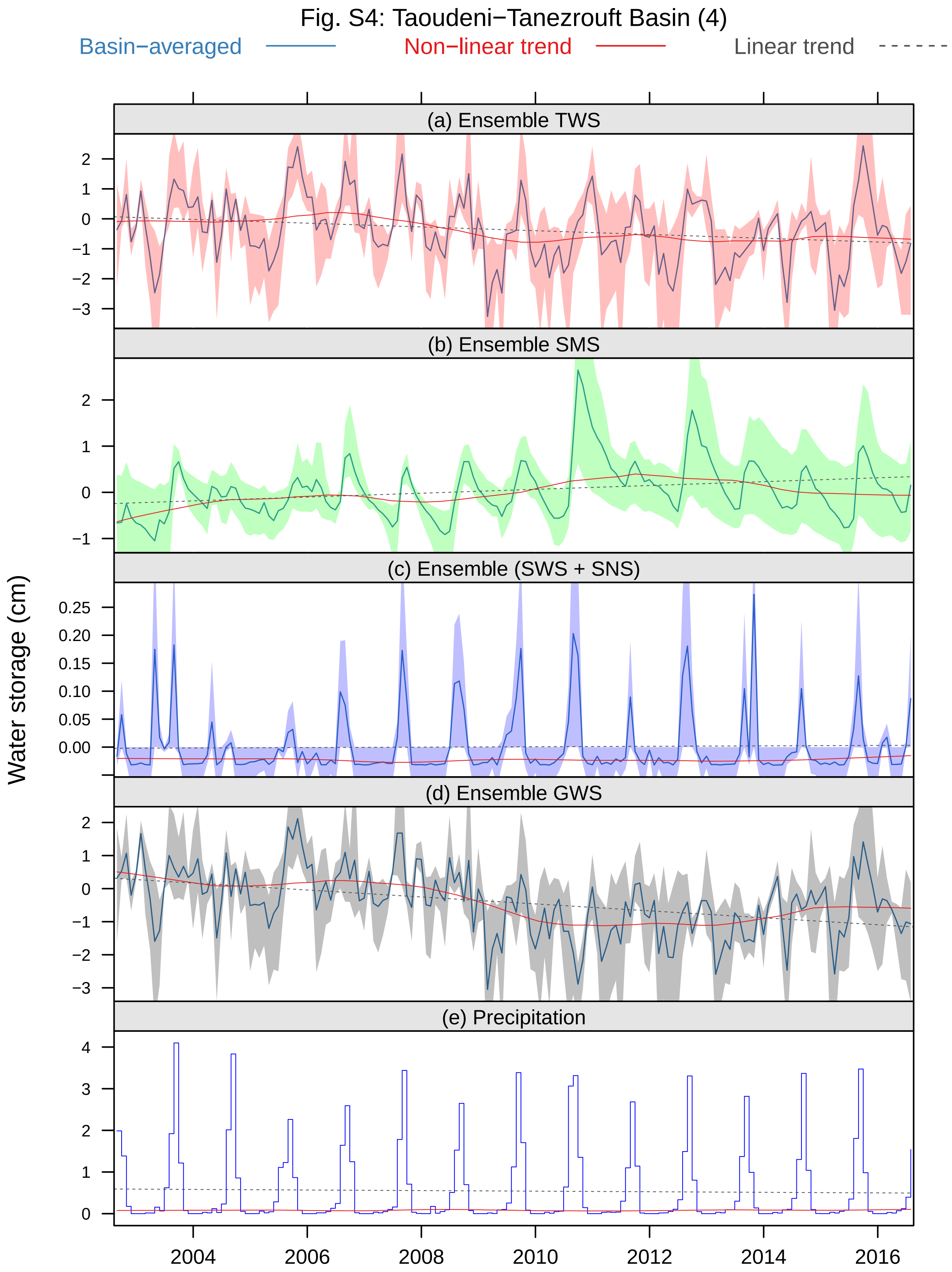
Fig. S4: Taoudeni−Tanezrouft Basin (4)
Basin−averaged
Non−linear trend
Linear trend
(a) Ensemble TWS
(b) Ensemble SMS
(c) Ensemble (SWS + SNS)
(d) Ensemble GWS
(e) Precipitation
Water storage (cm)
2004
2006
2008
2010
2012
2014
2016

Fig. S5: Senegal−Mauritanian Basin (5)

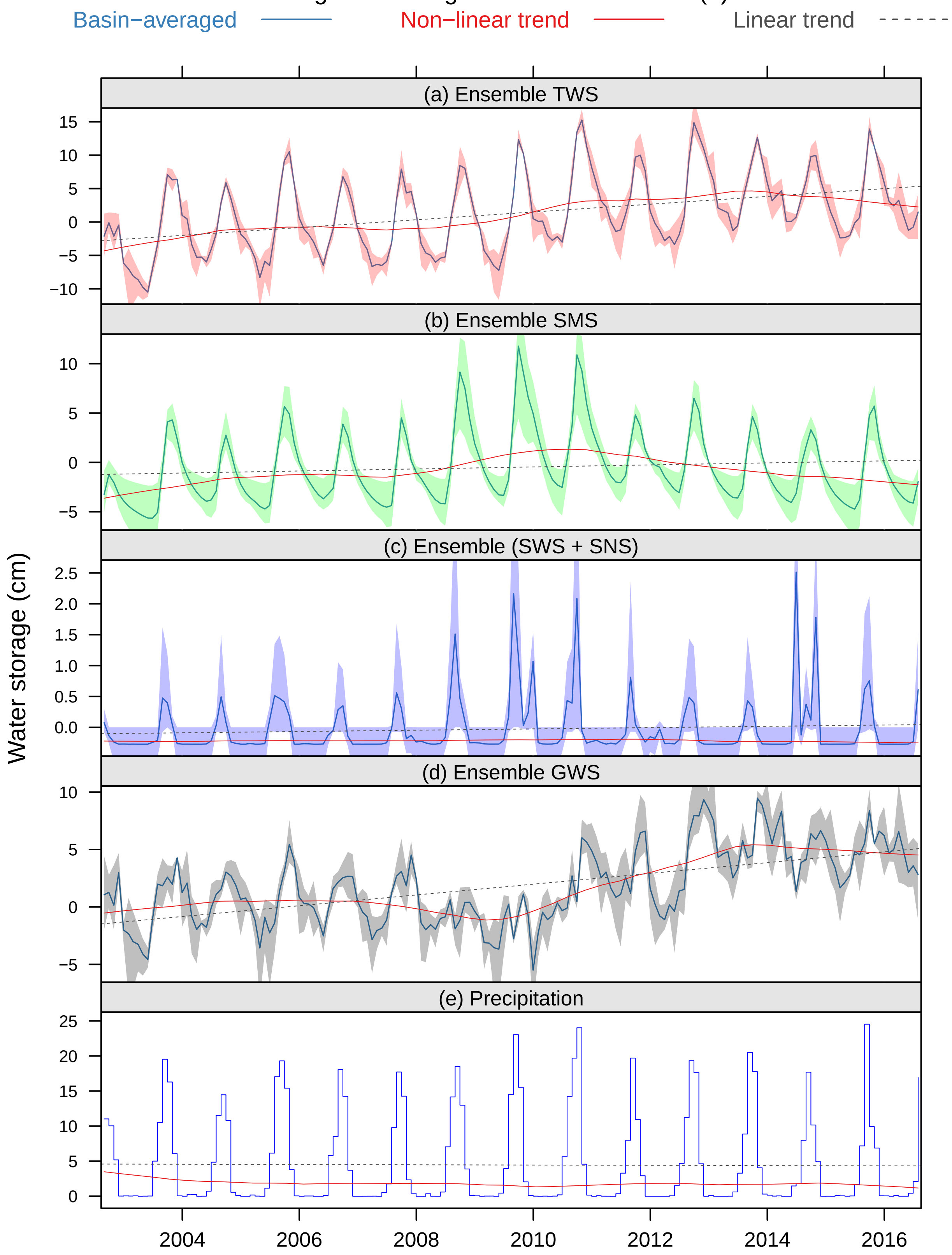

Fig. S6: Iullemmeden−Irhazer Aquifer System (6)

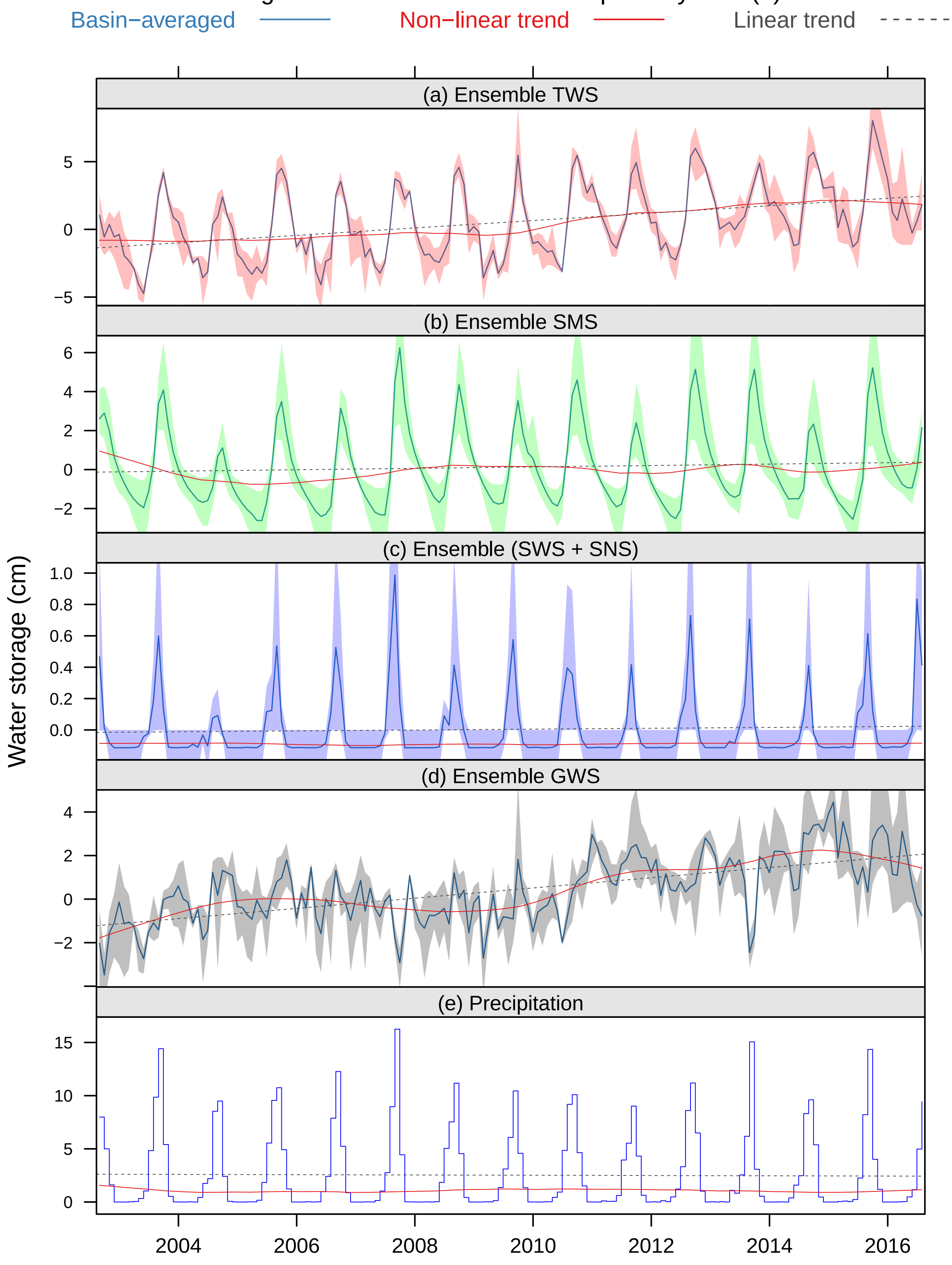

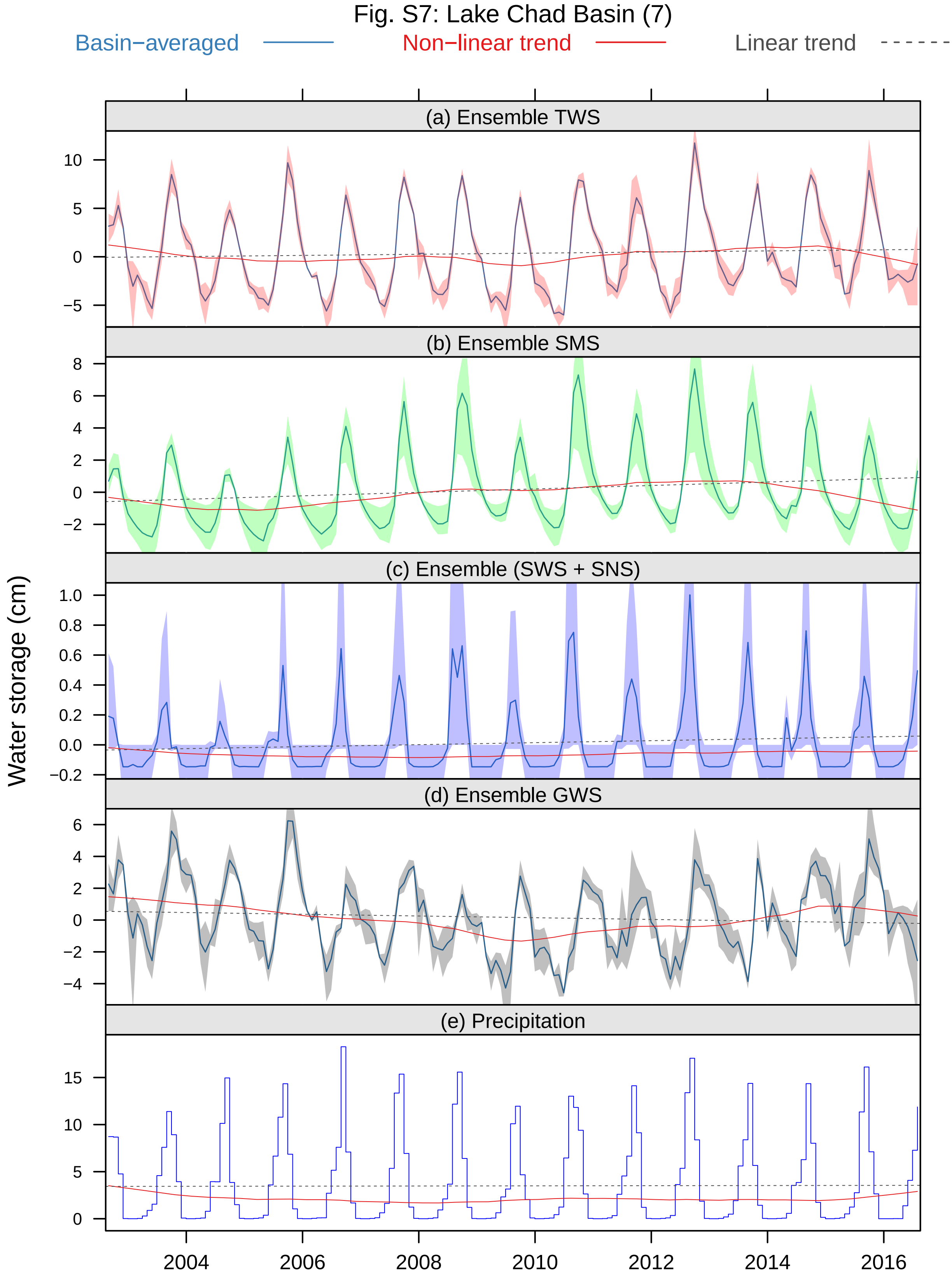
Fig. S7: Lake Chad Basin (7)
Basin−averaged
Non−linear trend
Linear trend
(a) Ensemble TWS
(b) Ensemble SMS
(c) Ensemble (SWS + SNS)
(d) Ensemble GWS
(e) Precipitation
Water storage (cm)
2004
2006
2008
2010
2012
2014
2016

Fig. S8: Umm Ruwaba Aquifer (Sudd Basin) (8)

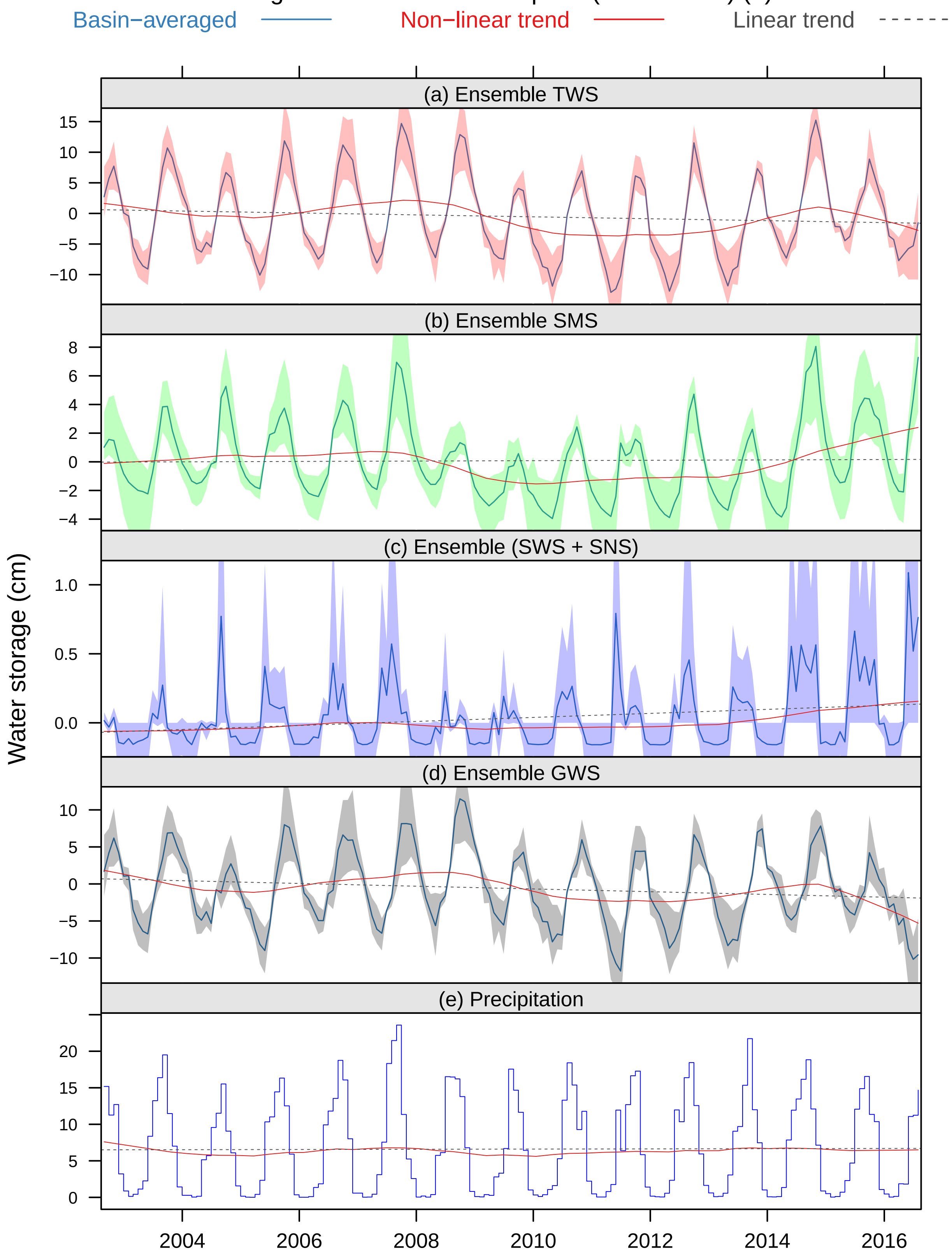

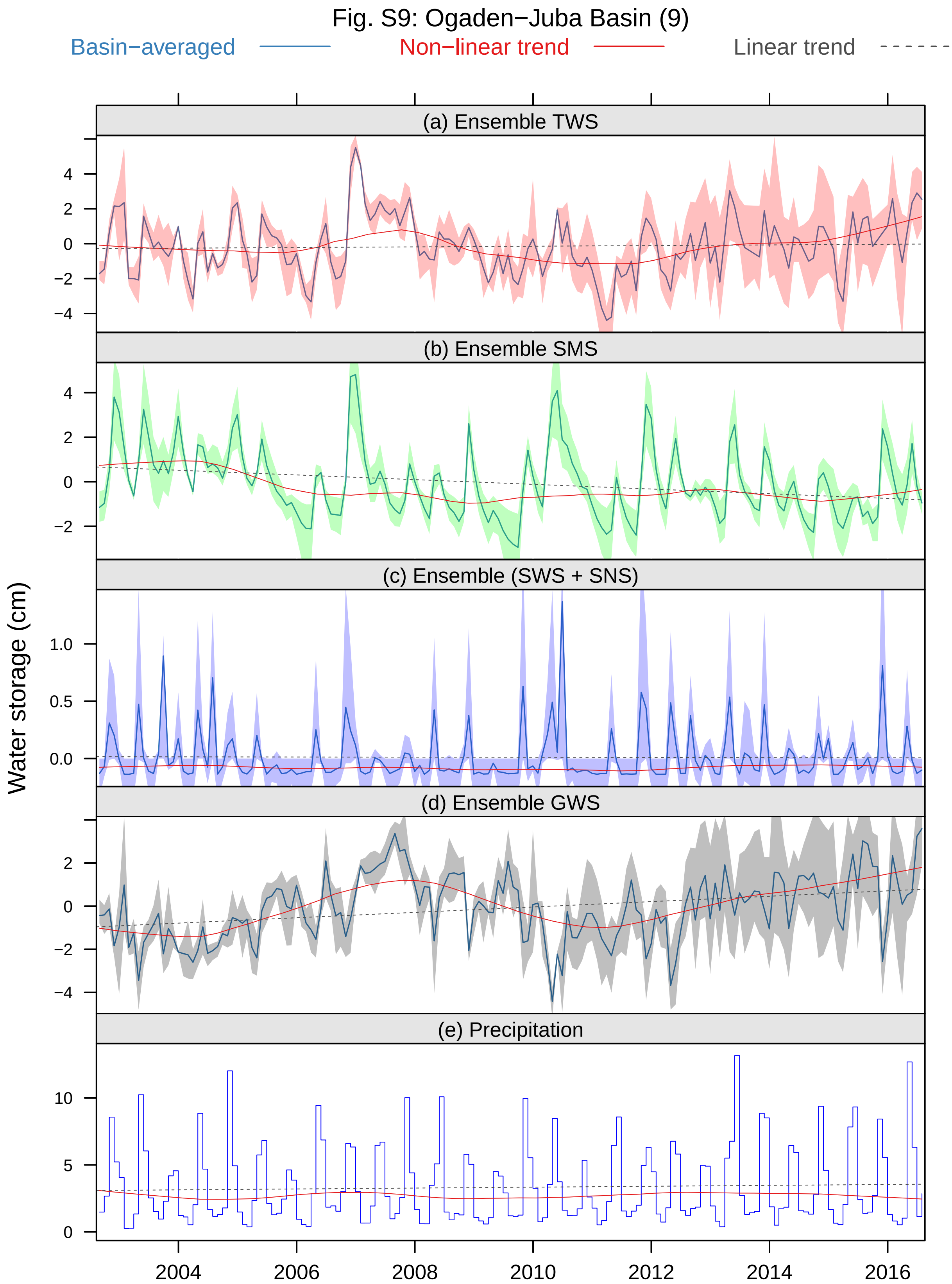
Fig. S9: Ogaden−Juba Basin (9)
Basin−averaged
Non−linear trend
Linear trend
(a) Ensemble TWS
(b) Ensemble SMS
(c) Ensemble (SWS + SNS)
(d) Ensemble GWS
(e) Precipitation
Water storage (cm)
4
2
0
−2
−4
1.0
0.5
0.0
10
5
2004
2006
2008
2010
2012
2014
2016

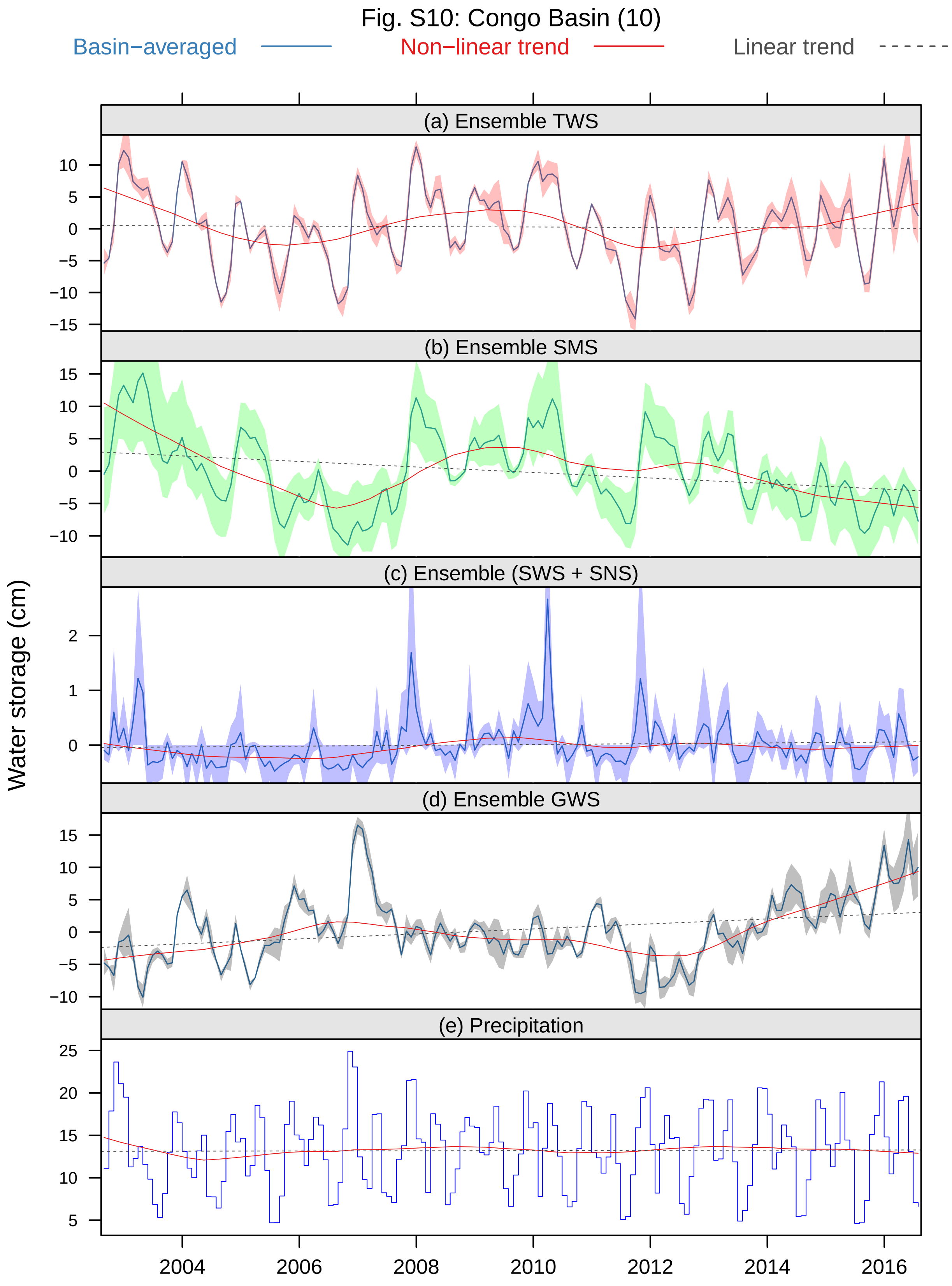
Fig. S10: Congo Basin (10)
Basin−averaged
Non−linear trend
Linear trend
(a) Ensemble TWS
(b) Ensemble SMS
(c) Ensemble (SWS + SNS)
(d) Ensemble GWS
(e) Precipitation
Water storage (cm)
2004
2006
2008
2010
2012
2014
2016

Fig. S11: Upper Kalahari−Cuvelai−Zambezi Basin (11)

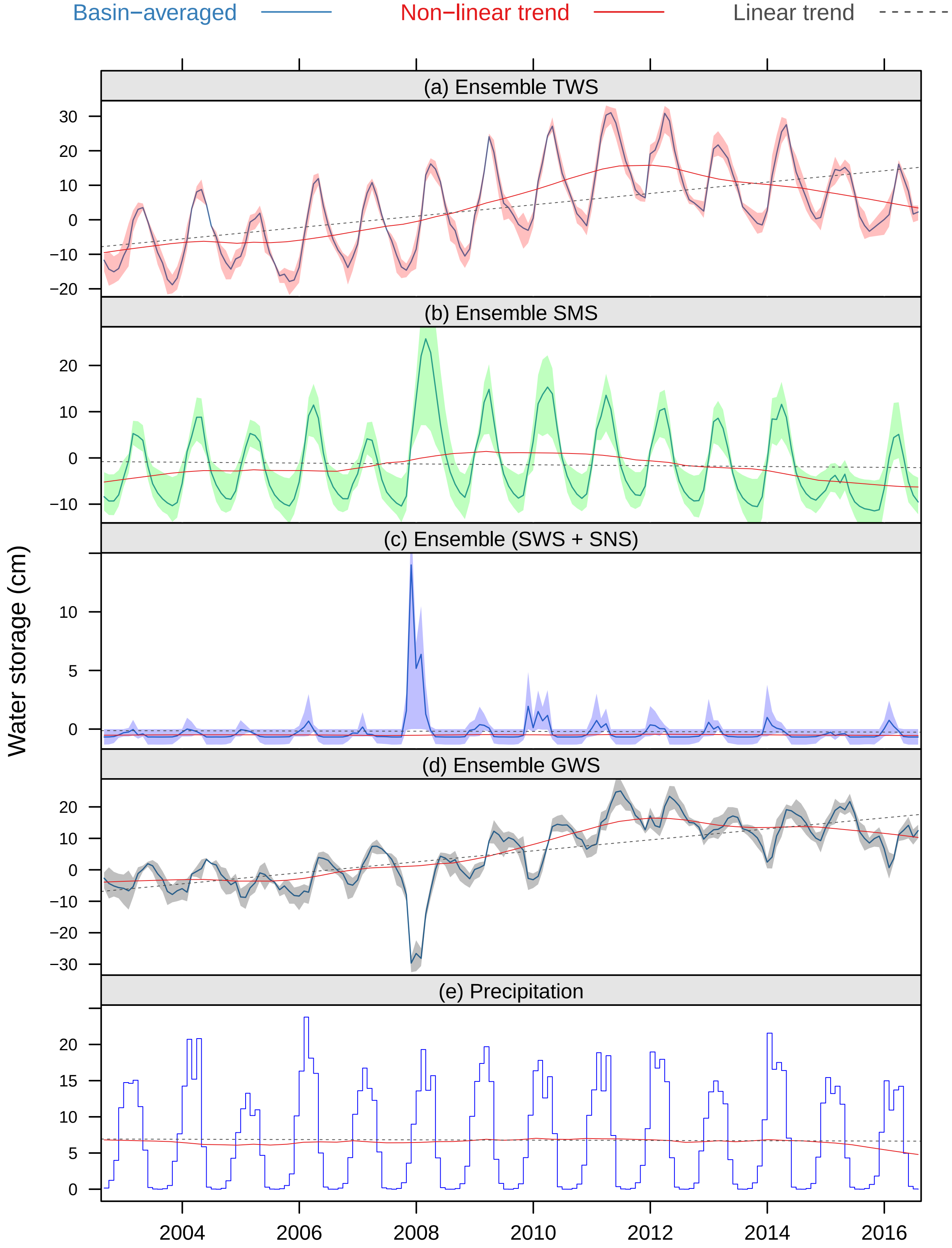

Fig. S12: Lower Kalahari−Stampriet Basin (12)

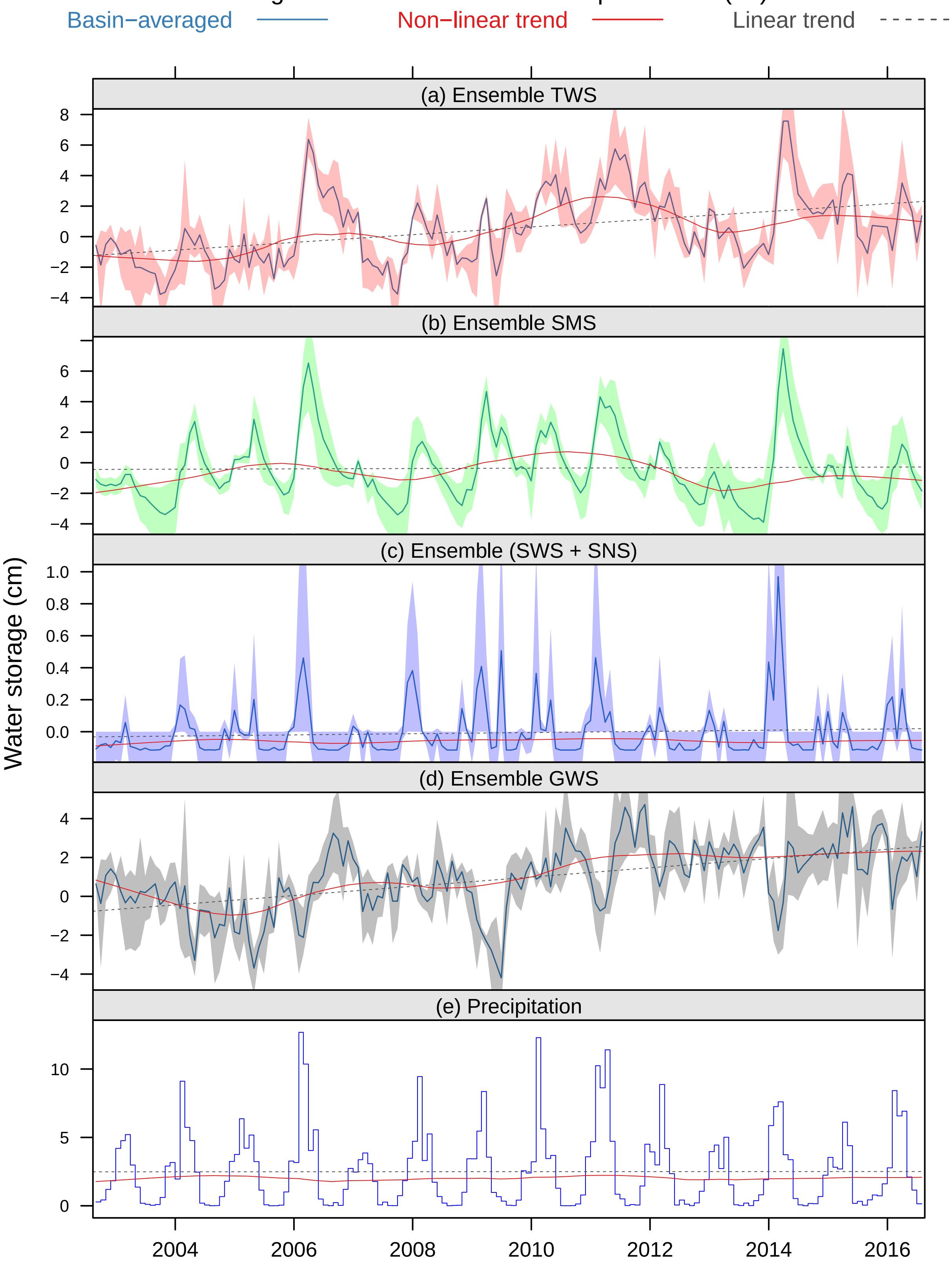

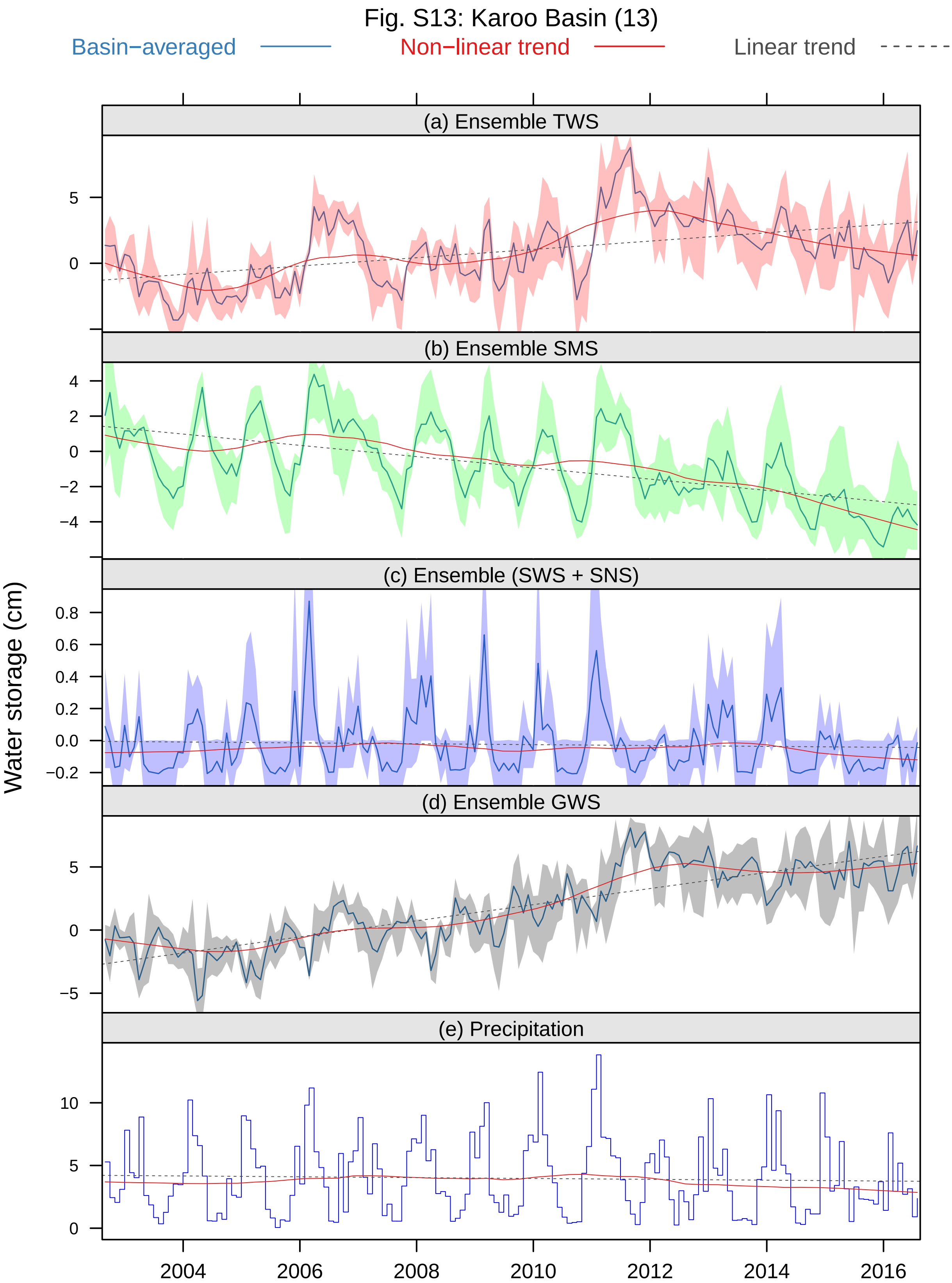
Fig. S13: Karoo Basin (13)
Basin−averaged
Non−linear trend
Linear trend
(a) Ensemble TWS
(b) Ensemble SMS
(c) Ensemble (SWS + SNS)
(d) Ensemble GWS
(e) Precipitation
Water storage (cm)
2004
2006
2008
2010
2012
2014
2016

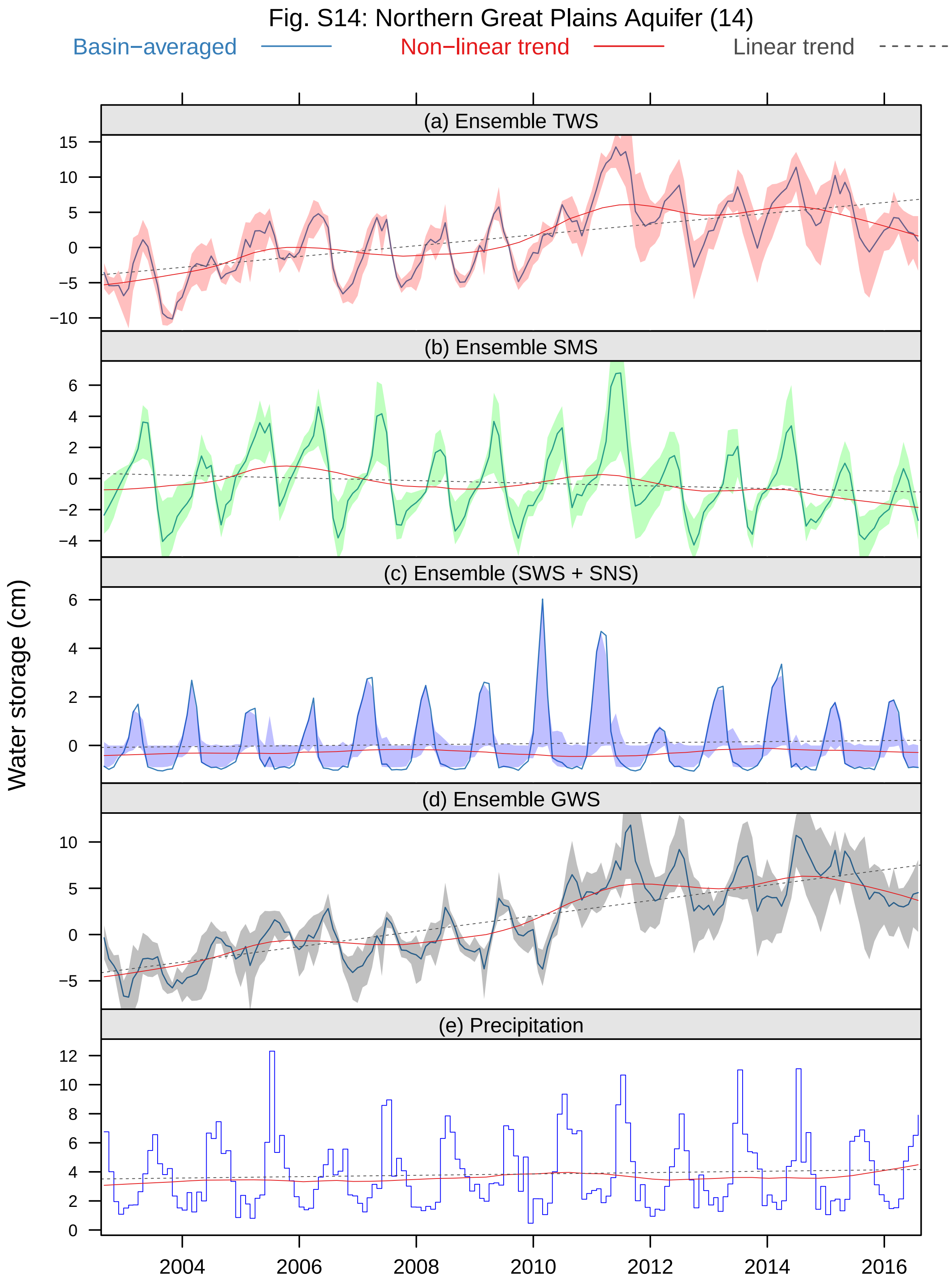
Fig. S14: Northern Great Plains Aquifer (14)
Basin−averaged
Non−linear trend
Linear trend
(a) Ensemble TWS
(b) Ensemble SMS
(c) Ensemble (SWS + SNS)
(d) Ensemble GWS
(e) Precipitation
Water storage (cm)
2004
2006
2008
2010
2012
2014
2016

Fig. S15: Cambro−Ordovician Aquifer System (15)

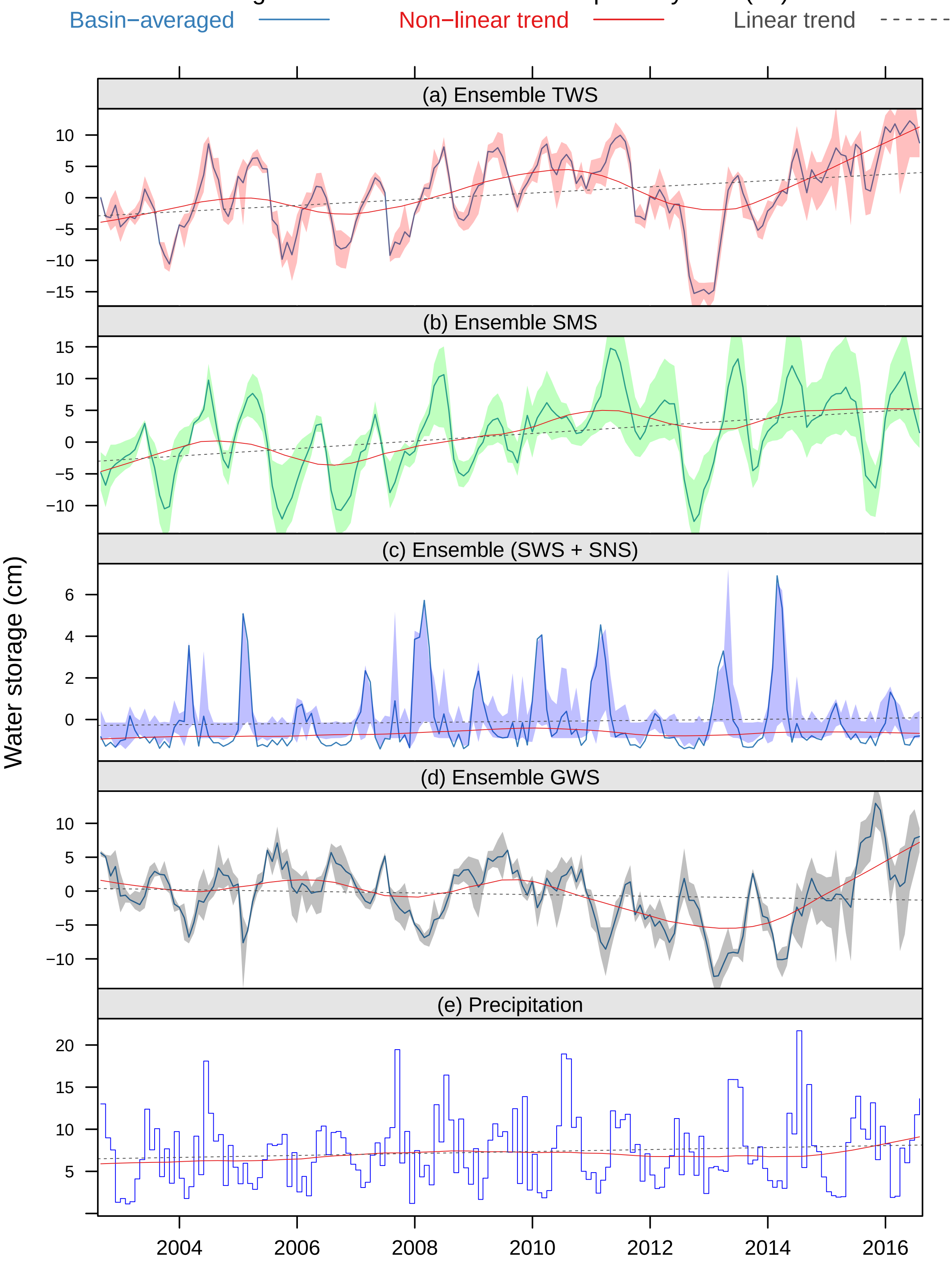

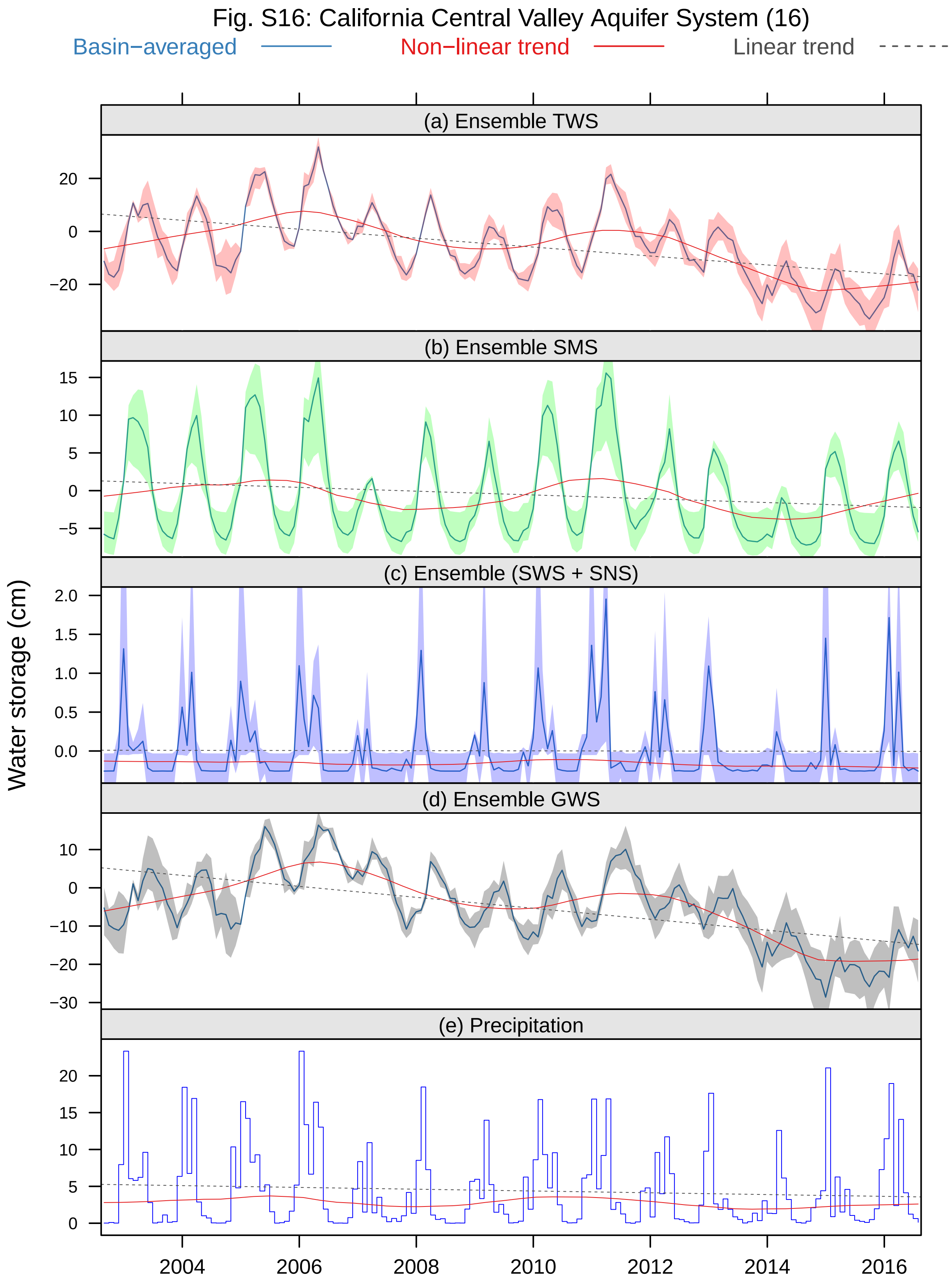

Fig. S16: California Central Valley Aquifer System (16)
Basin−averaged
Non−linear trend
Linear trend
(a) Ensemble TWS
(b) Ensemble SMS
(c) Ensemble (SWS + SNS)
(d) Ensemble GWS
(e) Precipitation
Water storage (cm)
2004
2006
2008
2010
2012
2014
2016

Fig. S17: Atlantic and Gulf Coastal Plains Aquifer (18)

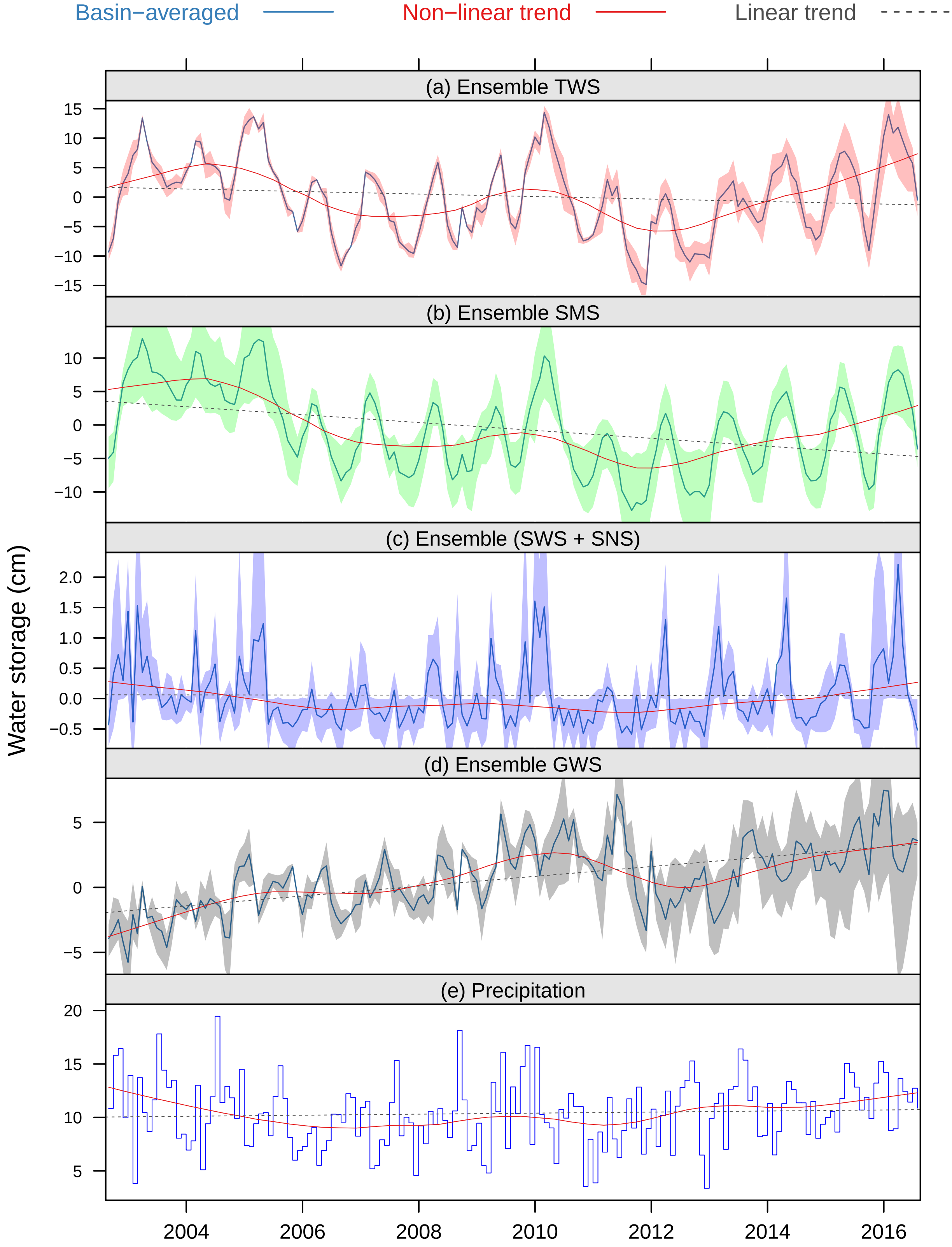

Fig. S18: Amazon Basin (19)

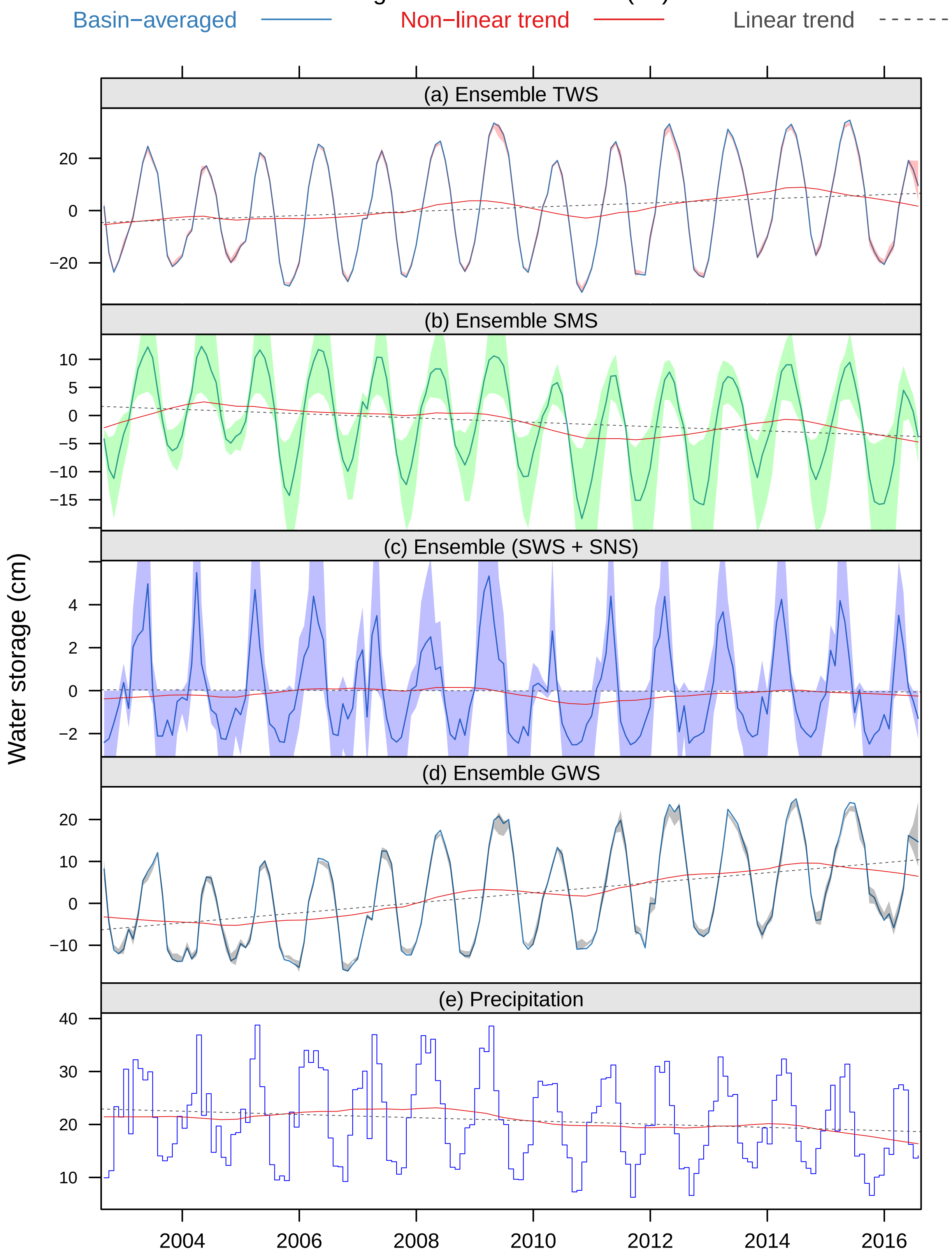

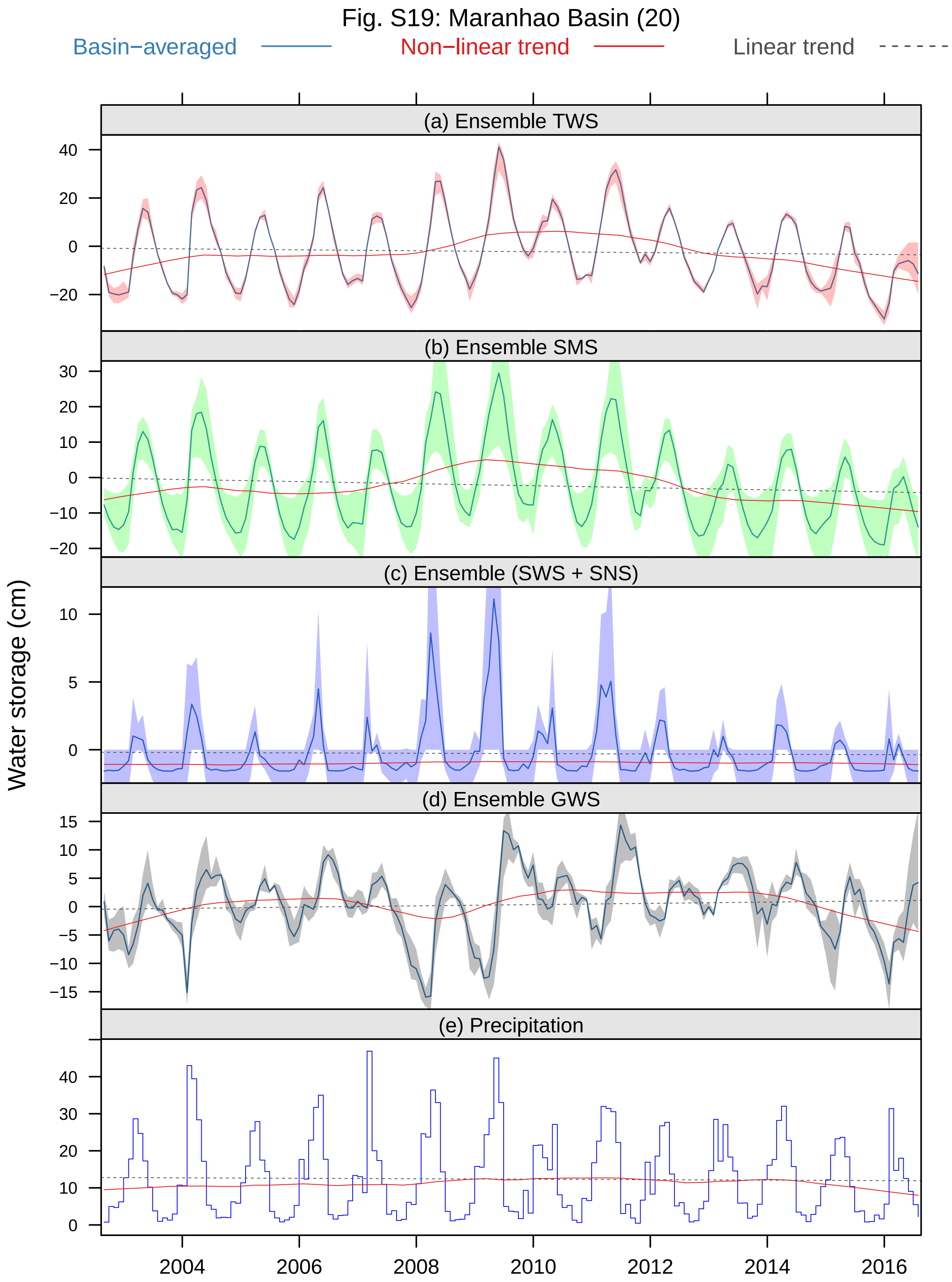

Fig. S19: Maranhao Basin (20)
Basin−averaged
Non−linear trend
Linear trend
(a) Ensemble TWS
(b) Ensemble SMS
(c) Ensemble (SWS + SNS)
(d) Ensemble GWS
(e) Precipitation
Water storage (cm)
2004
2006
2008
2010
2012
2014
2016

Fig. S20: Guarani Aquifer System (Parana Basin) (21)

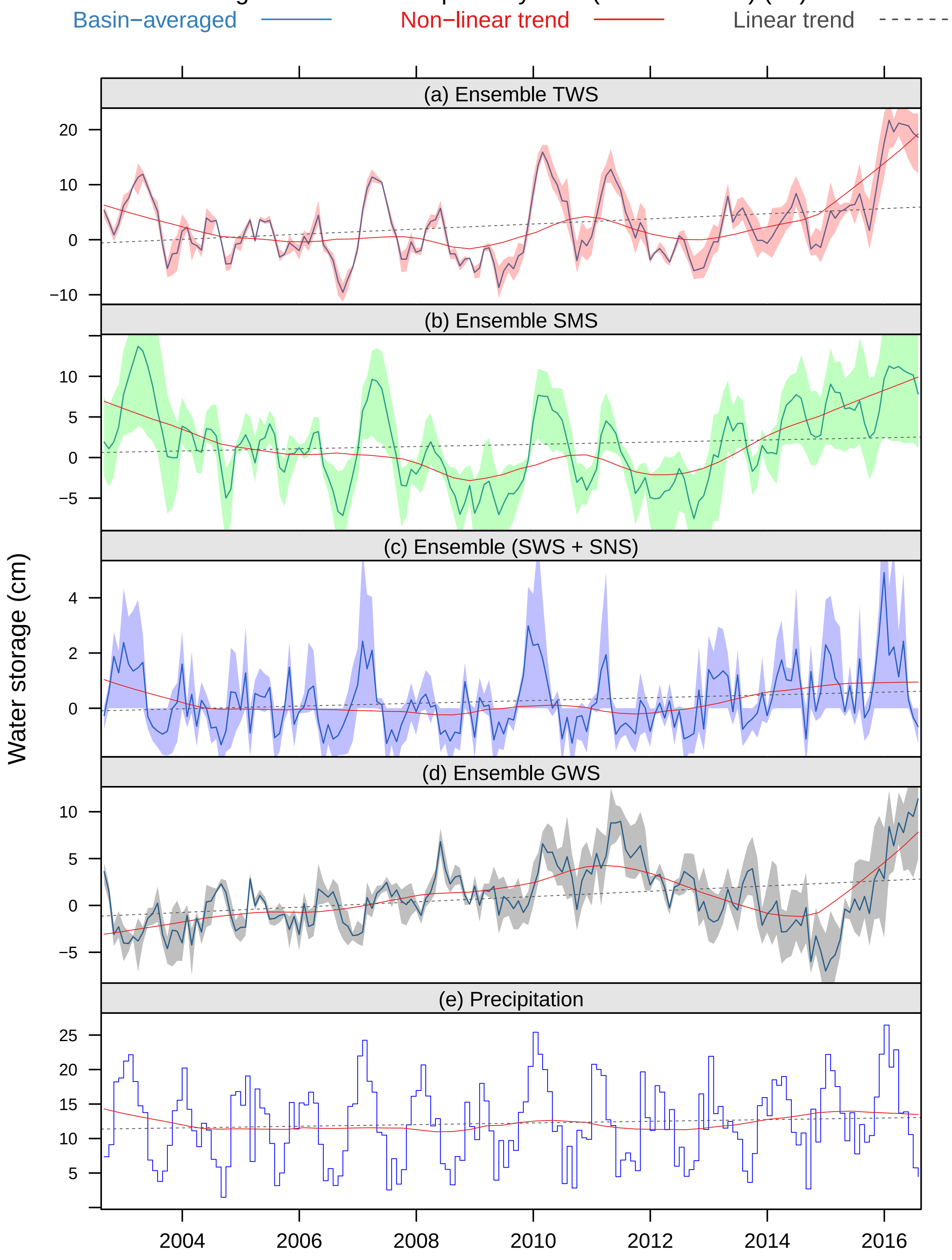

Fig. S21: Arabian Aquifer System (22)

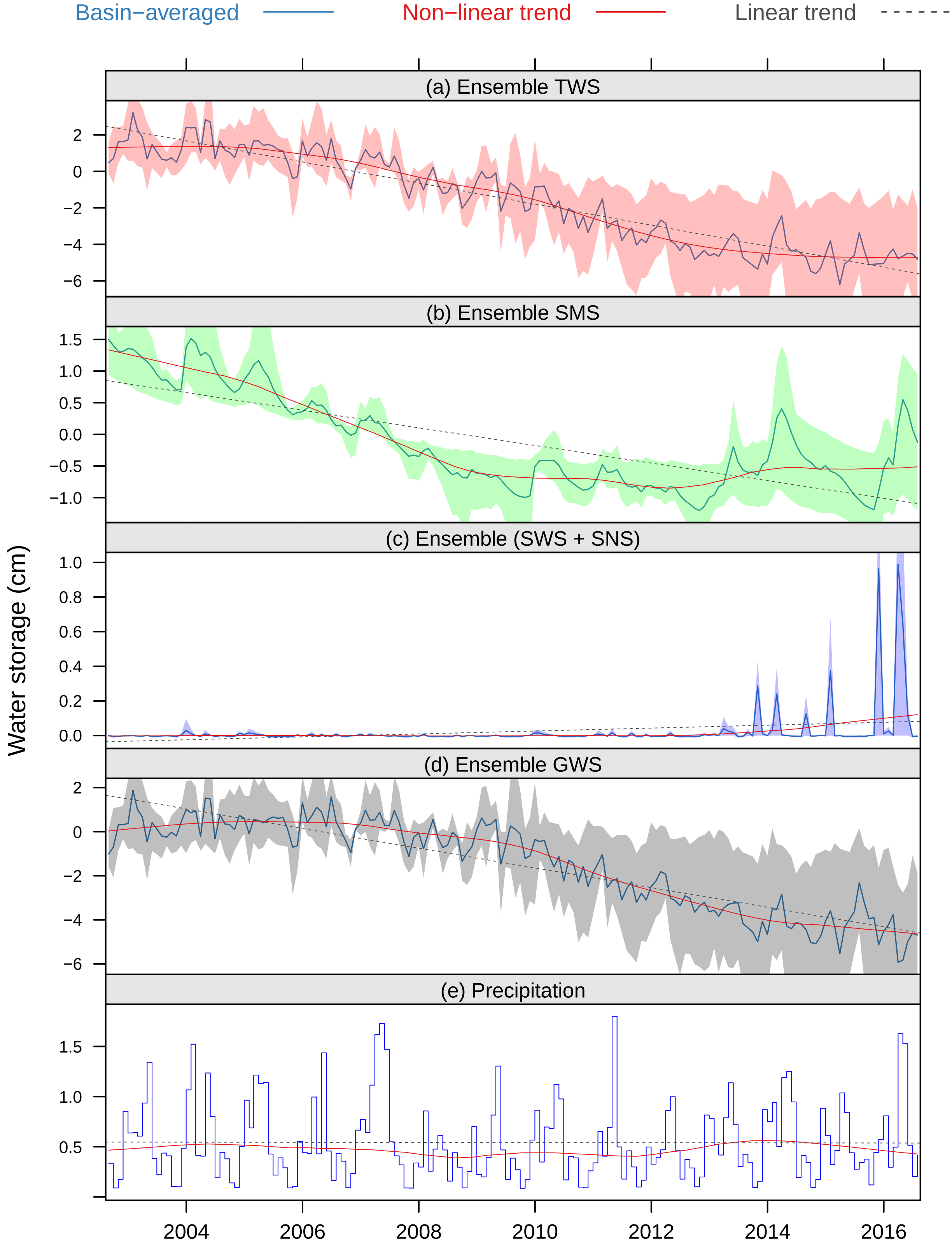

Fig. S22: Indus River Basin (23)

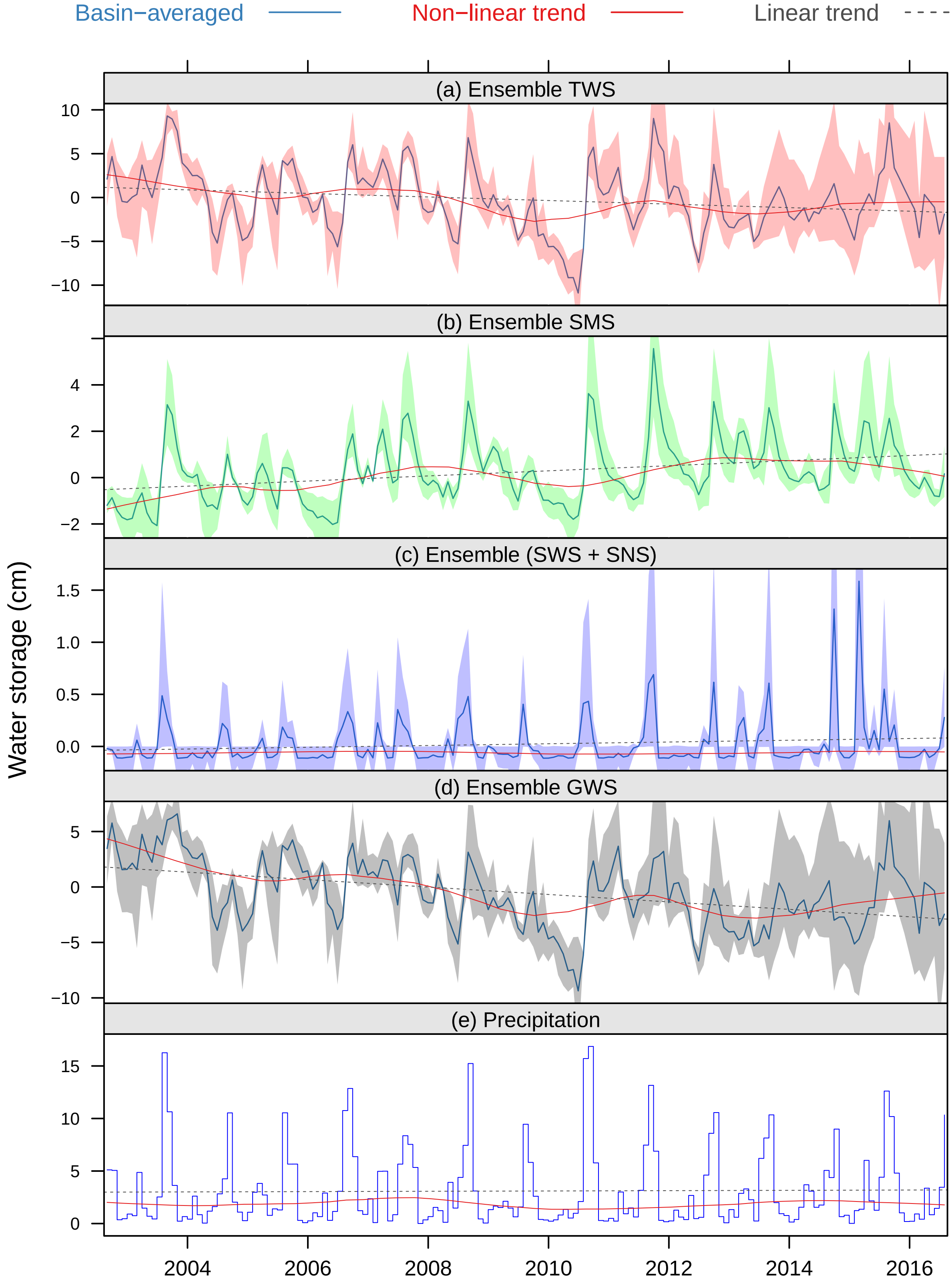

Fig. S23: Ganges−Brahmaputra River Basin (24)

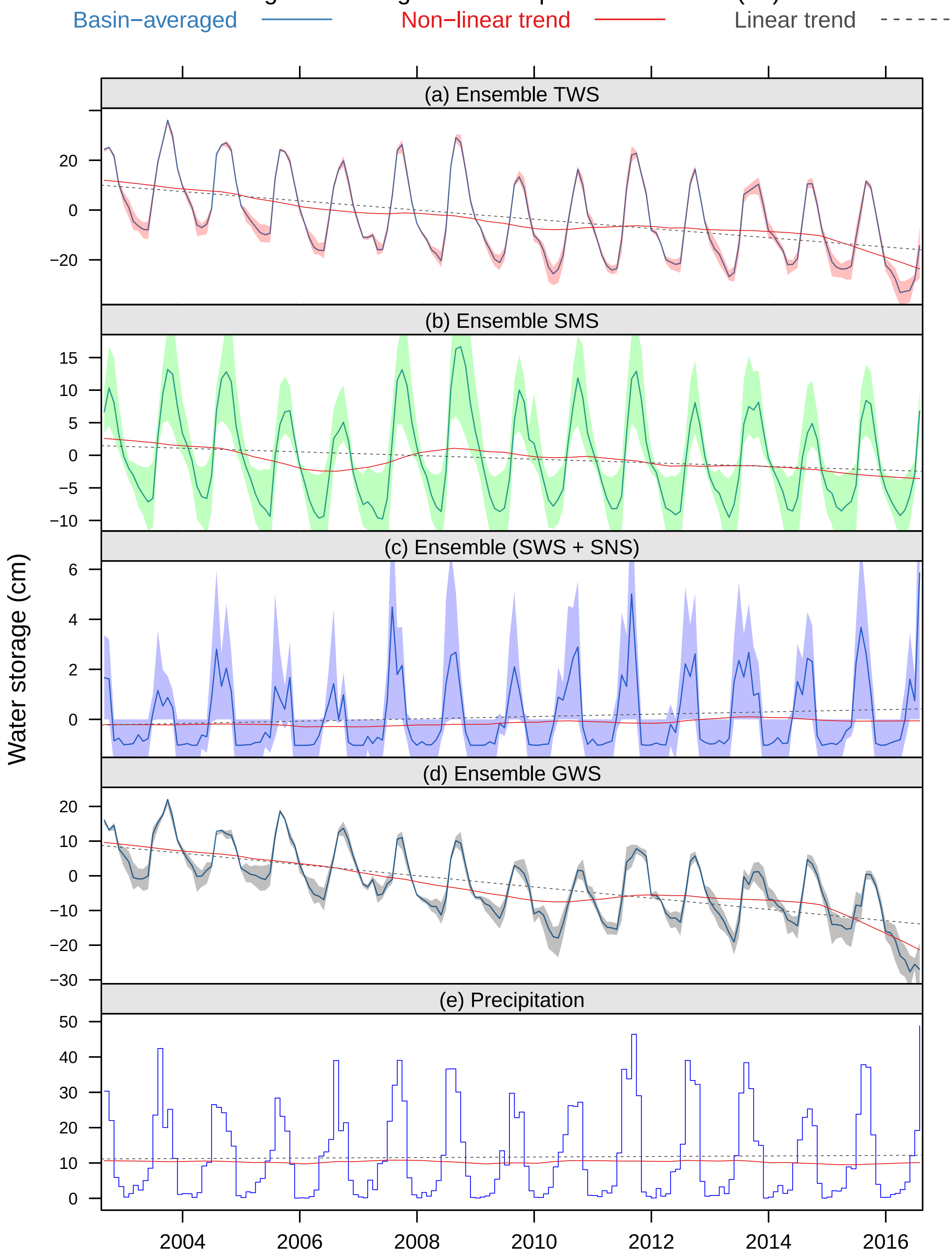

Fig. S24: West Siberian Artesian Basin (25)

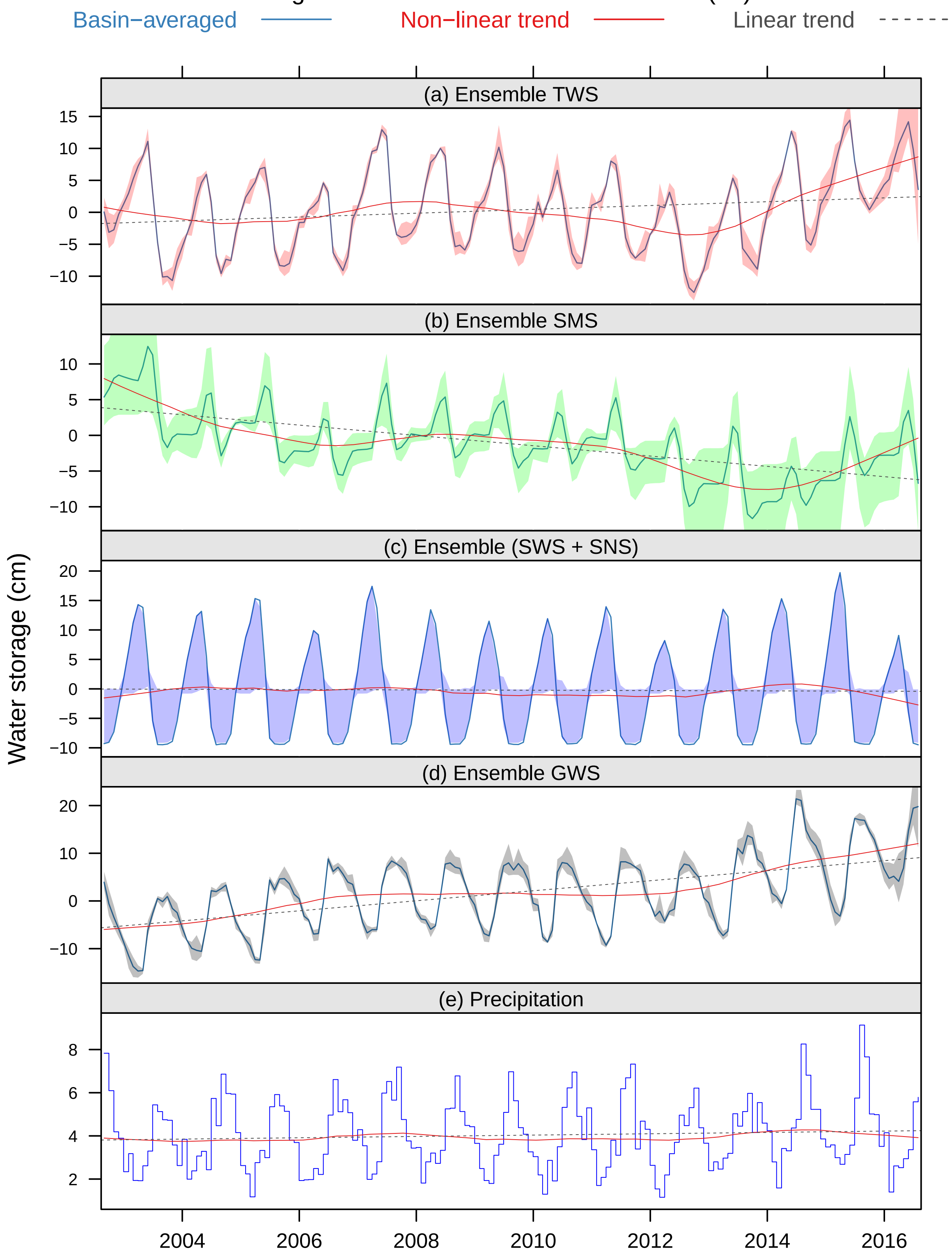

Fig. S25: Tunguss Basin (26)

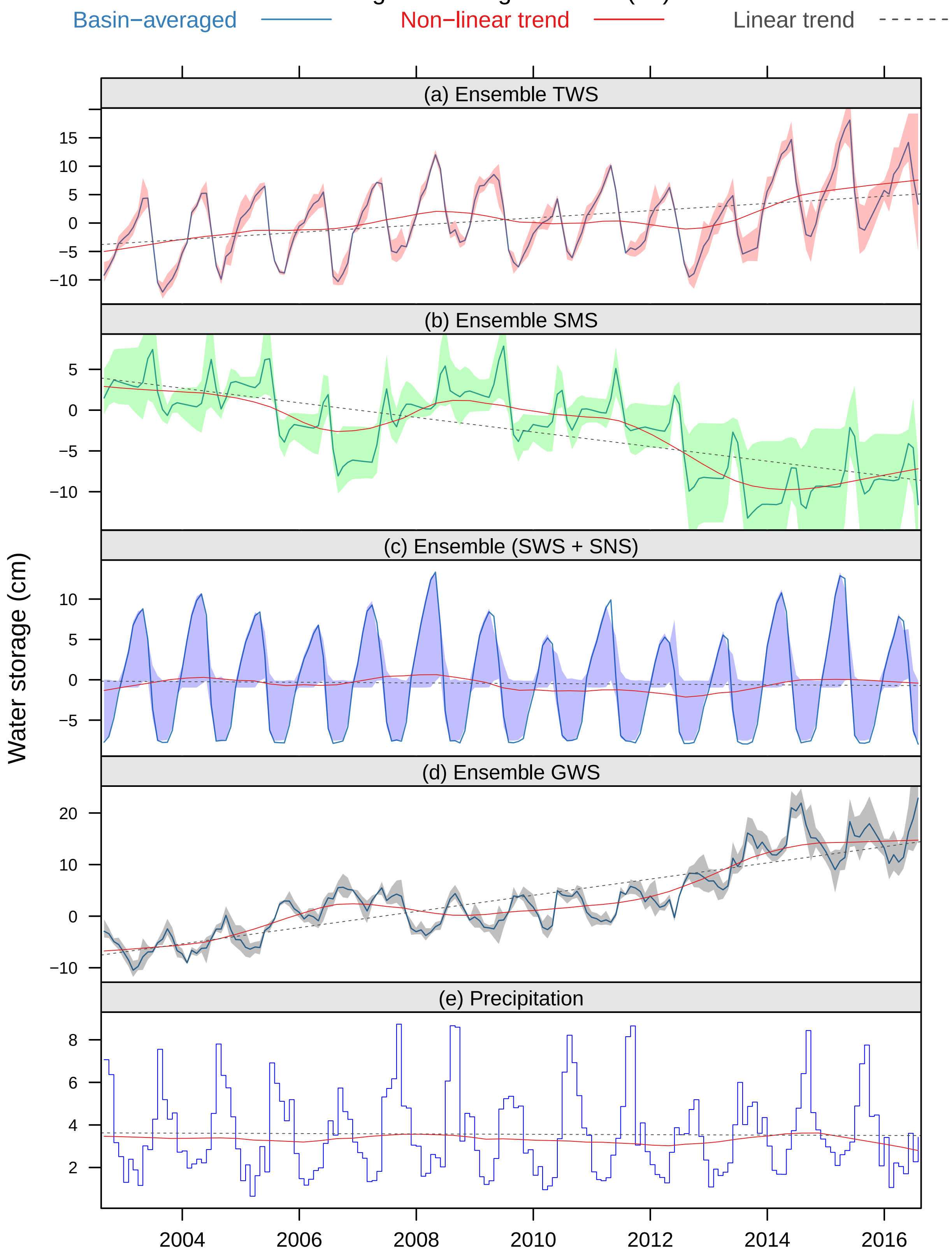

Fig. S26: Angara−Lena Basin (27)

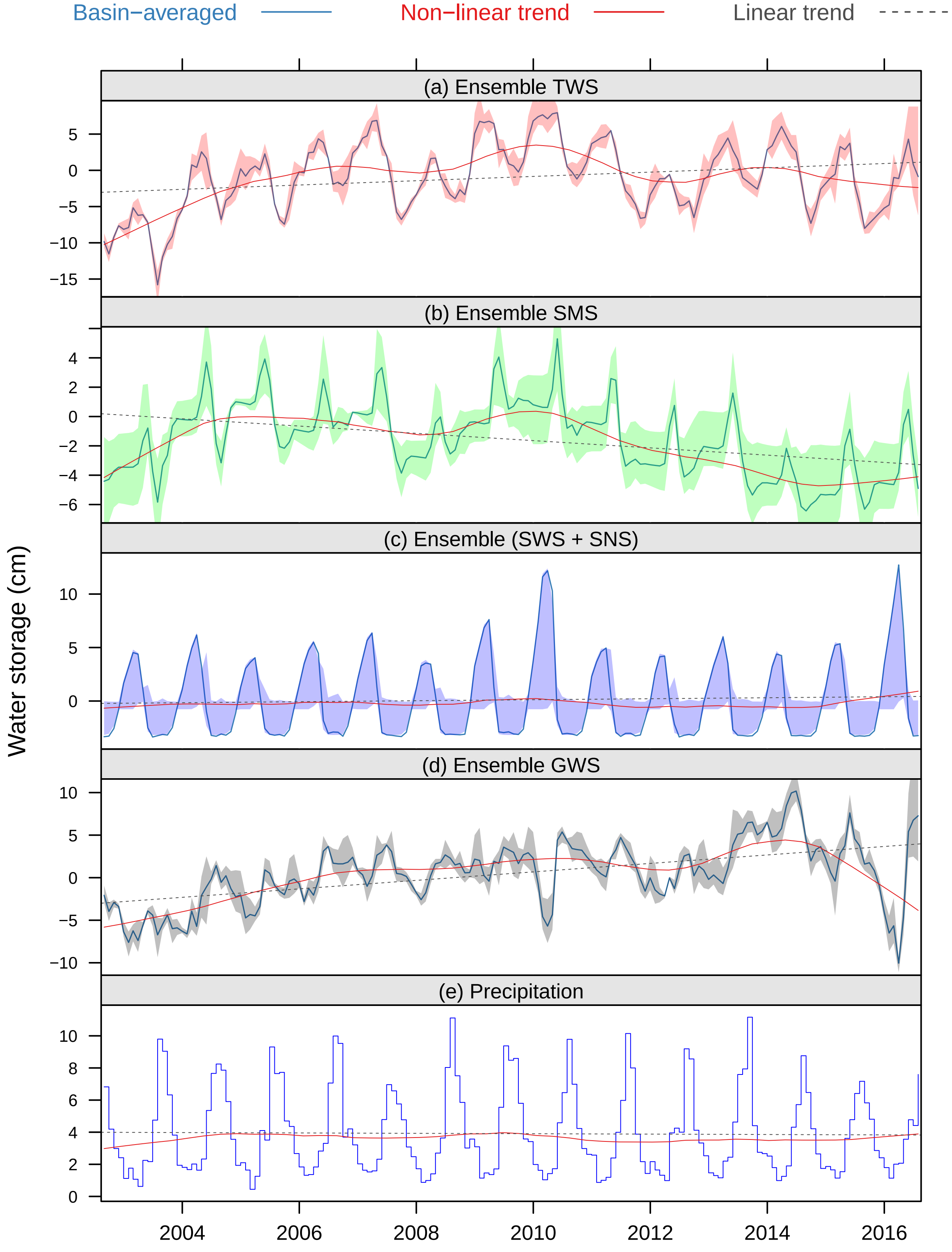

Fig. S27: Yakut Basin (28)

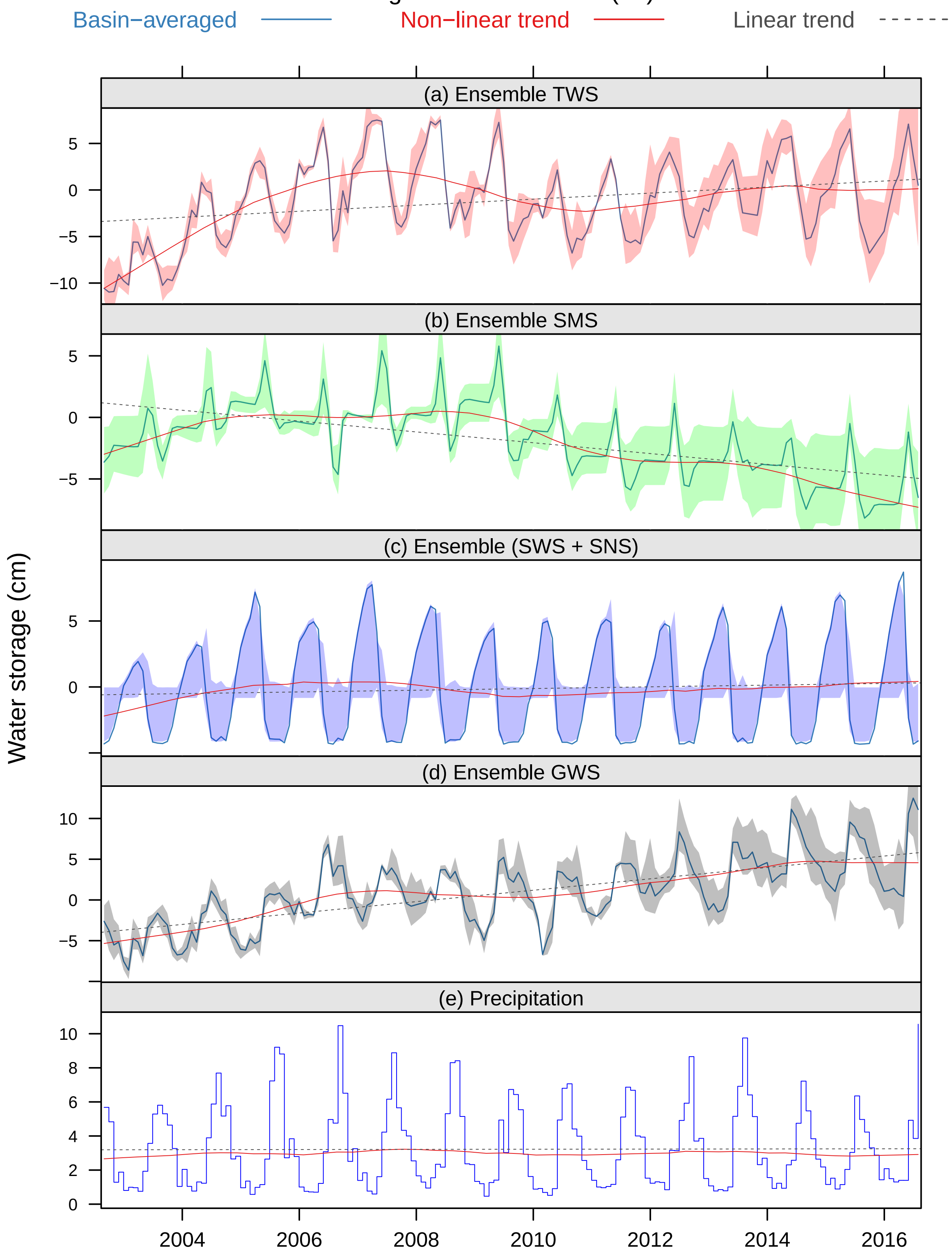

Fig. S28: North China Plains Aquifer System (29)

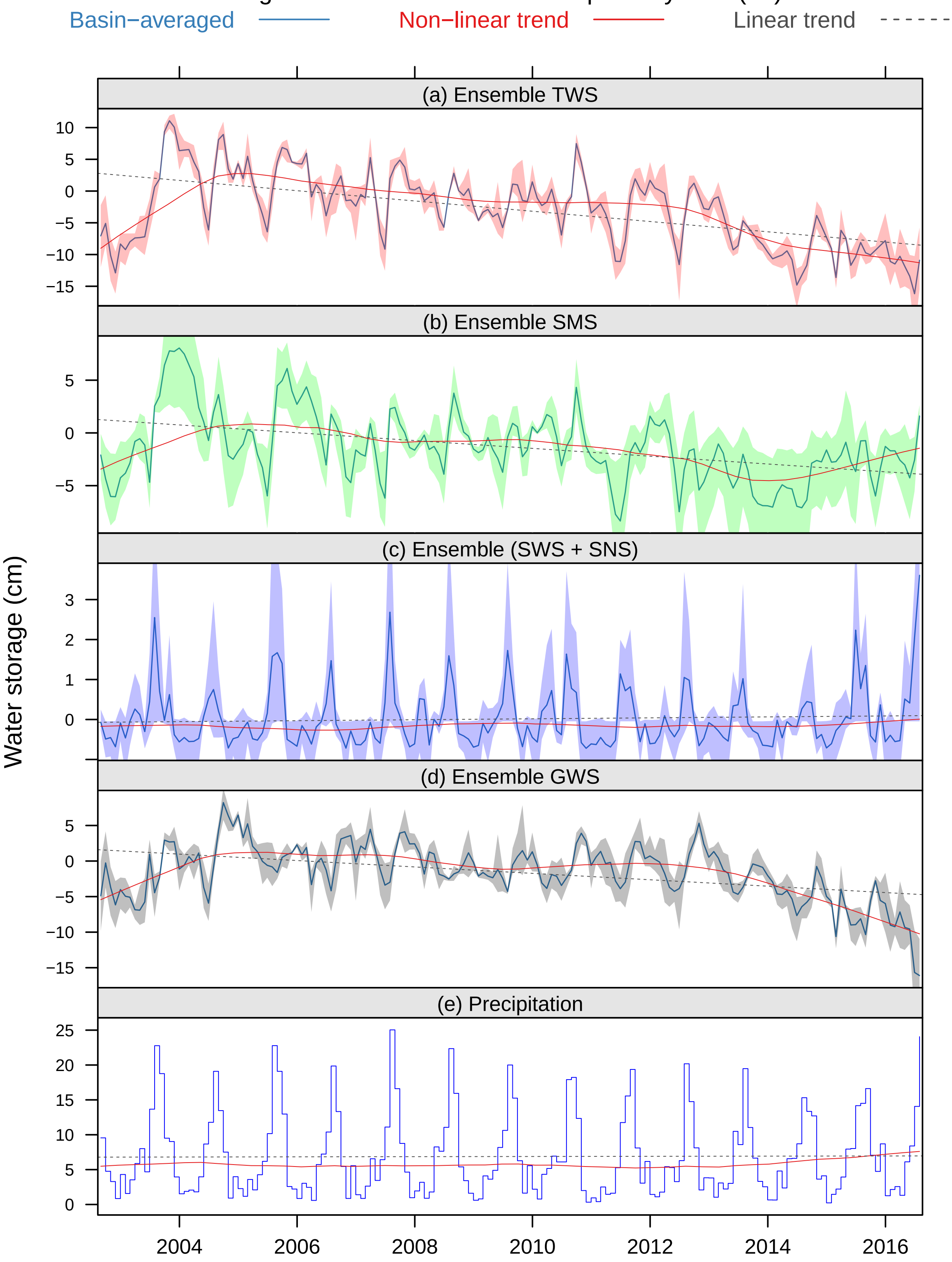

Fig. S29: Song−Liao Plain (30)

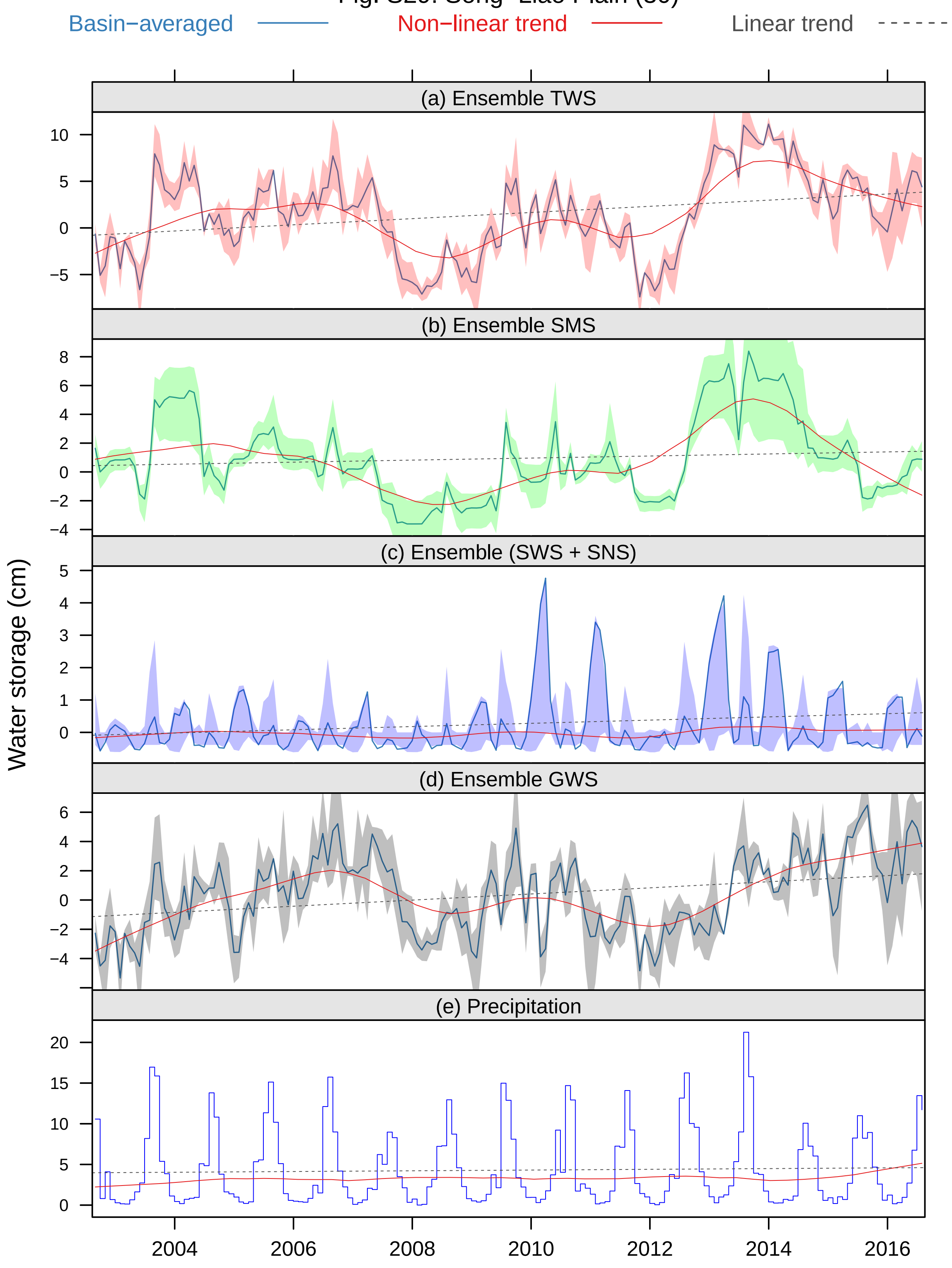

Fig. S30: Tarim Basin (31)

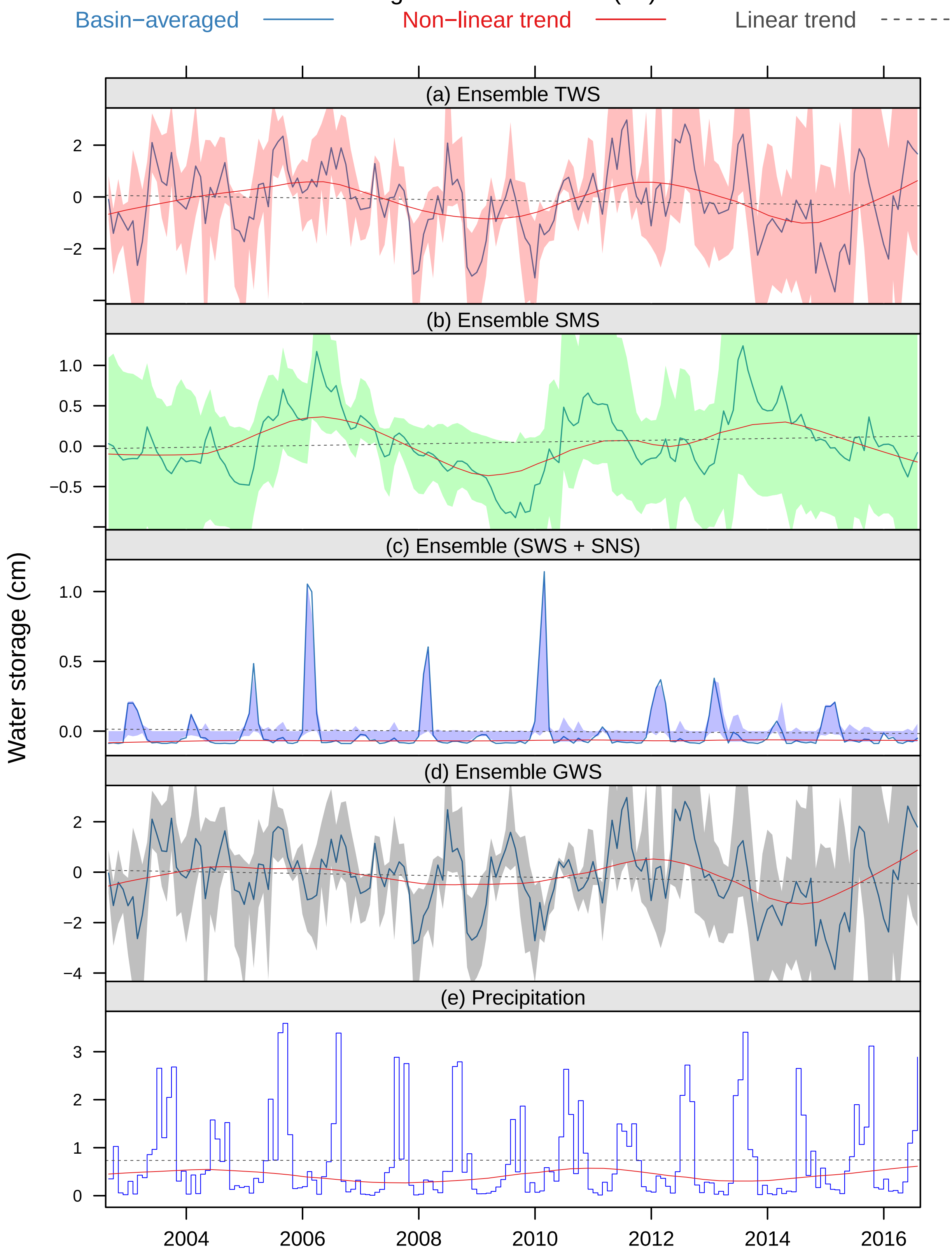

Fig. S31: Paris Basin (32)

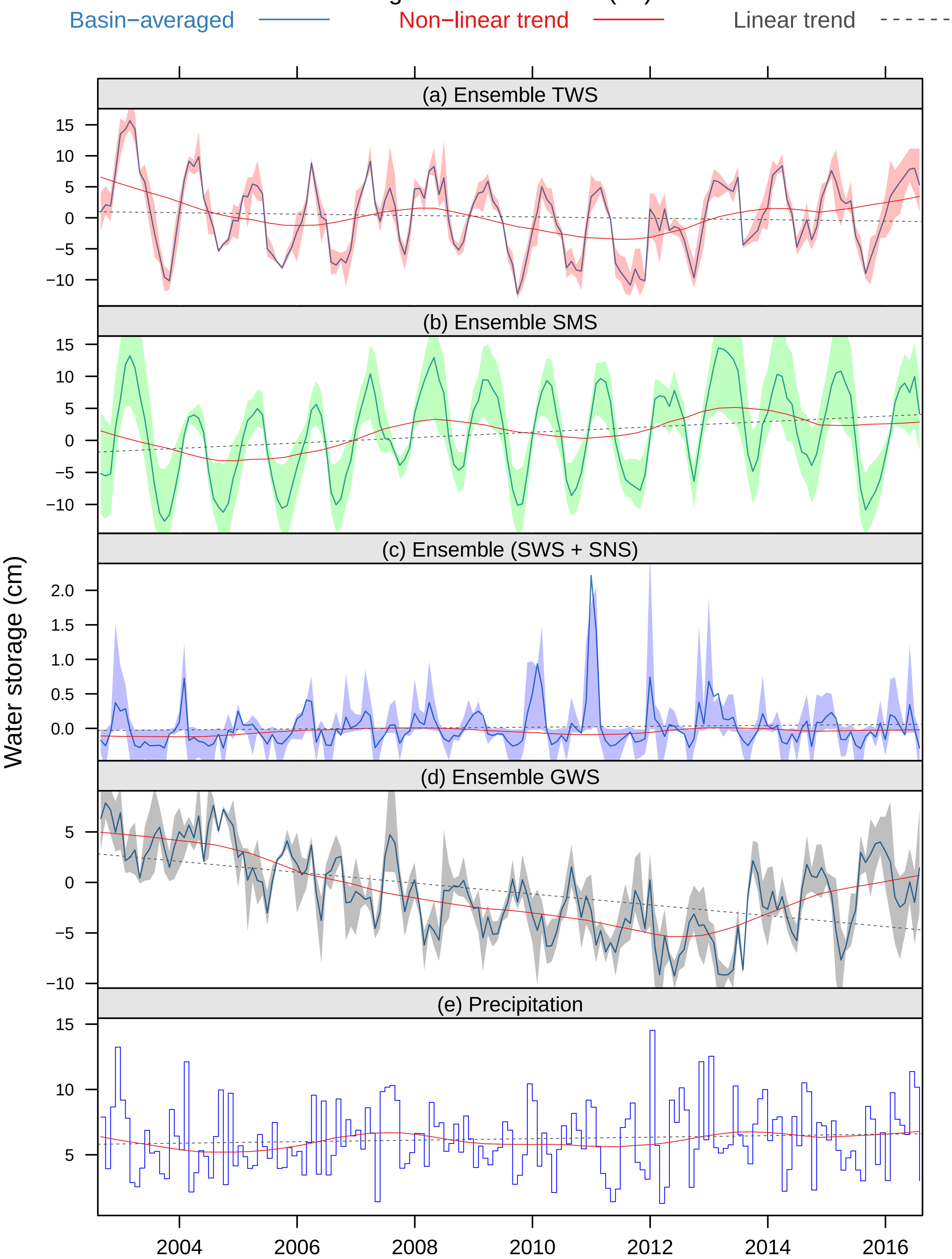

Fig. S32: East European Aquifer System (33)

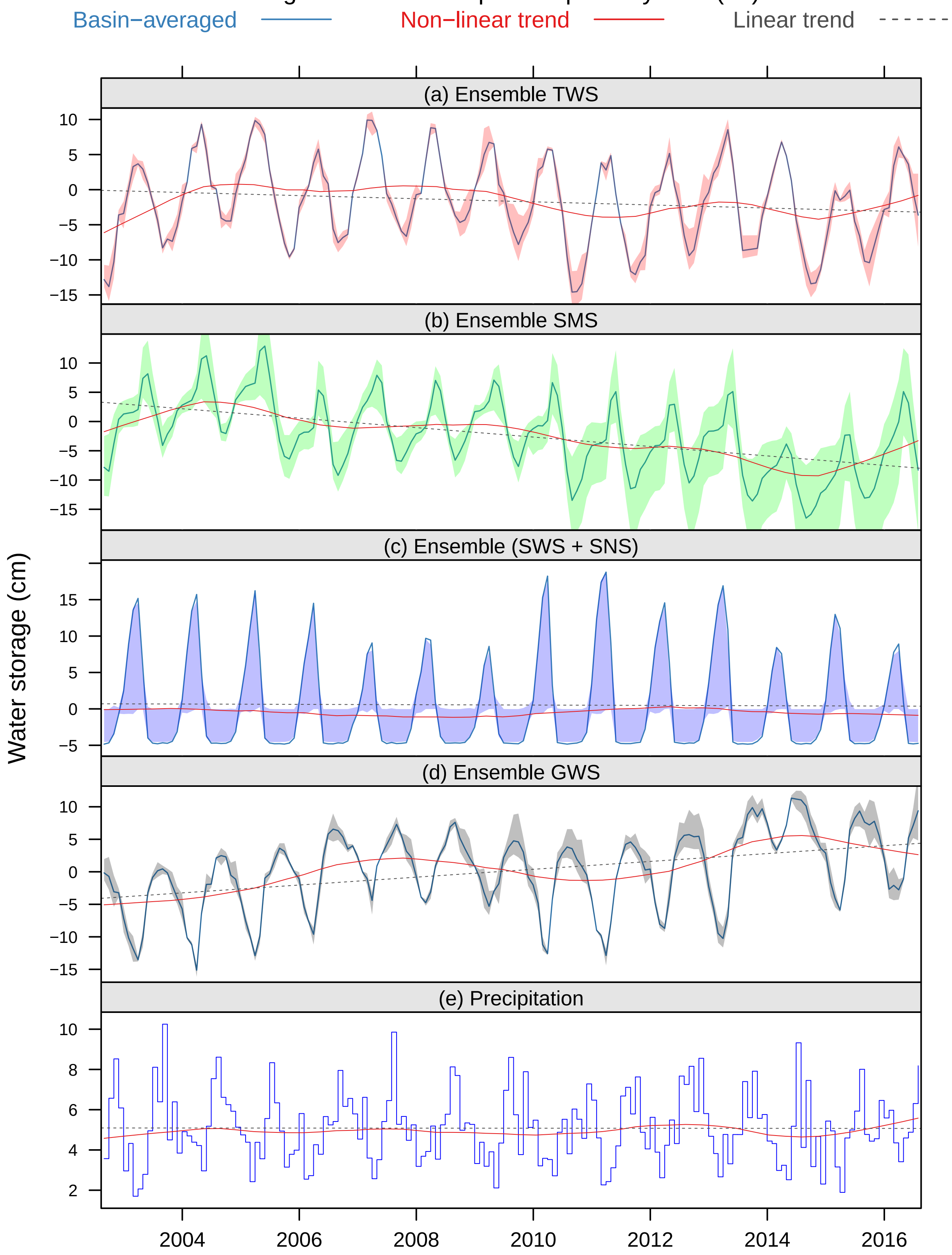

Fig. S33: North Caucasus Basin (34)

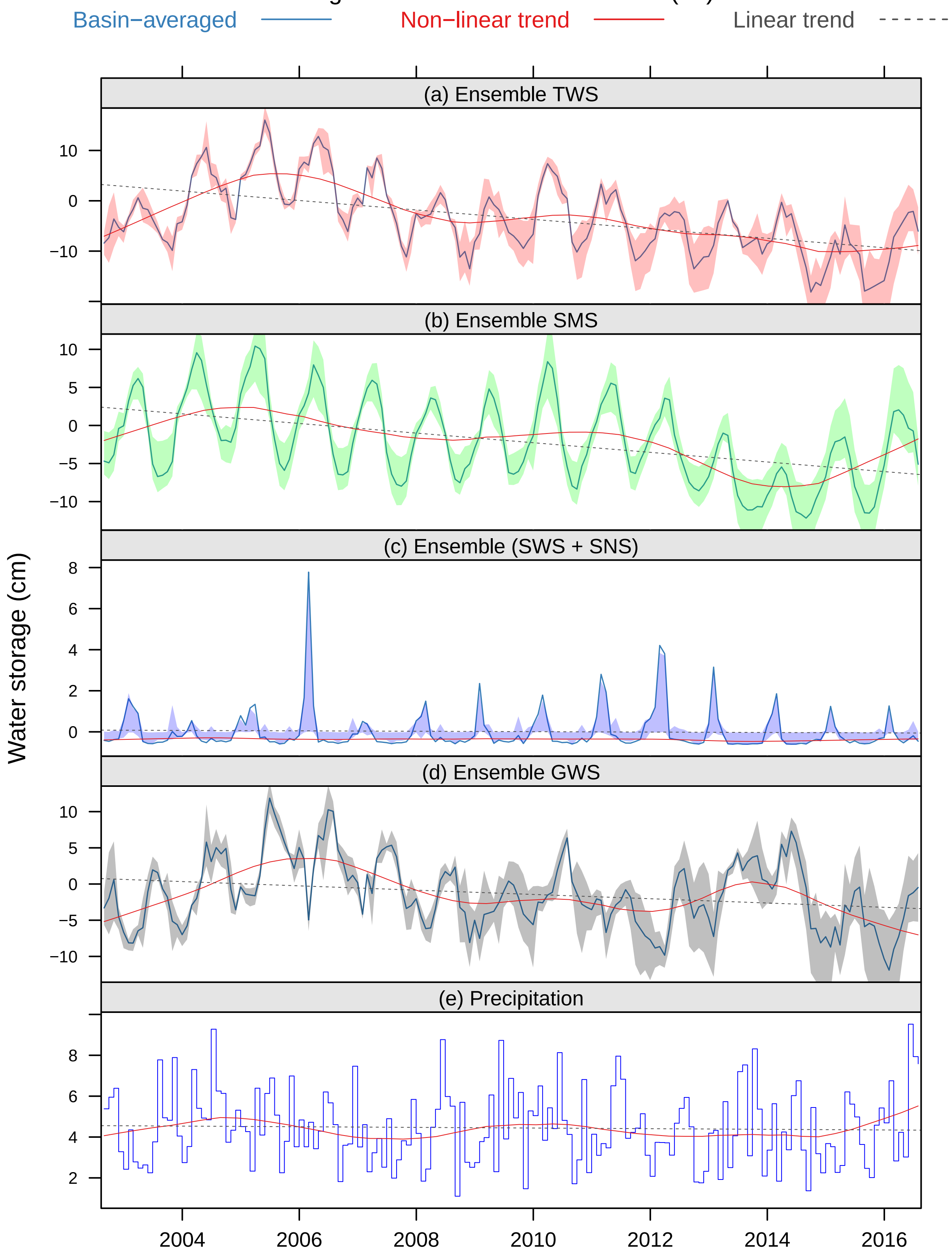

Fig. S34: Pechora Basin (35)

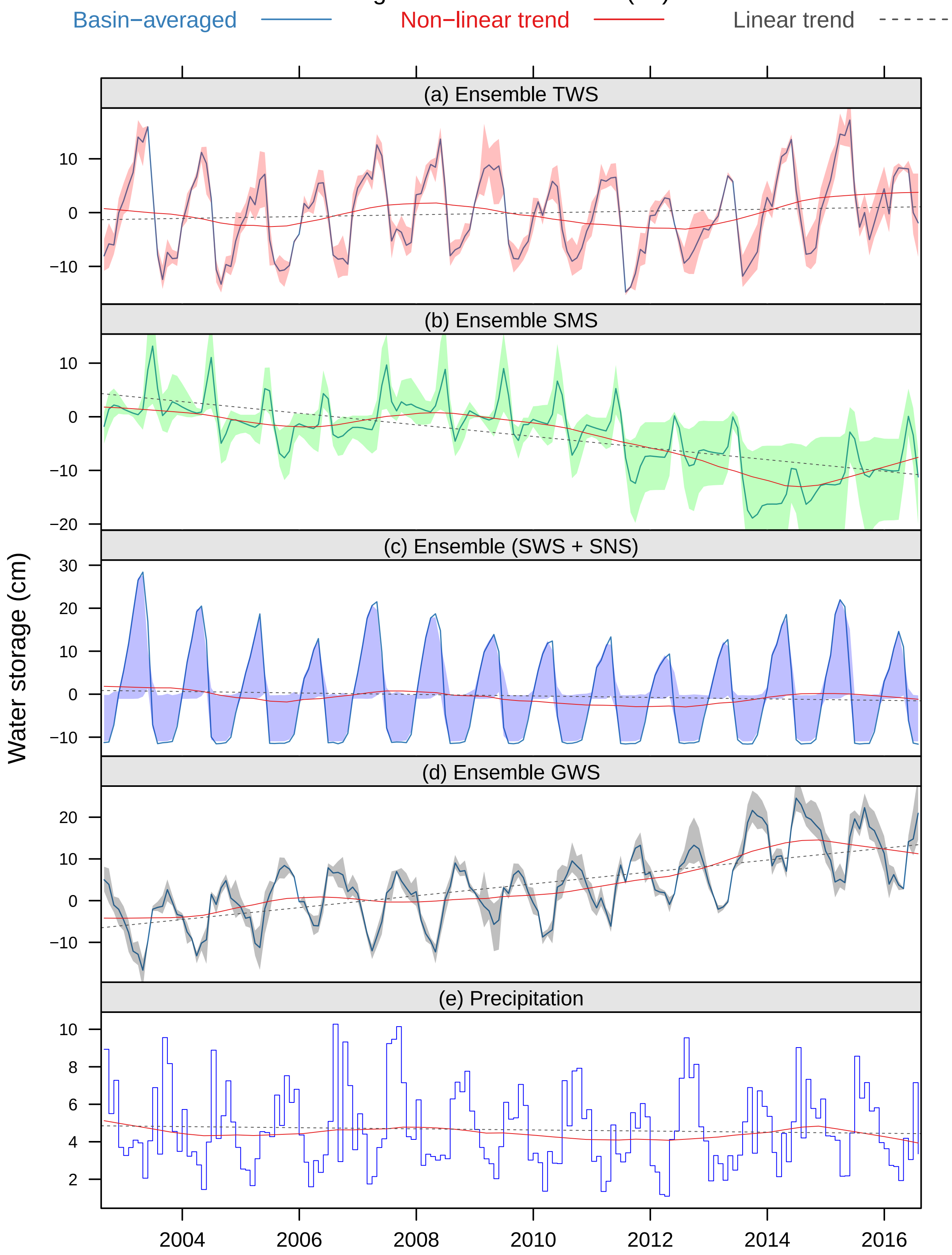

Fig. S35: Great Artesian Basin (36)

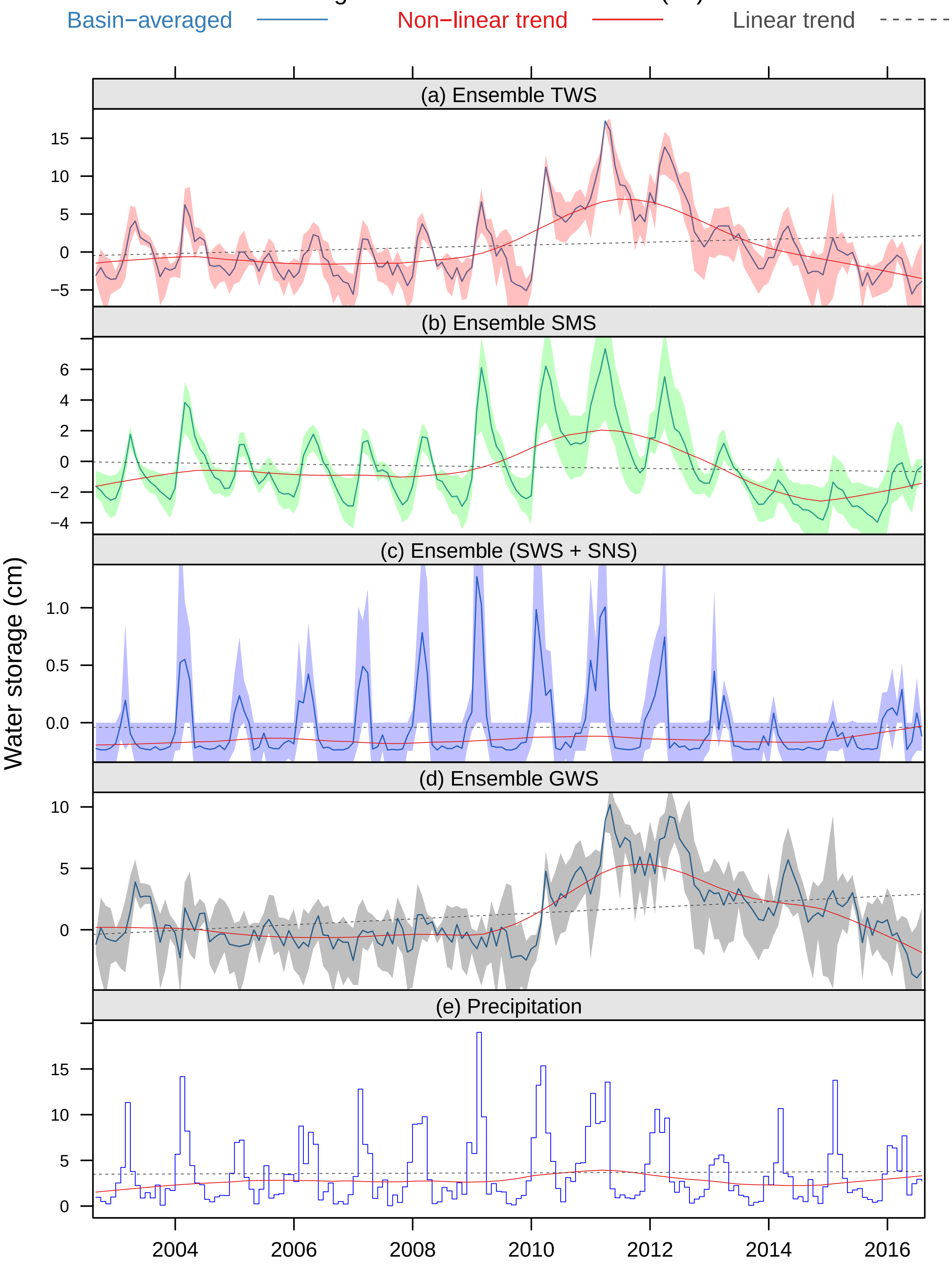

Fig. S36: Canning Basin (37)

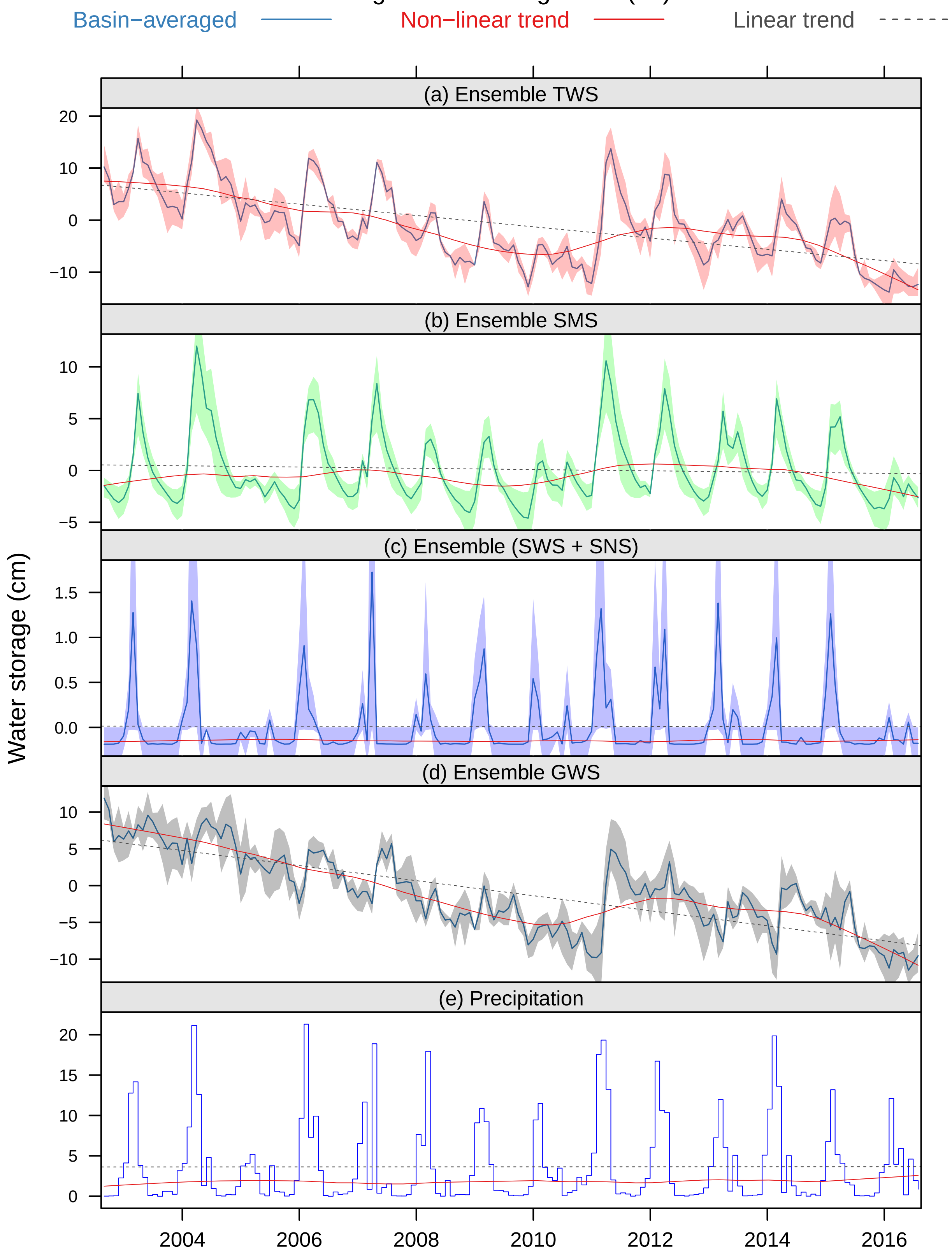

Fig. S37: STL decomposition of ensemble GRACE−TWS signal
High Plains Aquifer System (17)

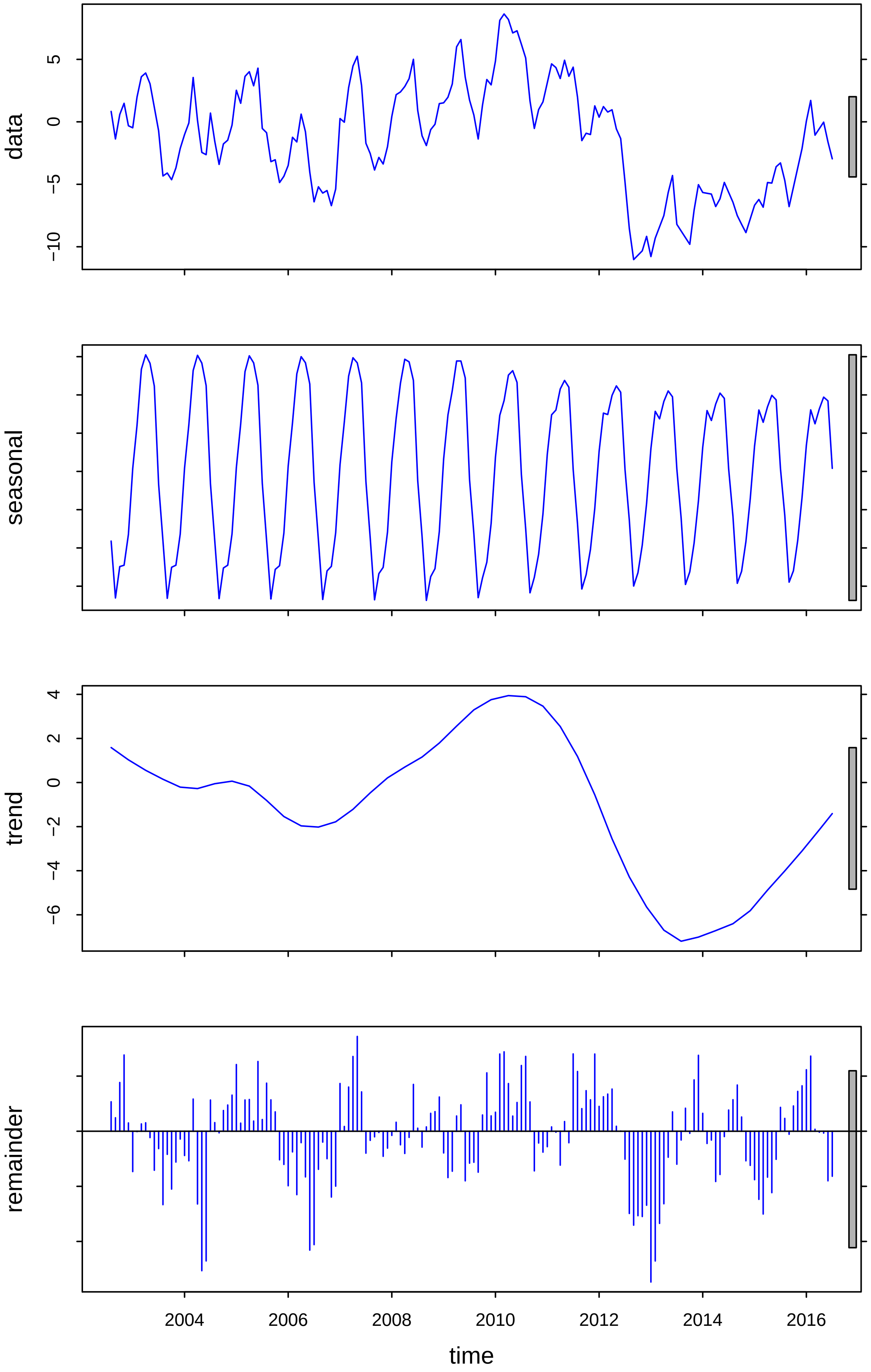

Fig. S38

(a)

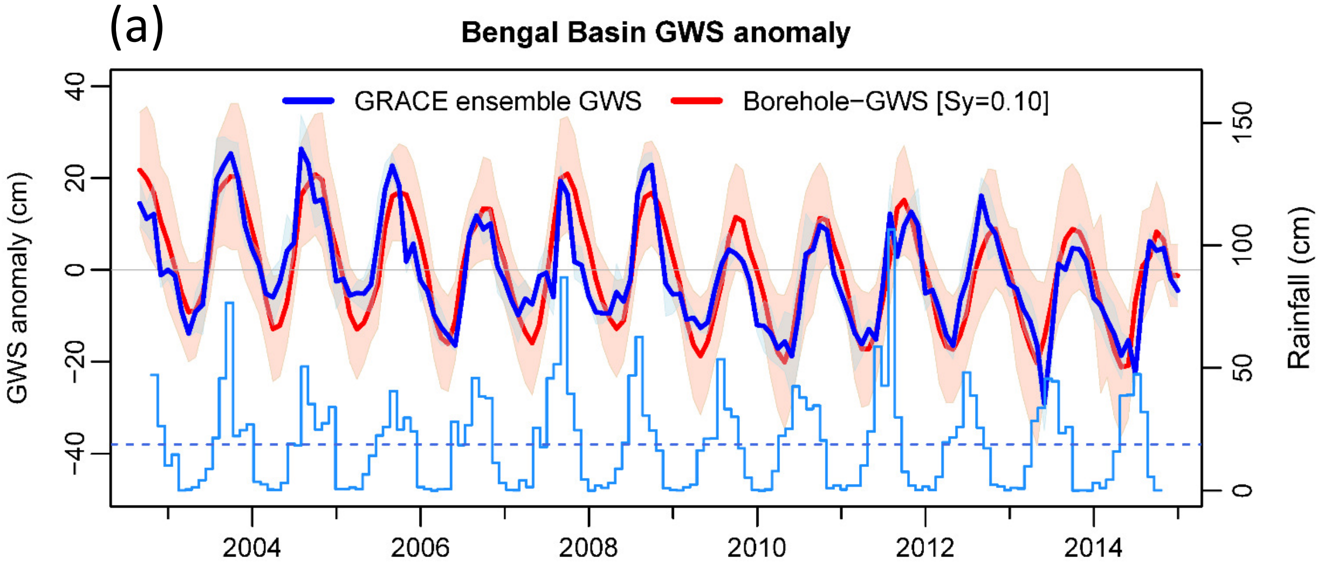

Bengal Basin GWS anomaly
GRACE ensemble GWS
Borehole−GWS [Sy=0.10]
GWS anomaly (cm)
Rainfall (cm)
40
20
0
−20
−40
150
100
50
0
2004
2006
2008
2010
2012
2014

(b)

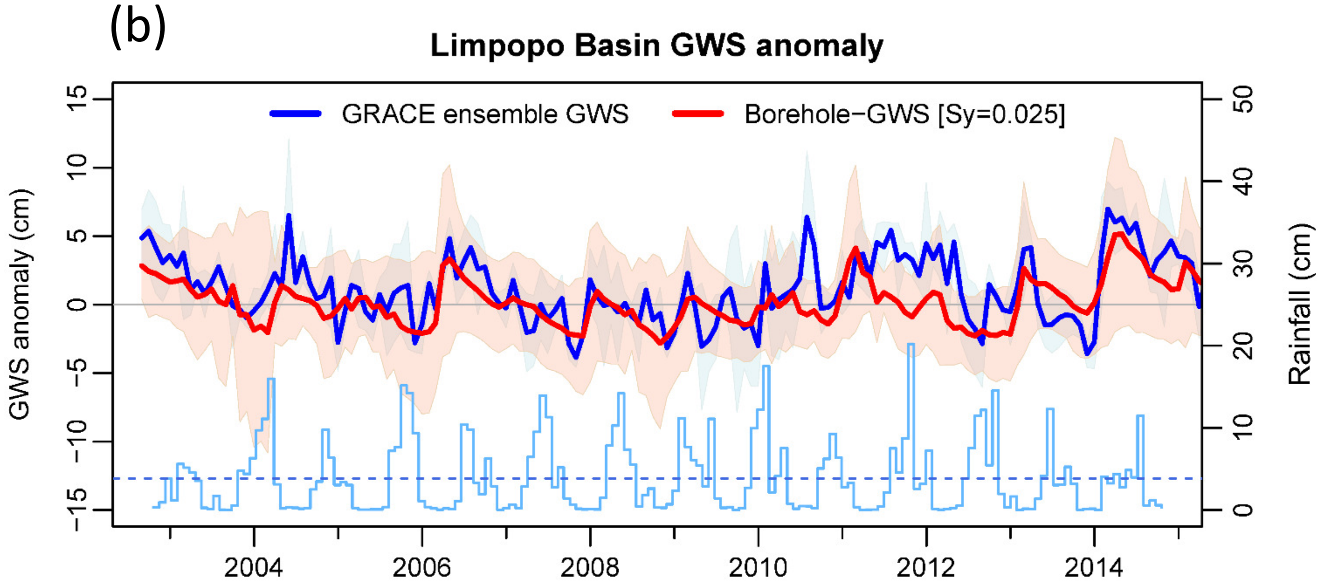

Limpopo Basin GWS anomaly
GRACE ensemble GWS
Borehole−GWS [Sy=0.025]
GWS anomaly (cm)
Rainfall (cm)
15
10
5
0
−5
−10
−15
50
40
30
20
10
0
2004
2006
2008
2010
2012
2014

Fig. S39: Bengal Basin

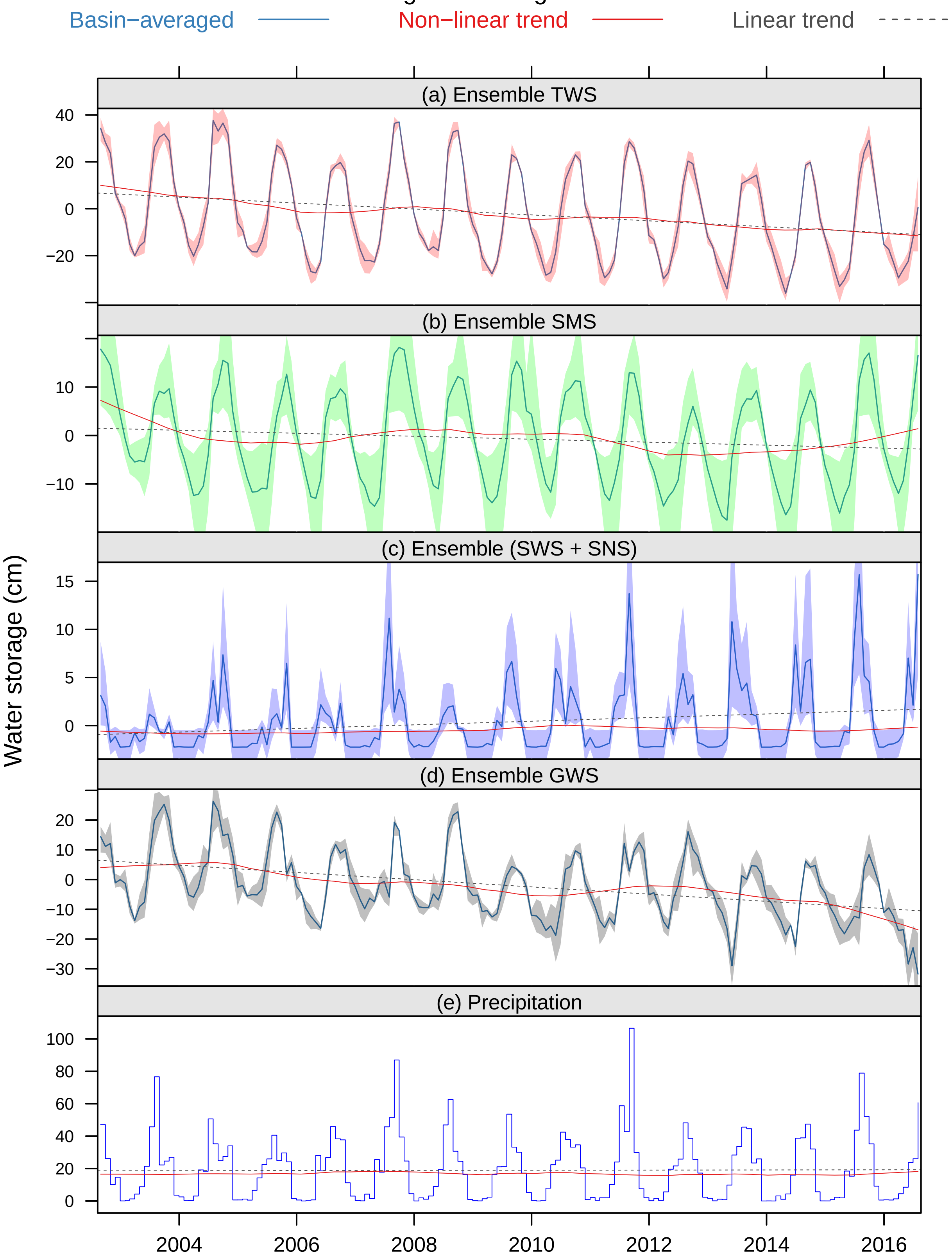

Fig. S40: Limpopo Basin

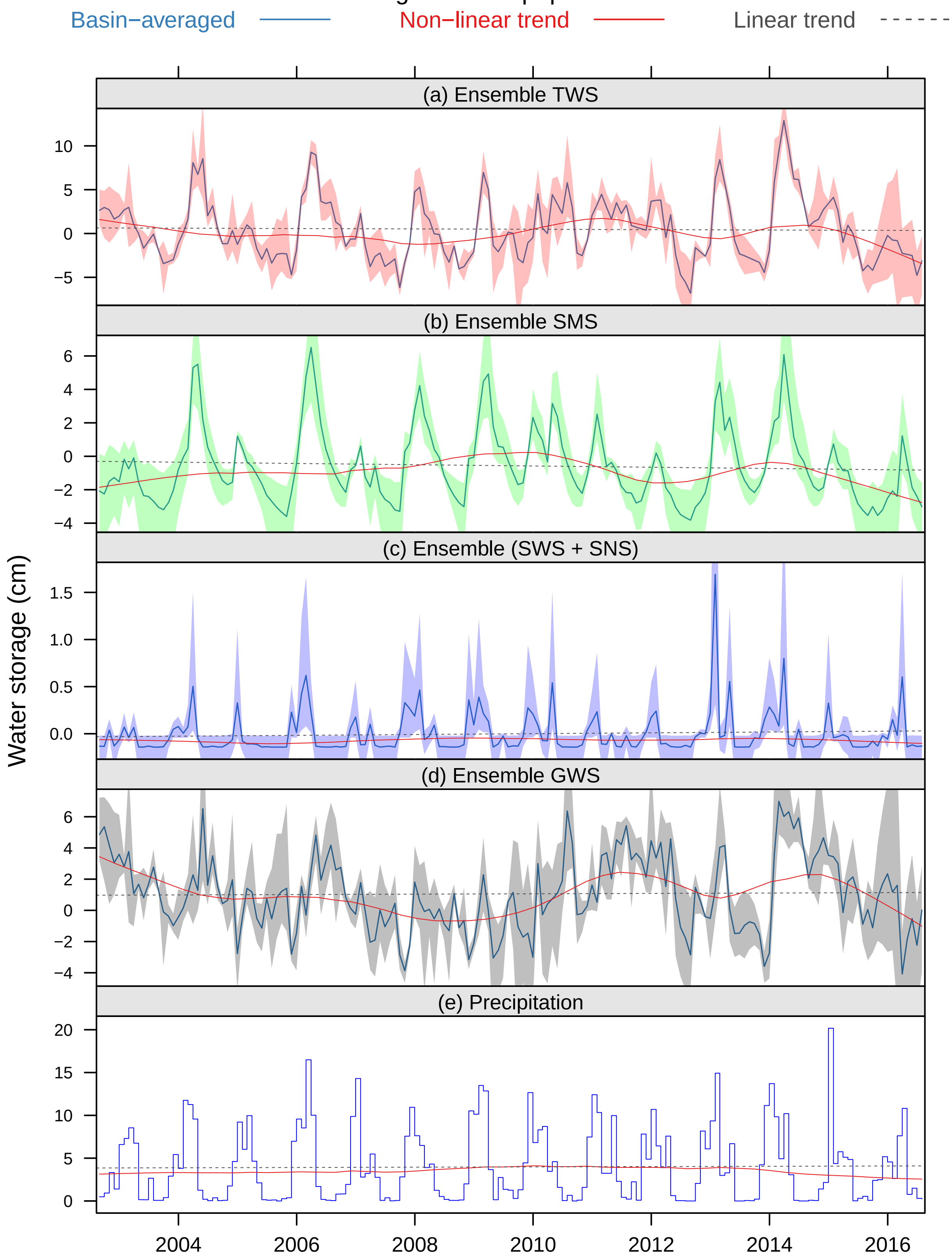

Fig. S41: Nubian Sandstone Aquifer System (1)

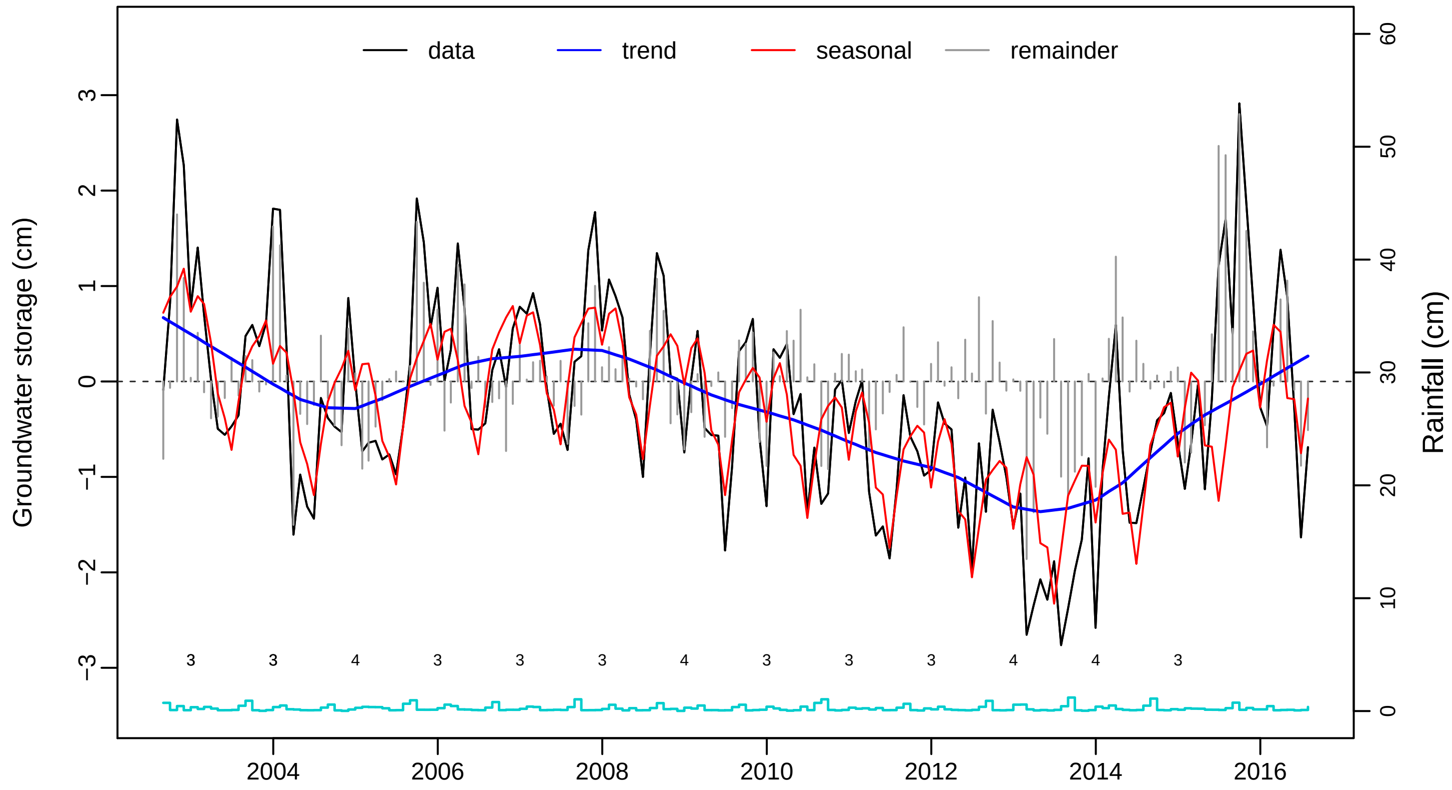

Seasonal−Trend−Remainder (GRACE GWS)
Proportion of variance

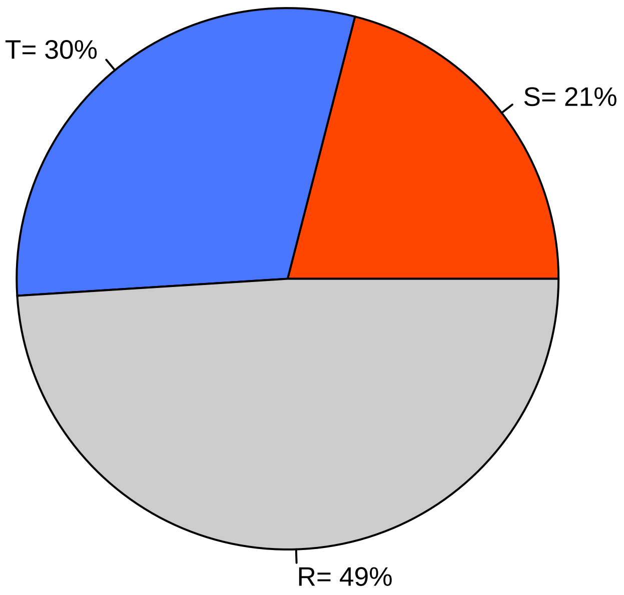

Fig. S42: Northwestern Sahara Aquifer System (2)

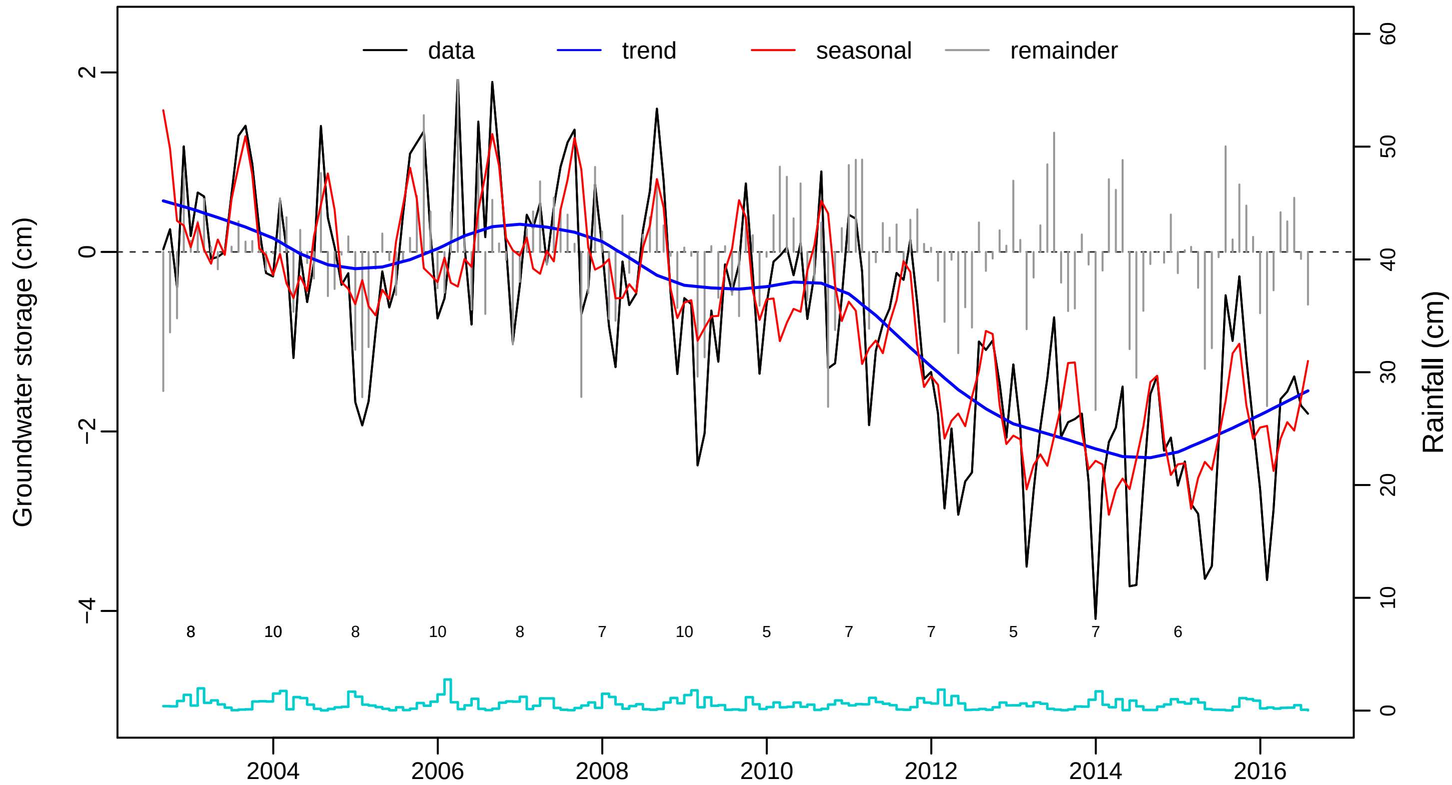

Seasonal−Trend−Remainder (GRACE GWS)
Proportion of variance

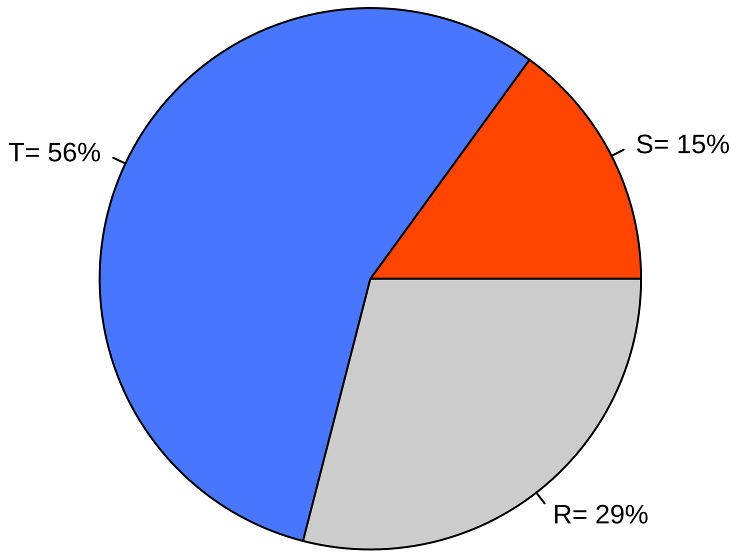

Fig. S43: Murzuk−Djado Basin (3)

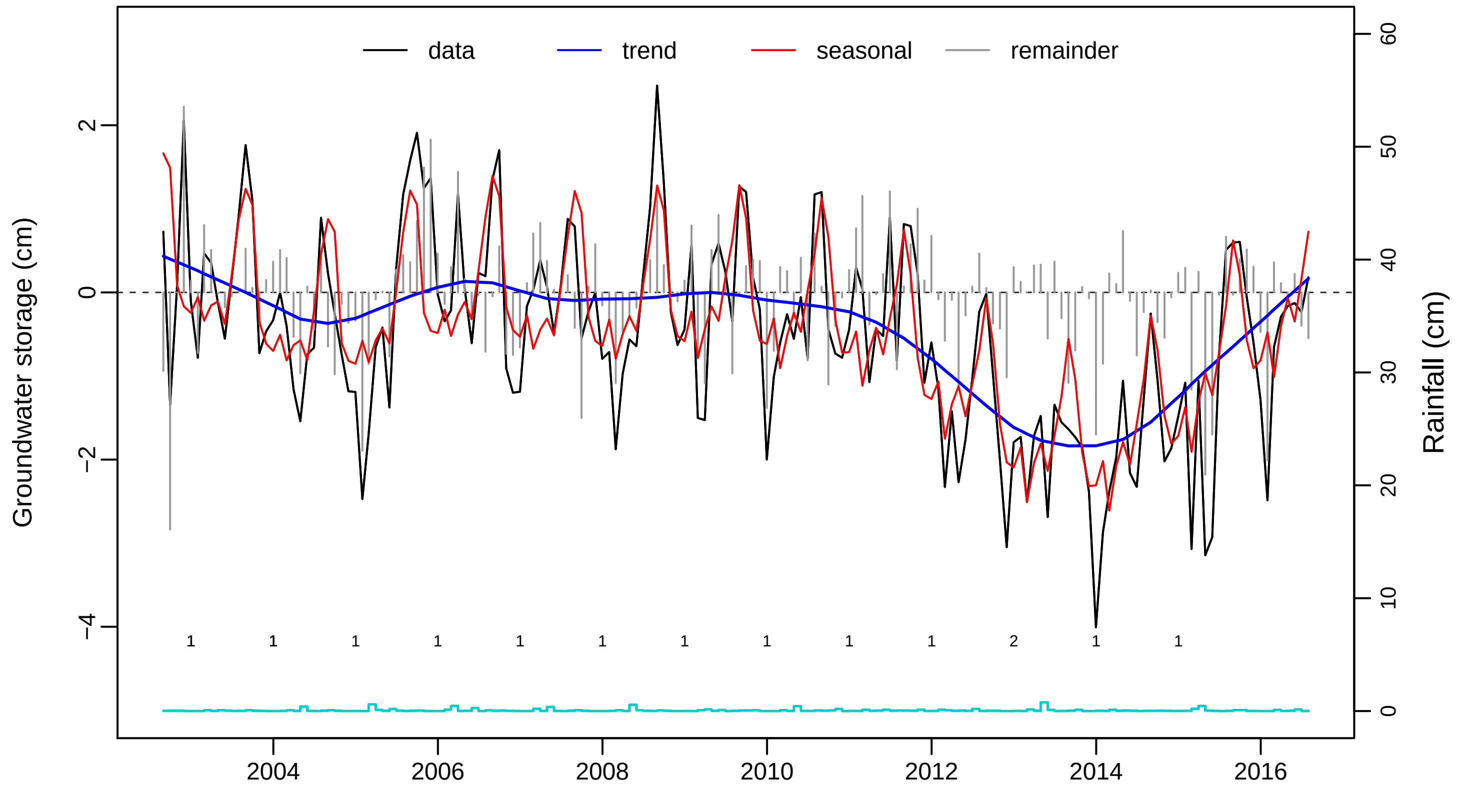

Seasonal−Trend−Remainder (GRACE GWS)
Proportion of variance

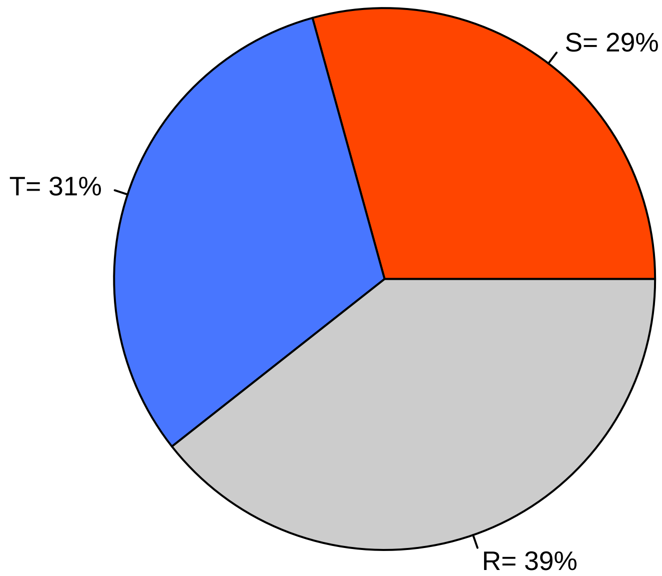

Fig. S44: Taoudeni−Tanezrouft Basin (4)

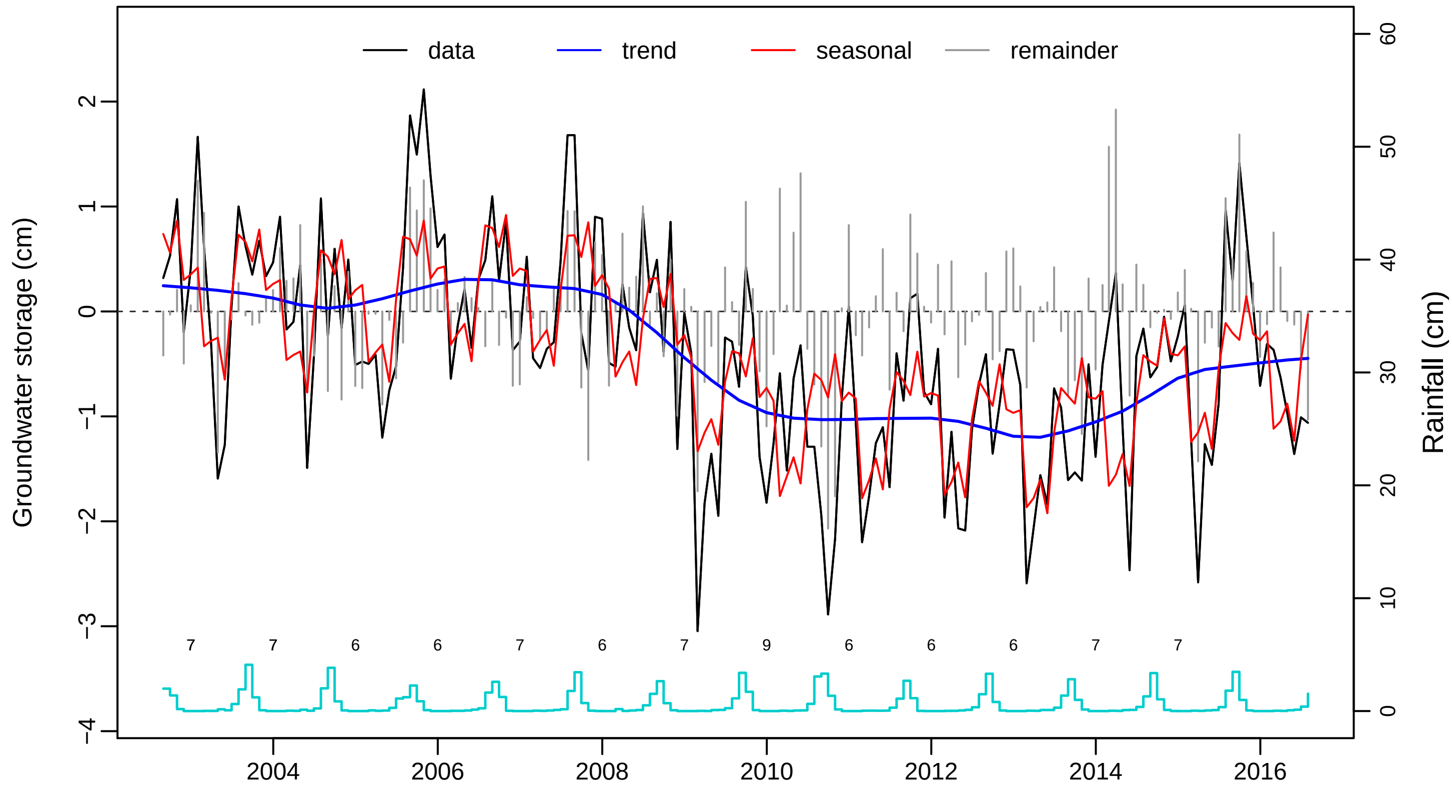

Seasonal−Trend−Remainder (GRACE GWS)
Proportion of variance

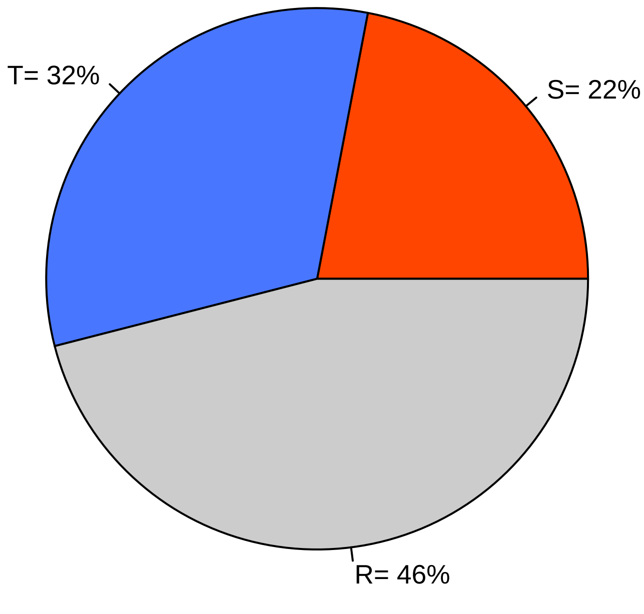

Fig. S45: Senegal−Mauritanian Basin (5)

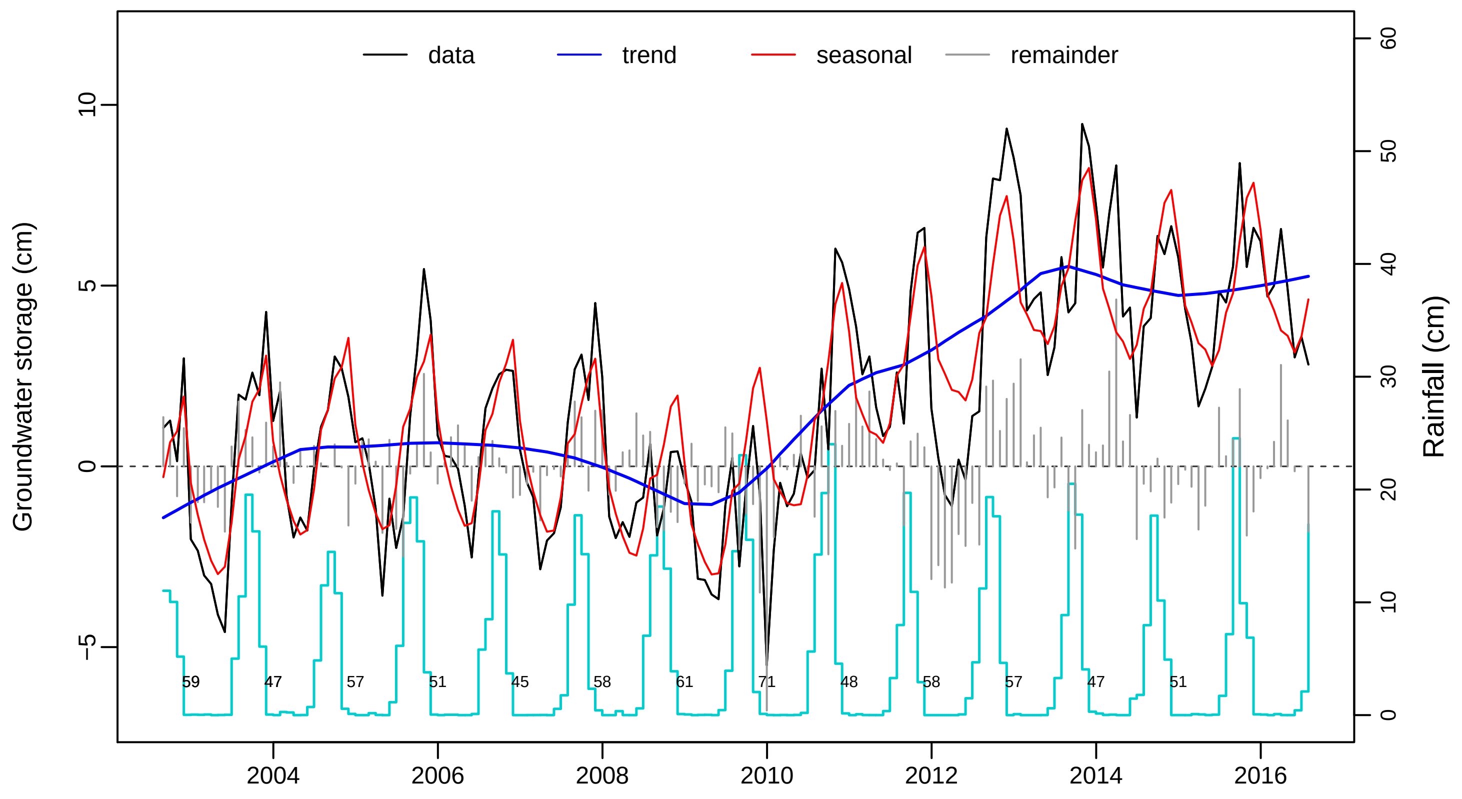

Seasonal−Trend−Remainder (GRACE GWS)
Proportion of variance

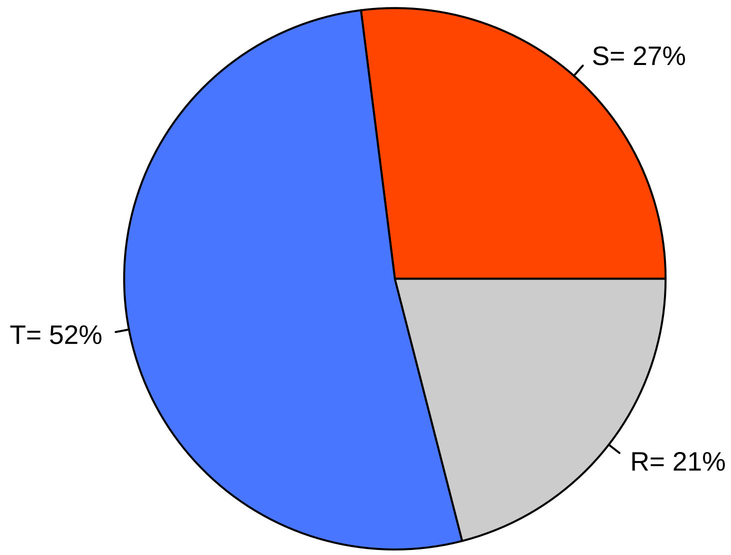

Fig. S46: Iullemmeden–Irhazer Aquifer System (6)

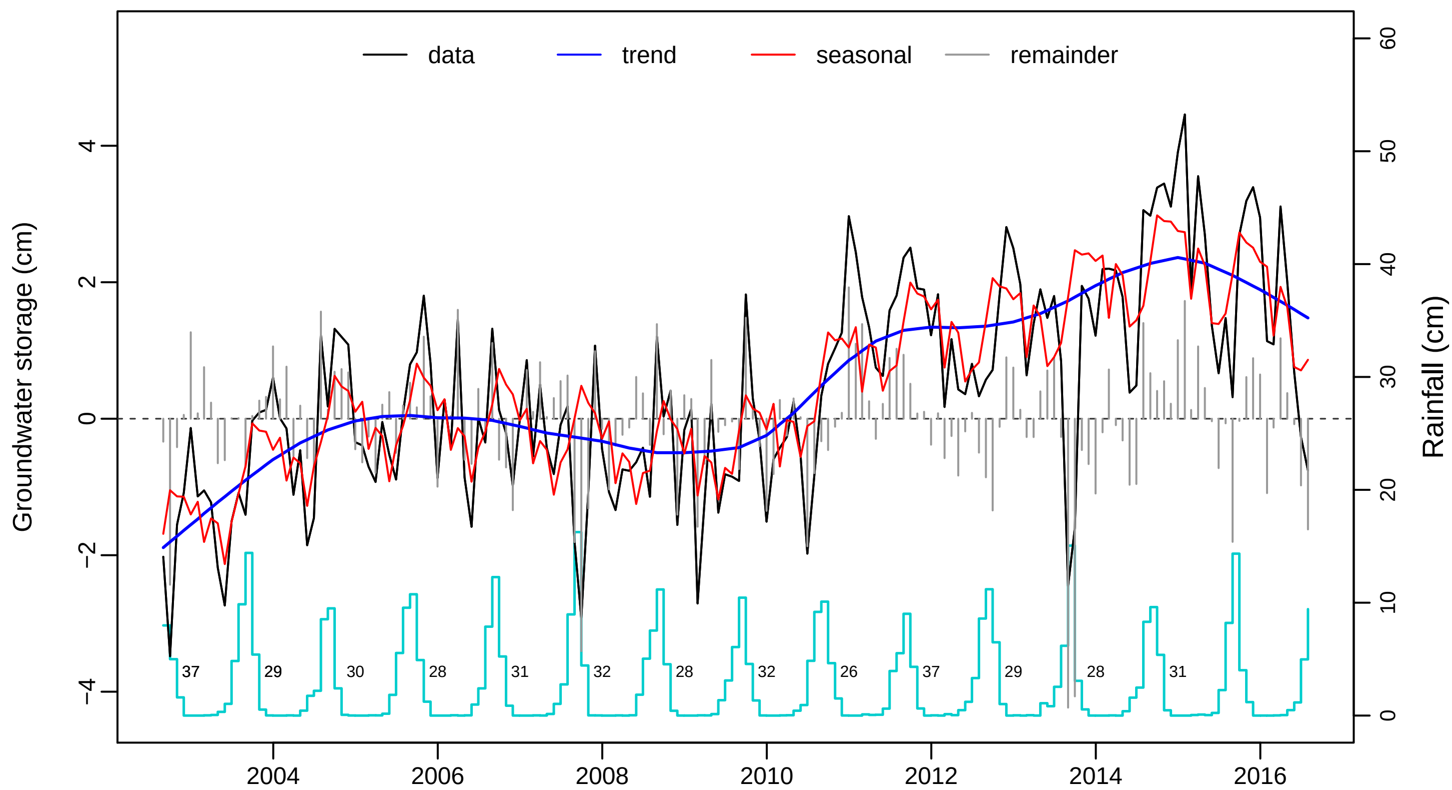

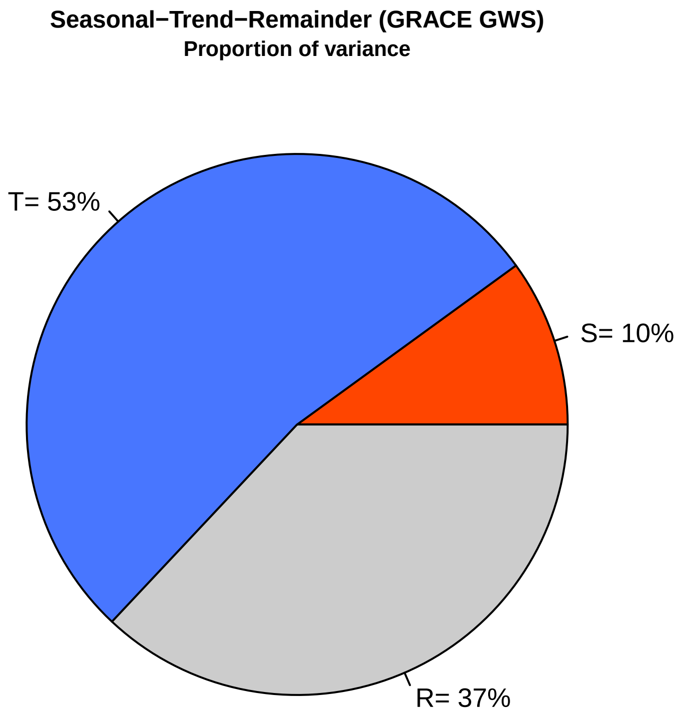

Fig. S47: Lake Chad Basin (7)

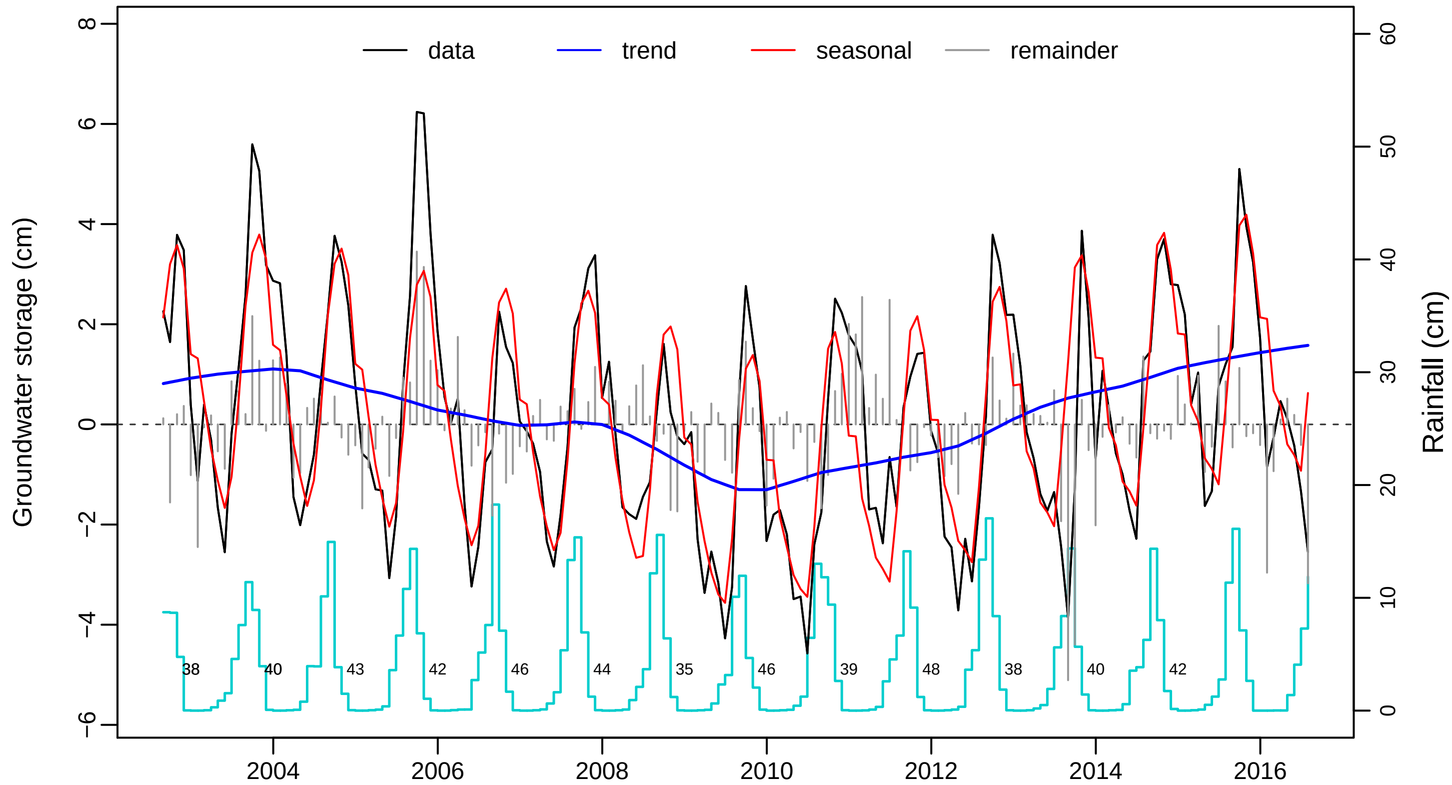

Seasonal−Trend−Remainder (GRACE GWS)
Proportion of variance

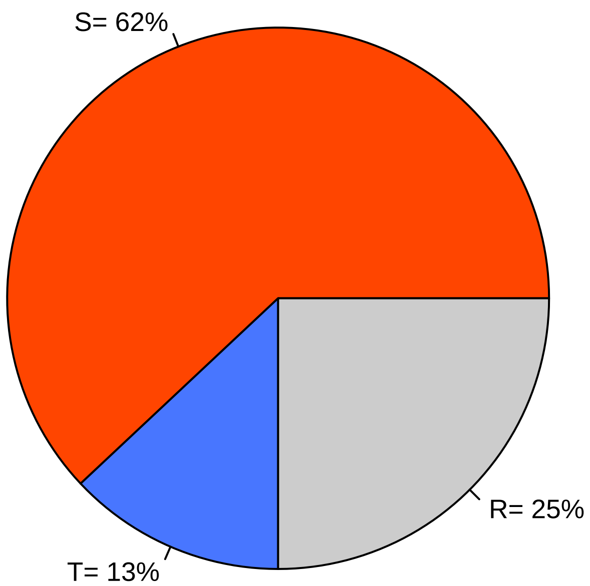

Fig. S48: Umm Ruwaba Aquifer (Sudd Basin) (8)

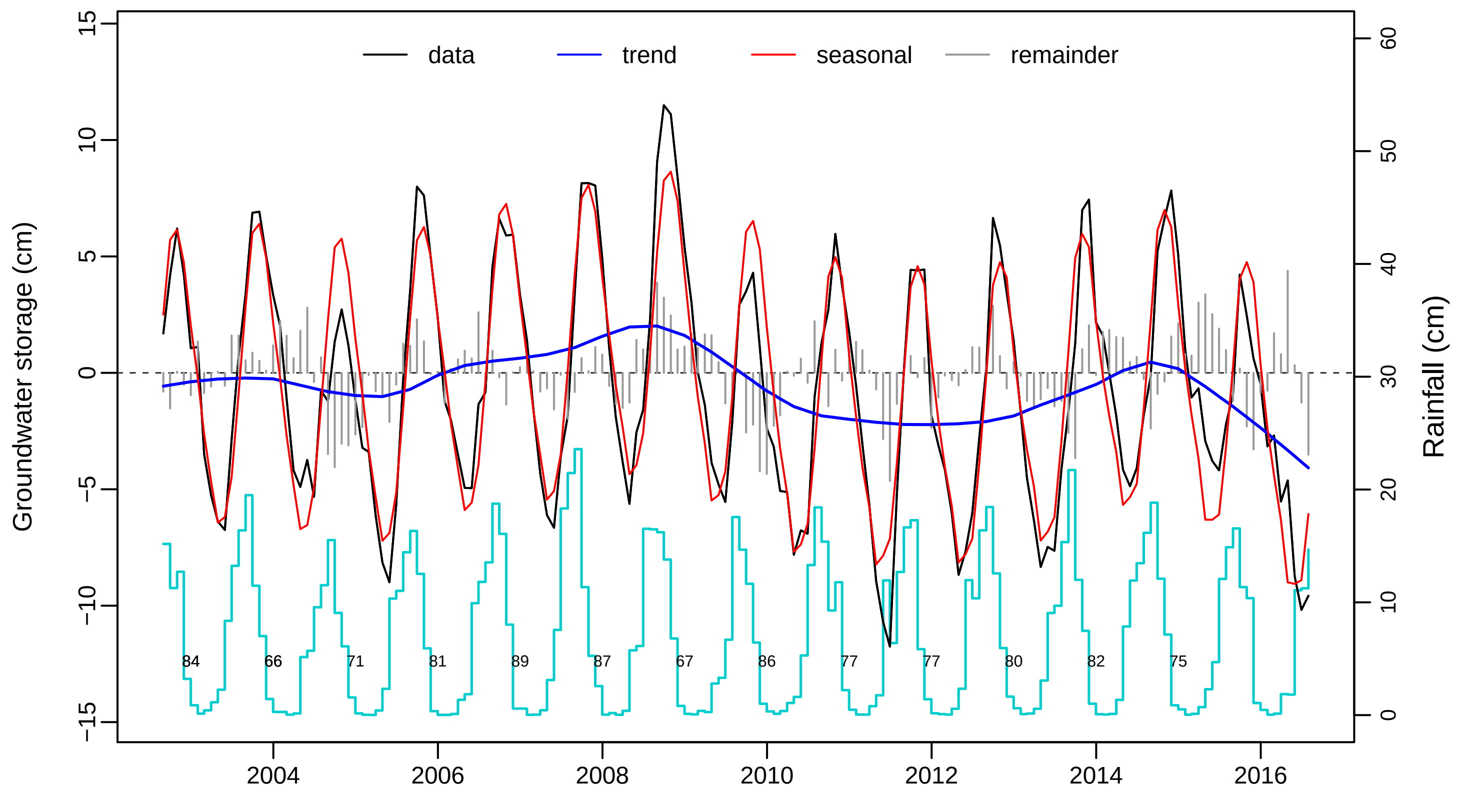

Seasonal−Trend−Remainder (GRACE GWS)
Proportion of variance

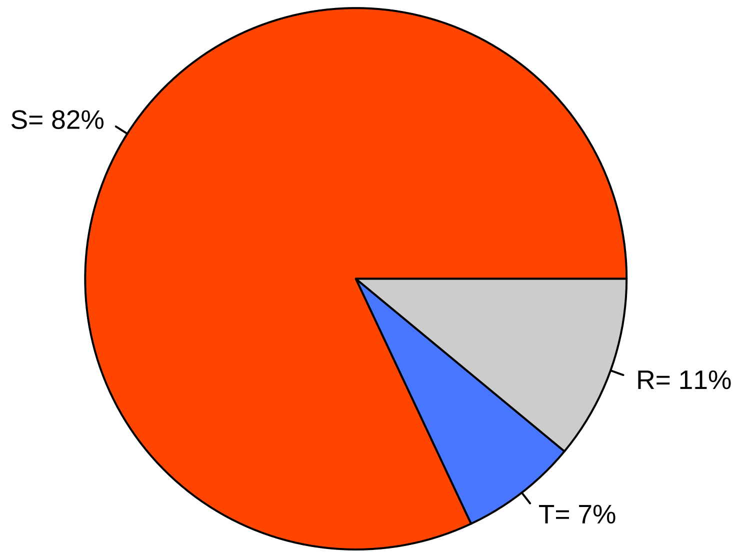

Fig. S49: Ogaden−Juba Basin (9)

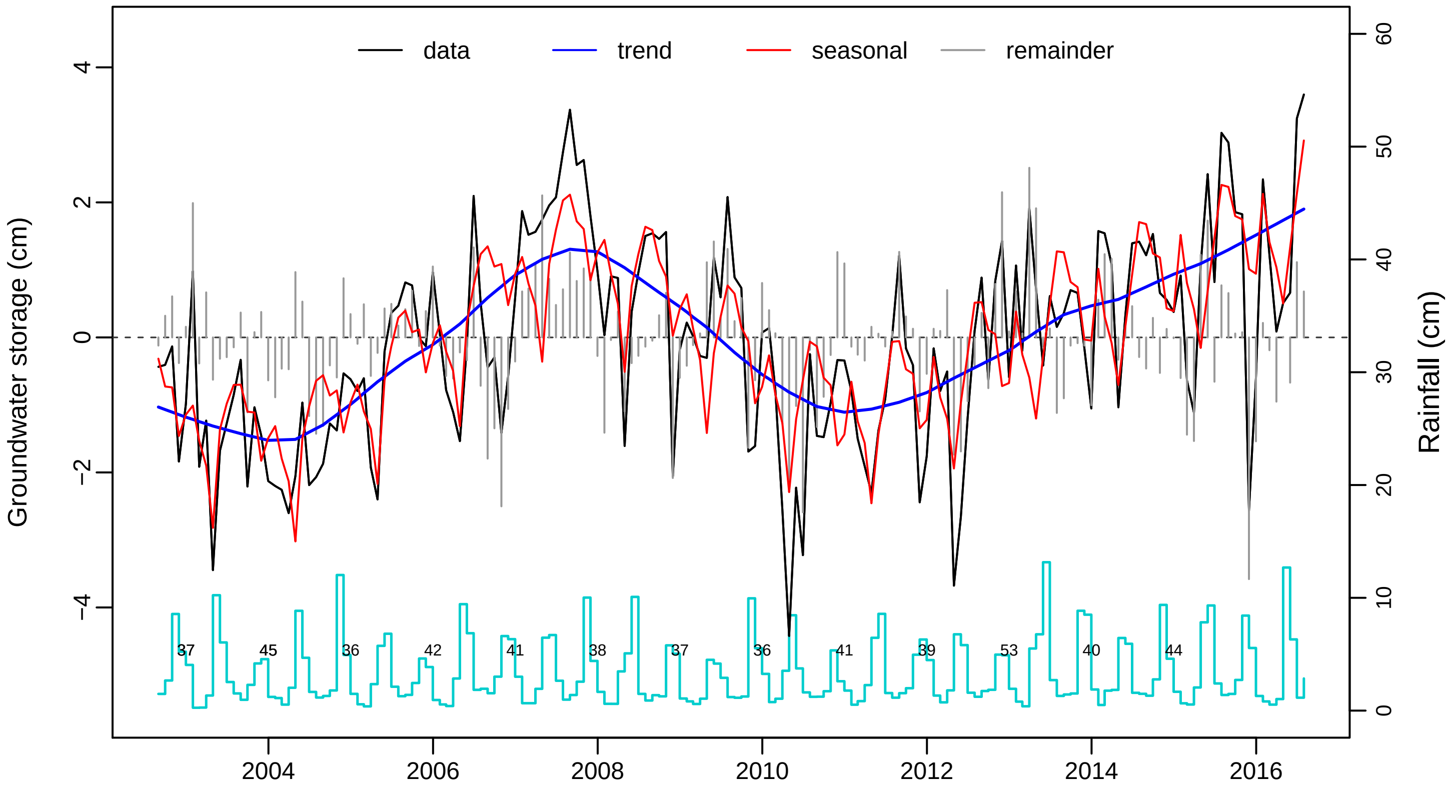

Seasonal−Trend−Remainder (GRACE GWS)
Proportion of variance

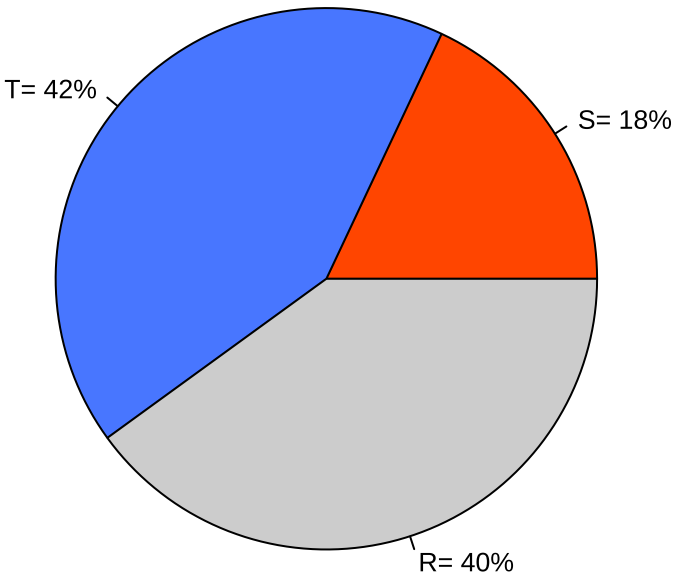

Fig. S50: Congo Basin (10)

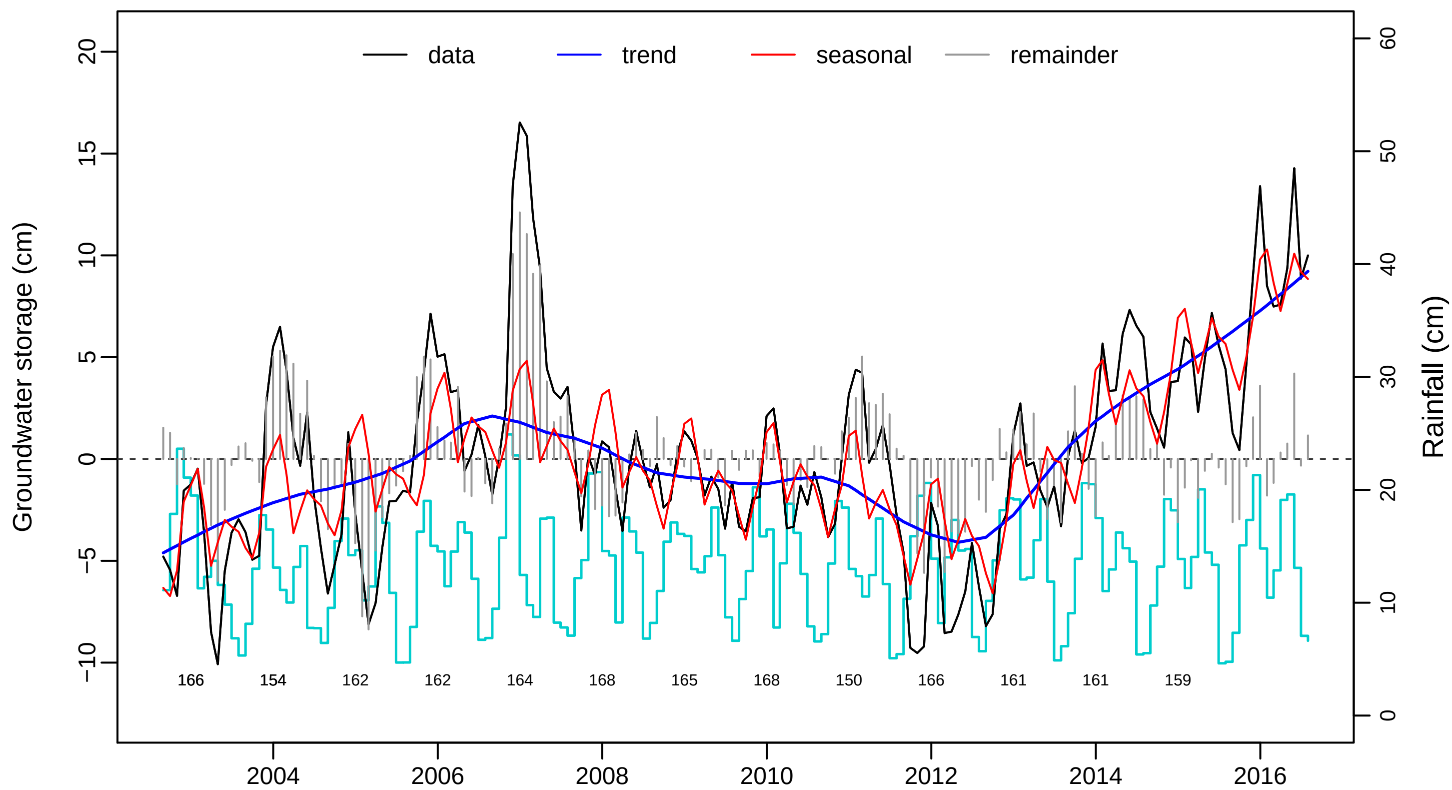

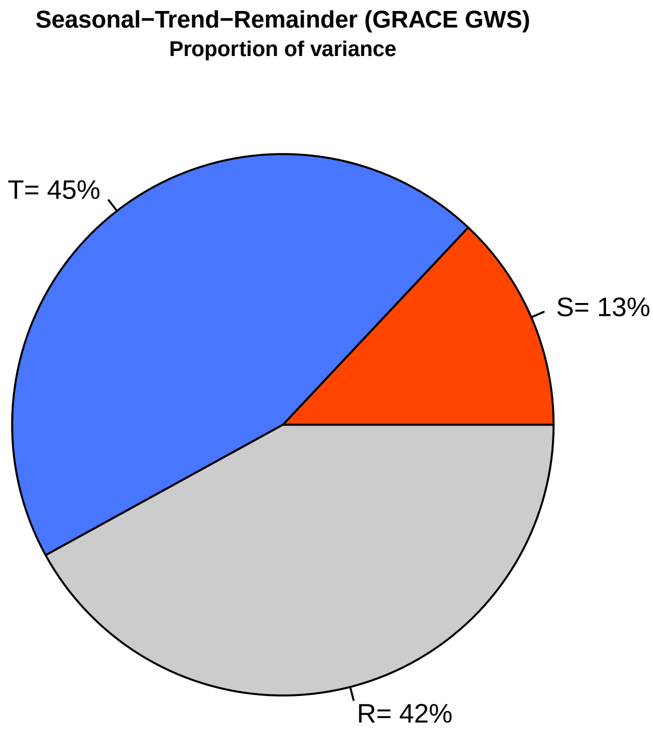

Fig. S51: Upper Kalahari−Cuvelai−Zambezi Basin (11)

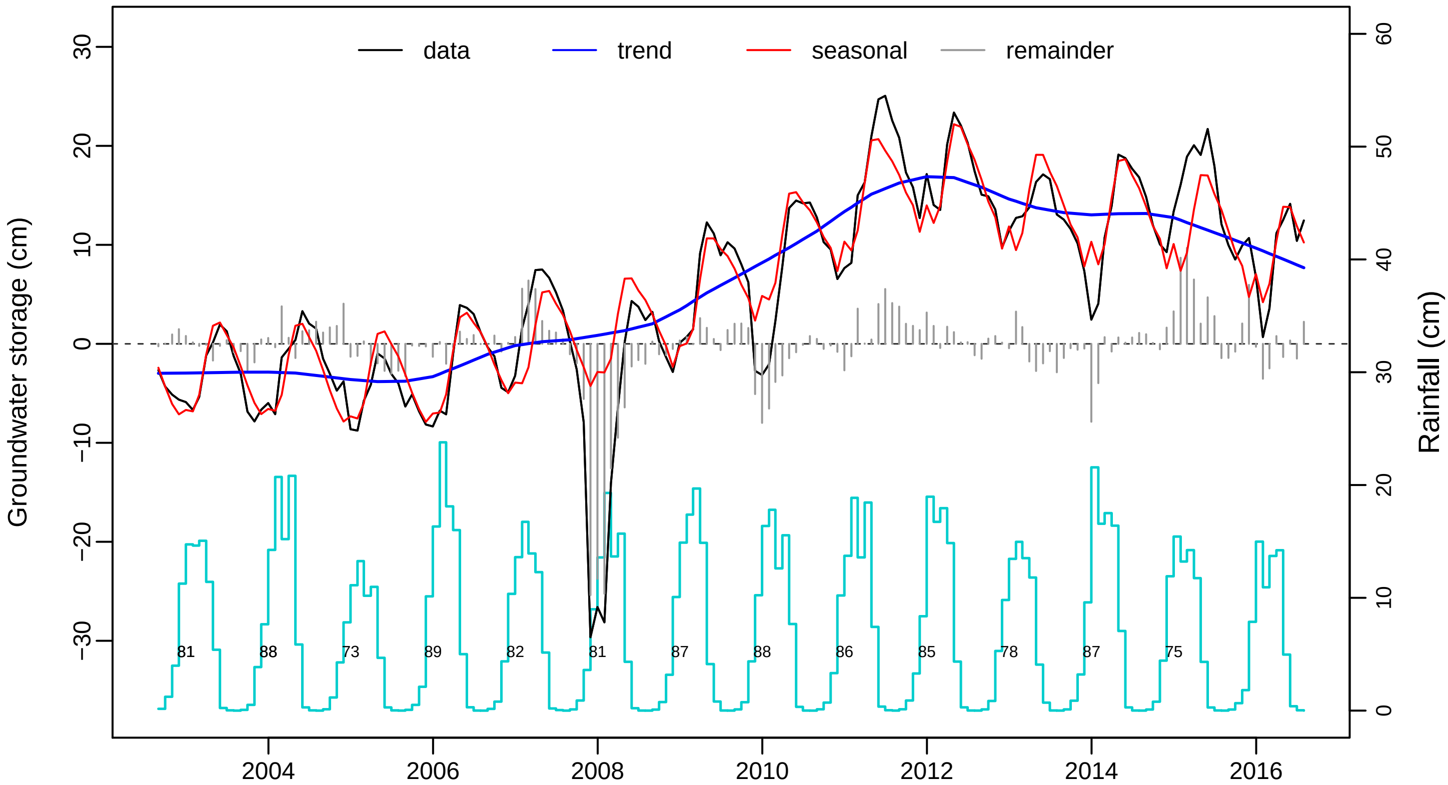

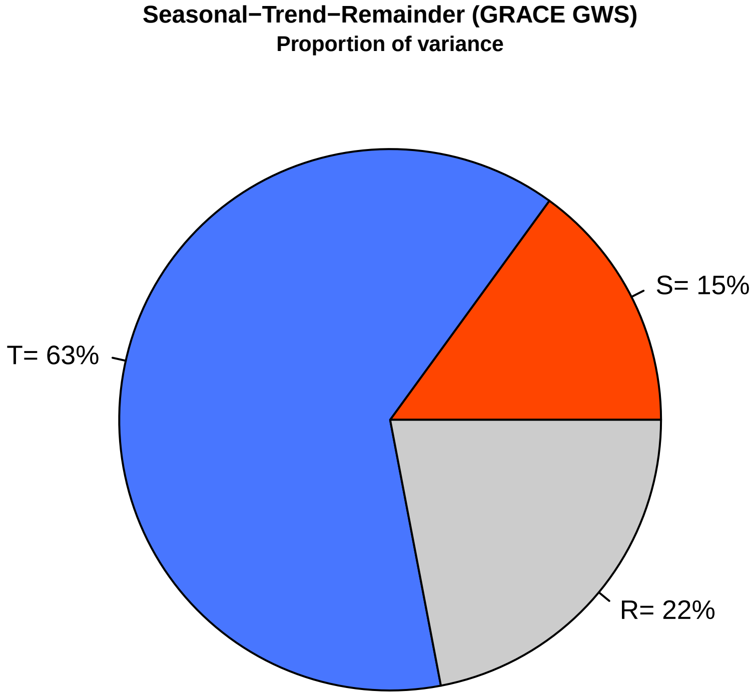

Fig. S52: Lower Kalahari−Stampriet Basin (12)

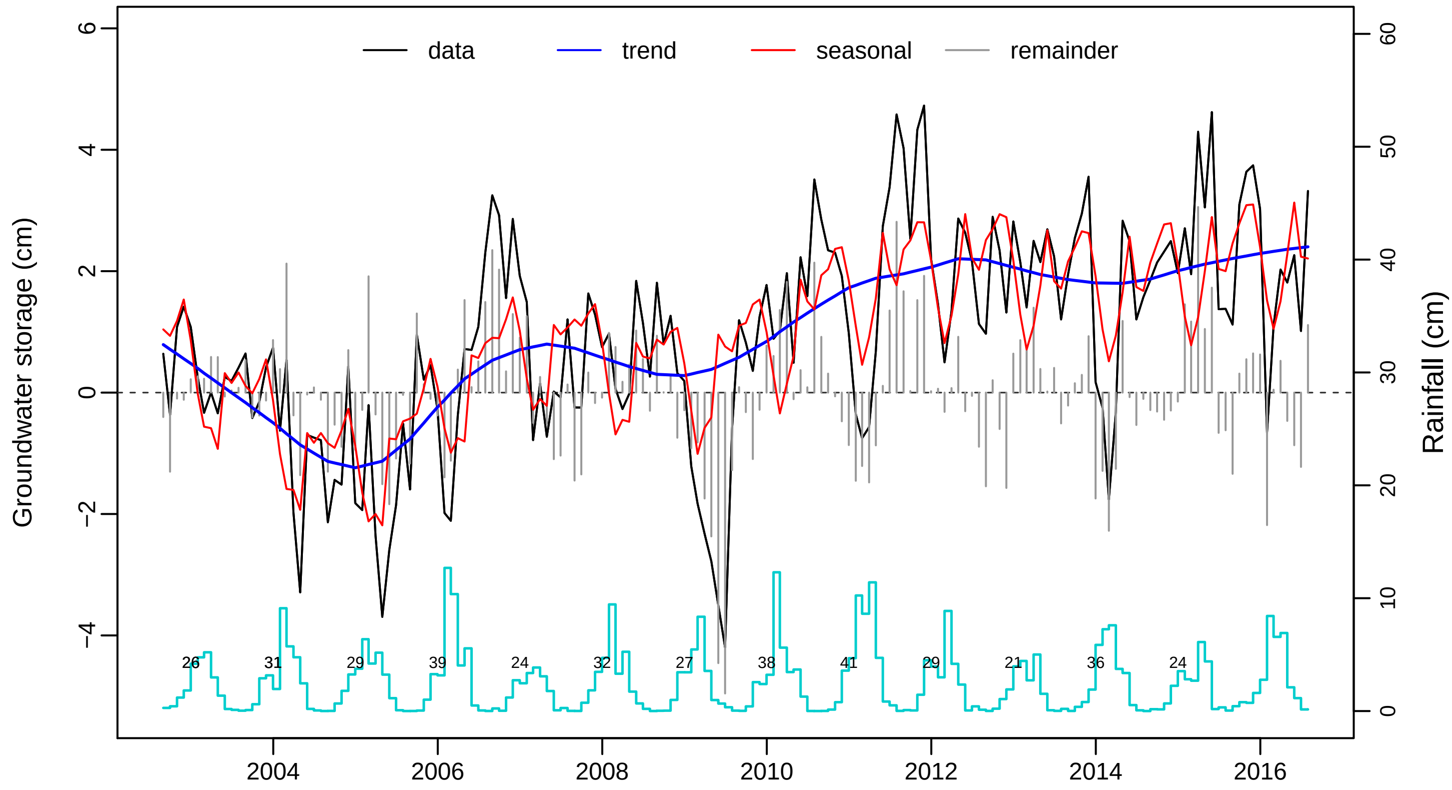

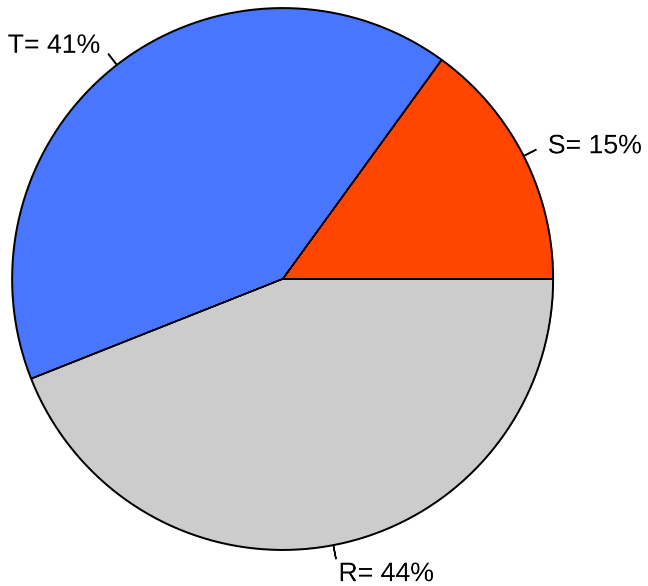

Fig. S53: Karoo Basin (13)

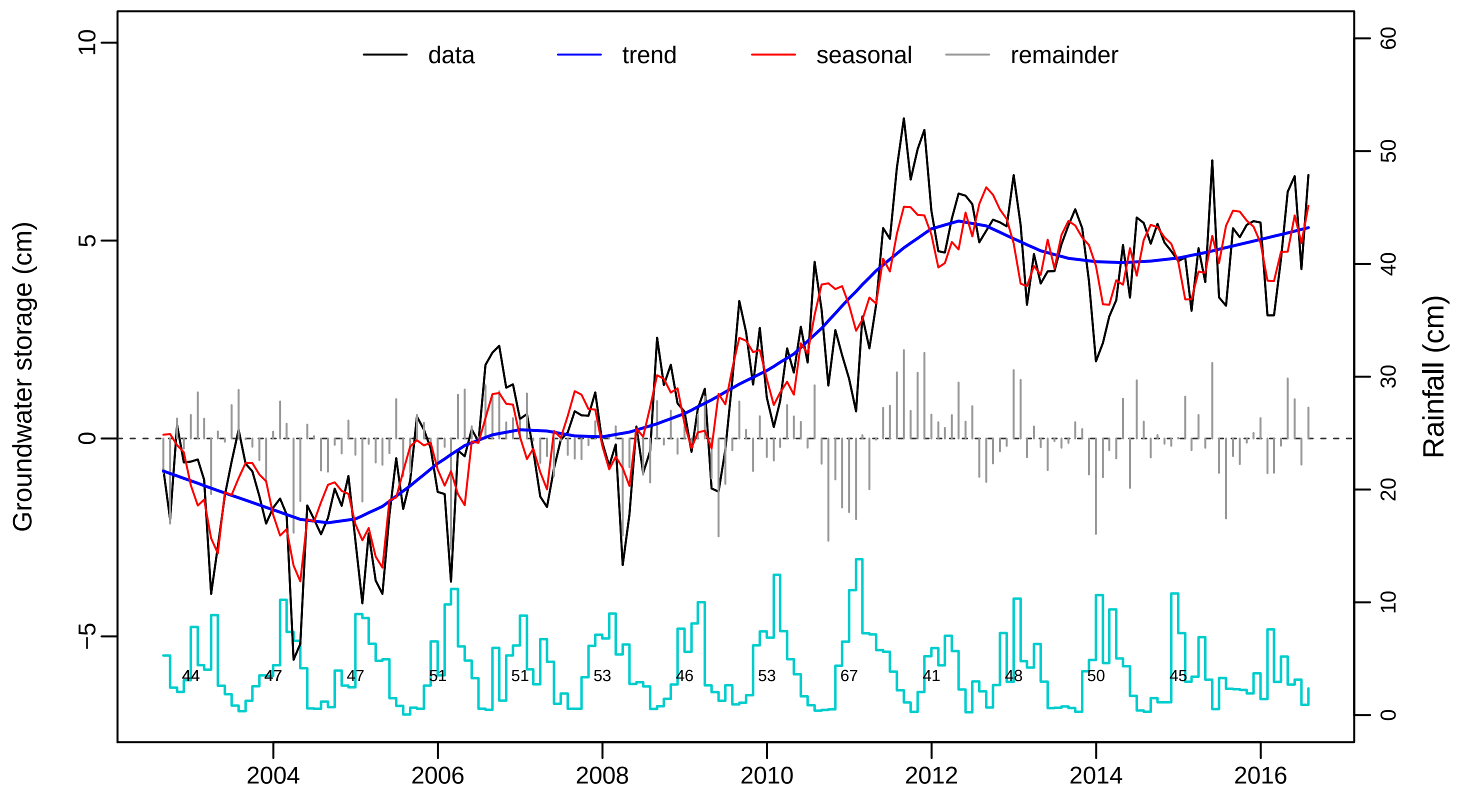

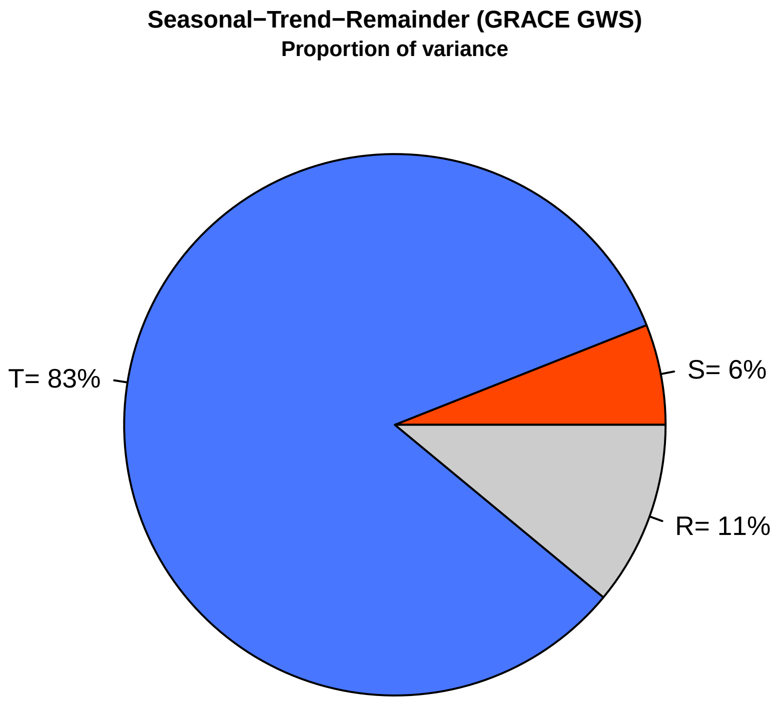

Fig. S54: Northern Great Plains Aquifer (14)

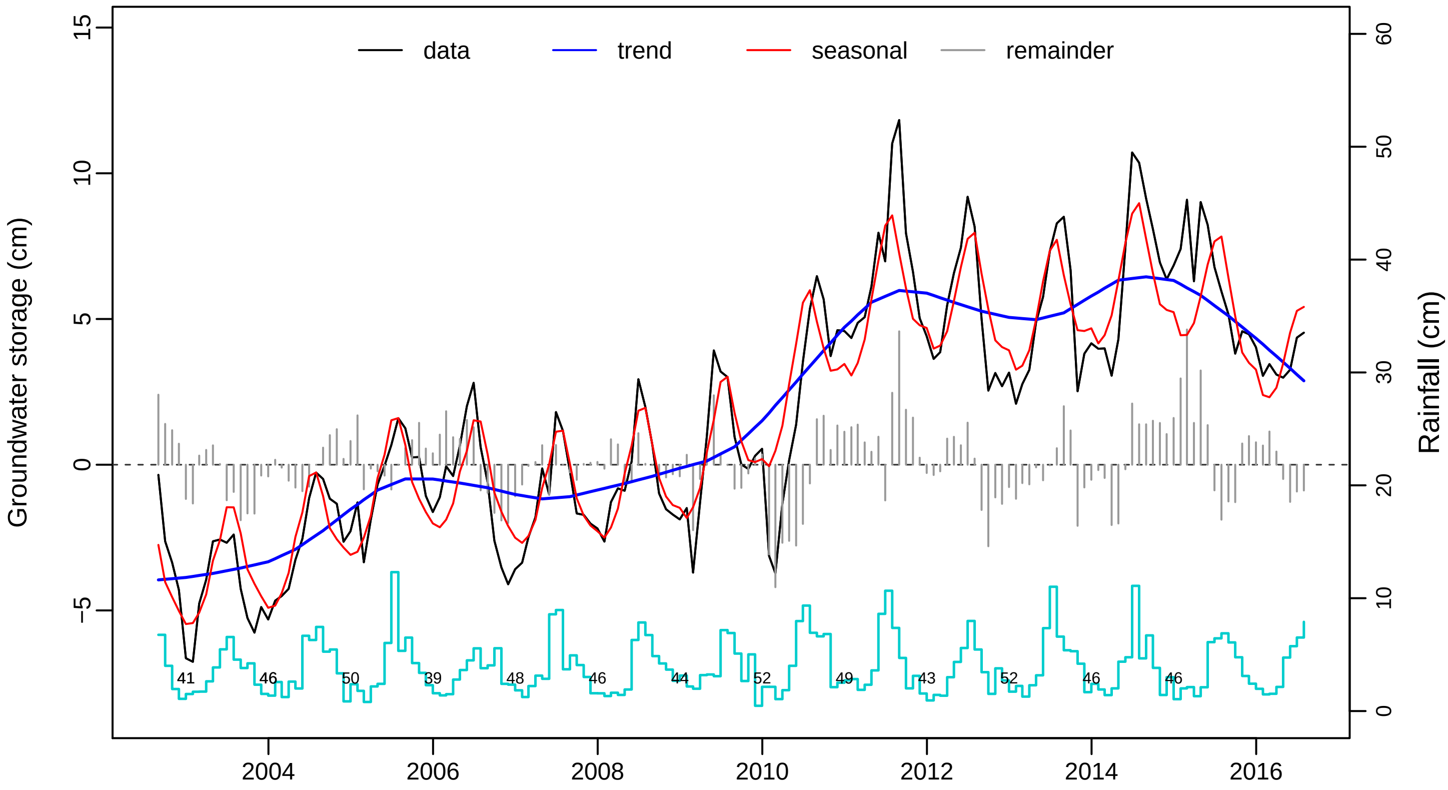

Seasonal−Trend−Remainder (GRACE GWS)
Proportion of variance

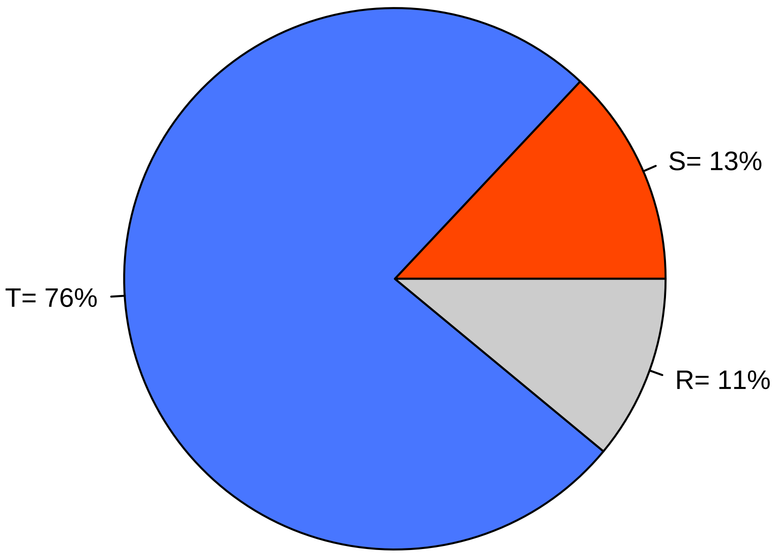

Fig. S55: Cambro−Ordovician Aquifer System (15)

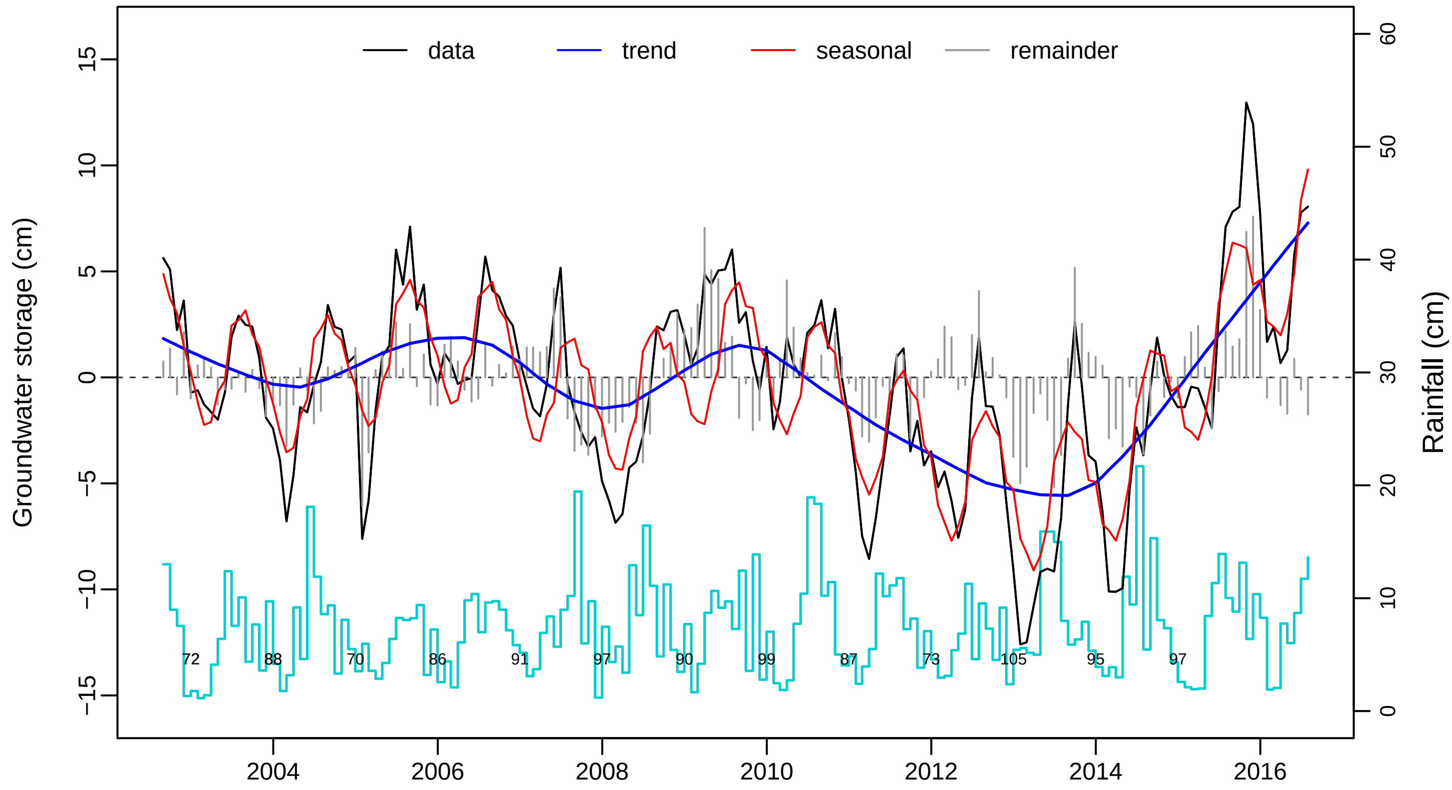

Seasonal−Trend−Remainder (GRACE GWS)
Proportion of variance

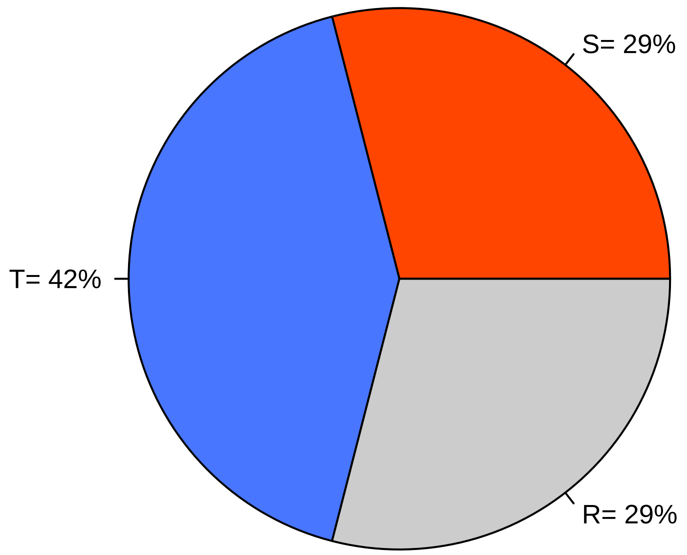

Fig. S56: California Central Valley Aquifer System (16)

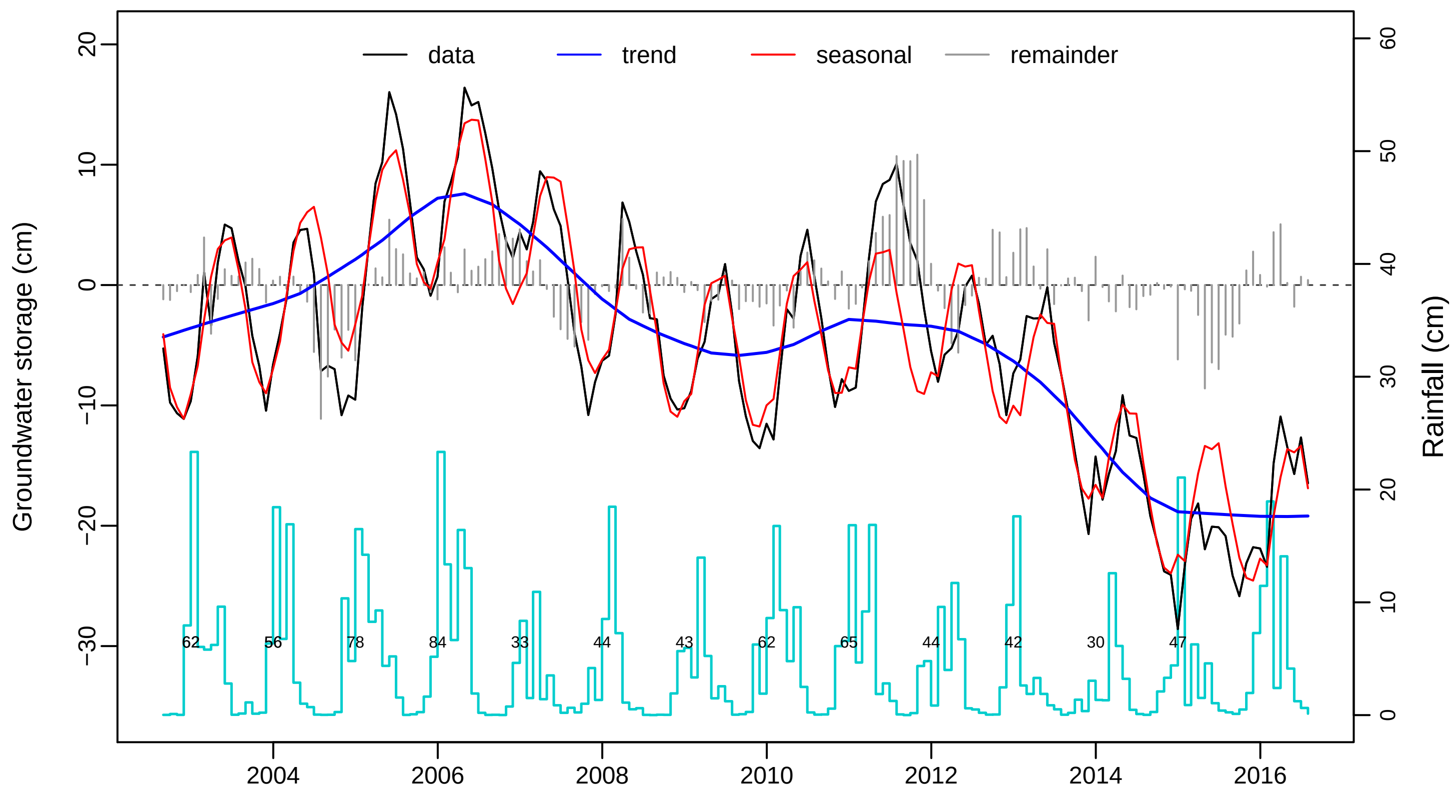

Seasonal−Trend−Remainder (GRACE GWS)
Proportion of variance

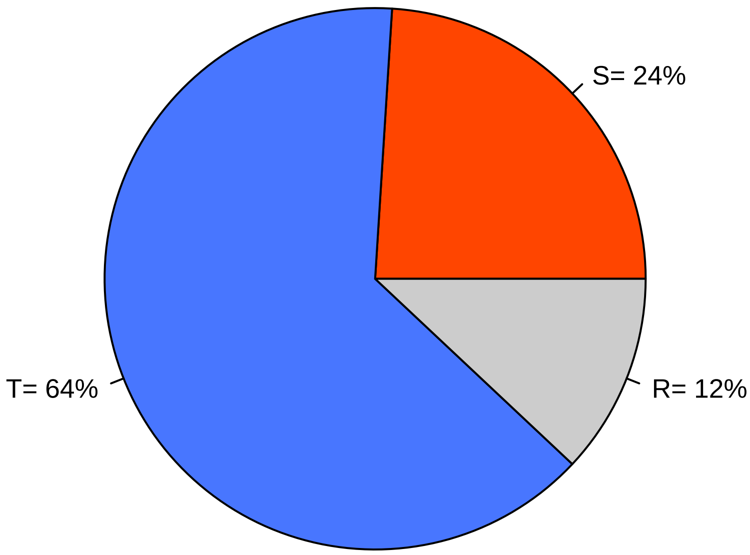

Fig. S57: Ogallala Aquifer (High Plains) (17)

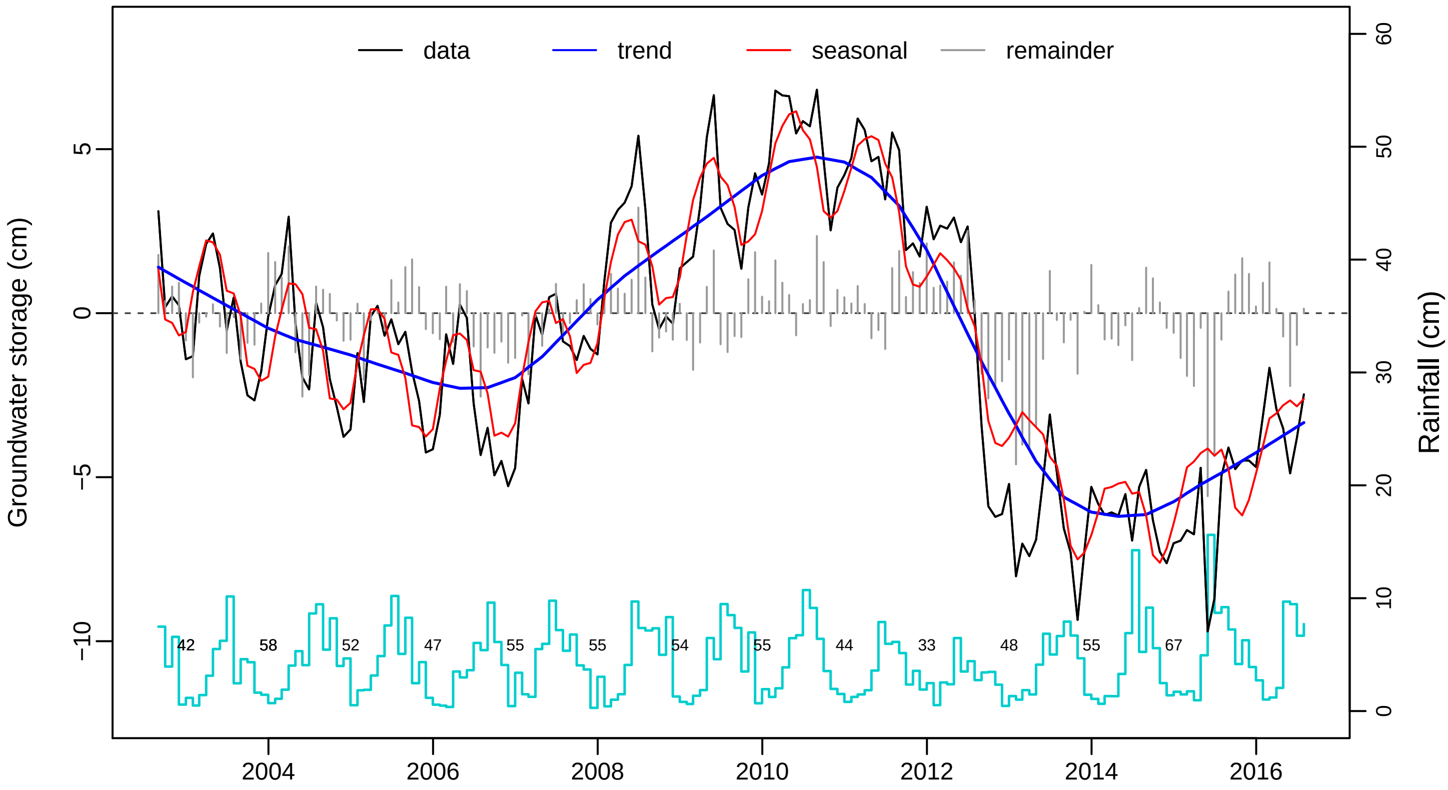

Seasonal−Trend−Remainder (GRACE GWS)
Proportion of variance

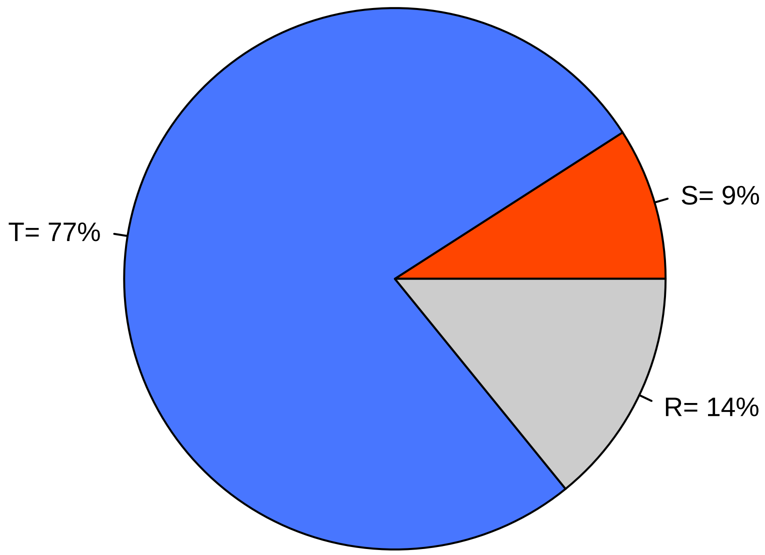

Fig. S58: Atlantic and Gulf Coastal Plains Aquifer (18)

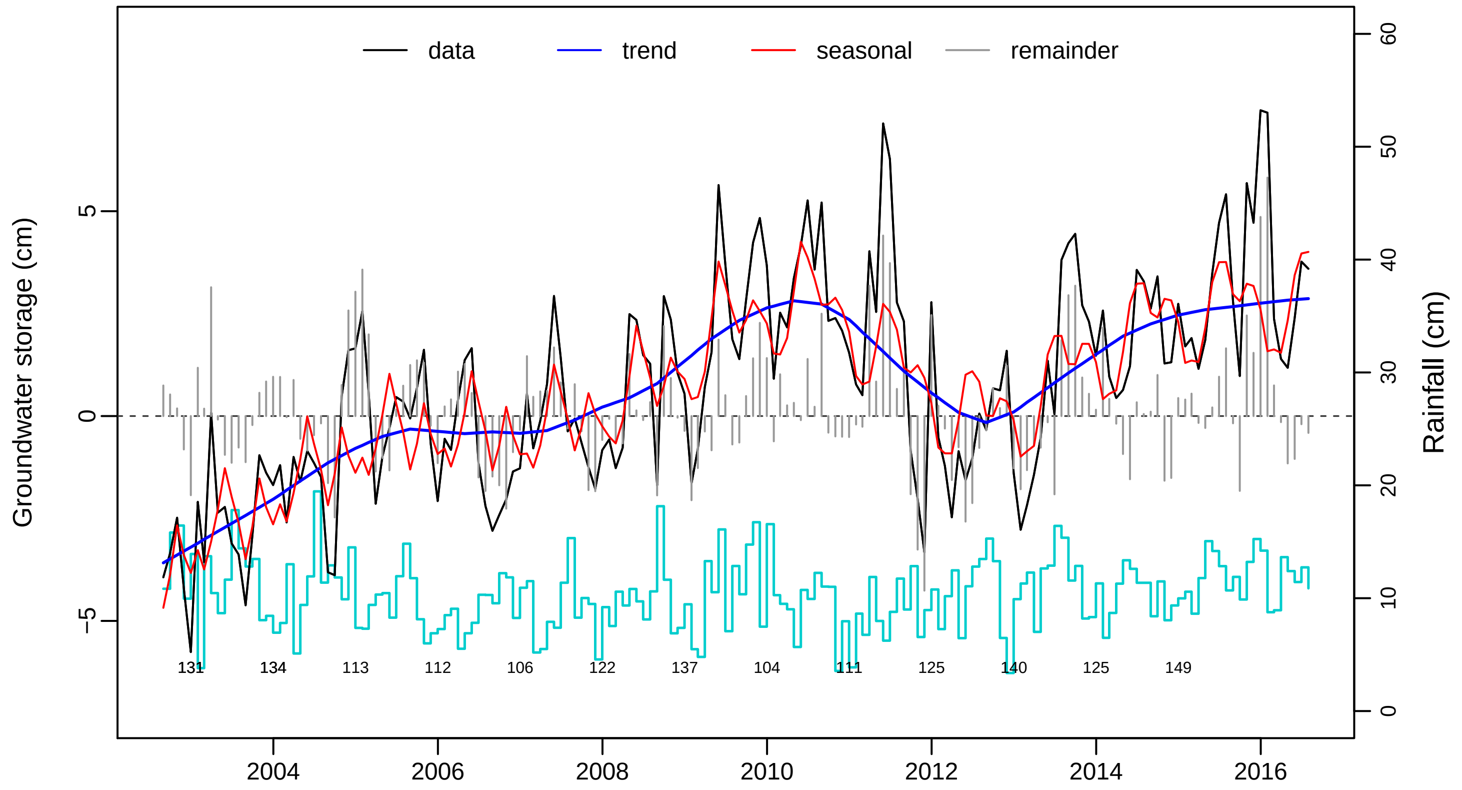

Seasonal−Trend−Remainder (GRACE GWS)
Proportion of variance

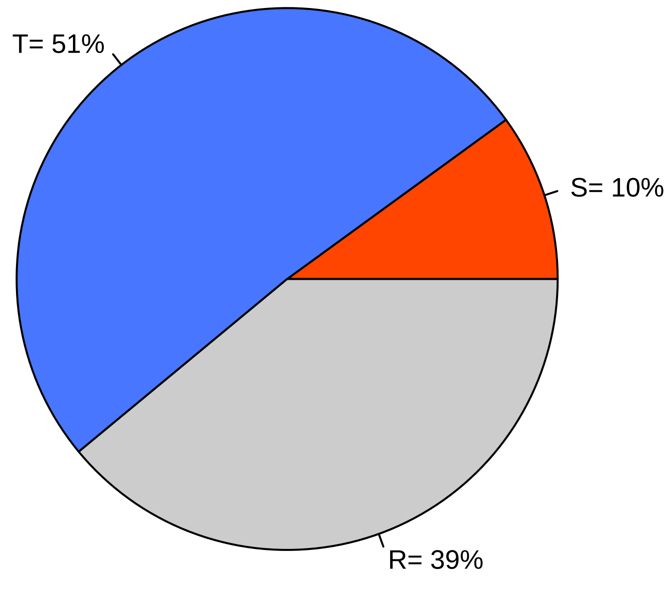

Fig. S59: Amazon Basin (19)

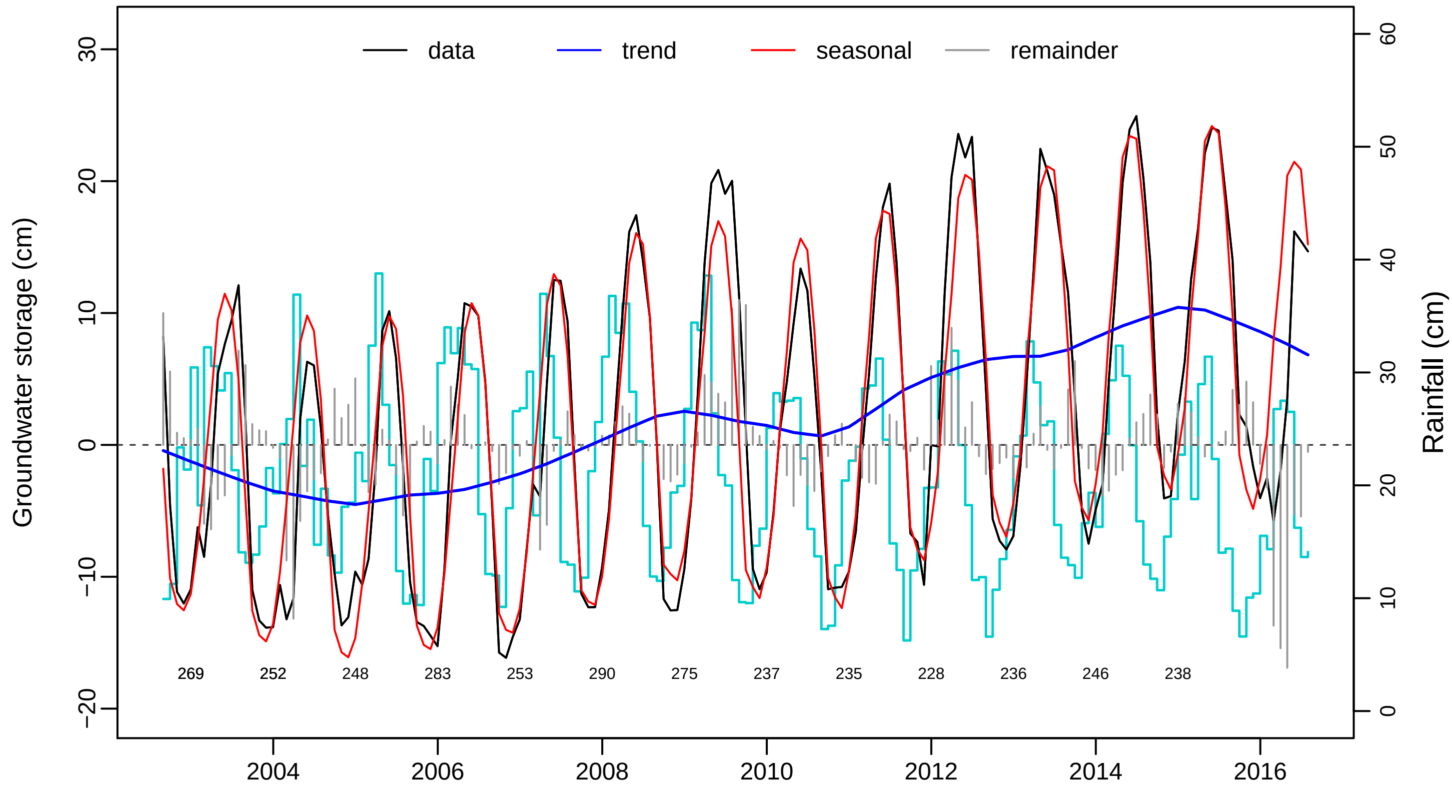

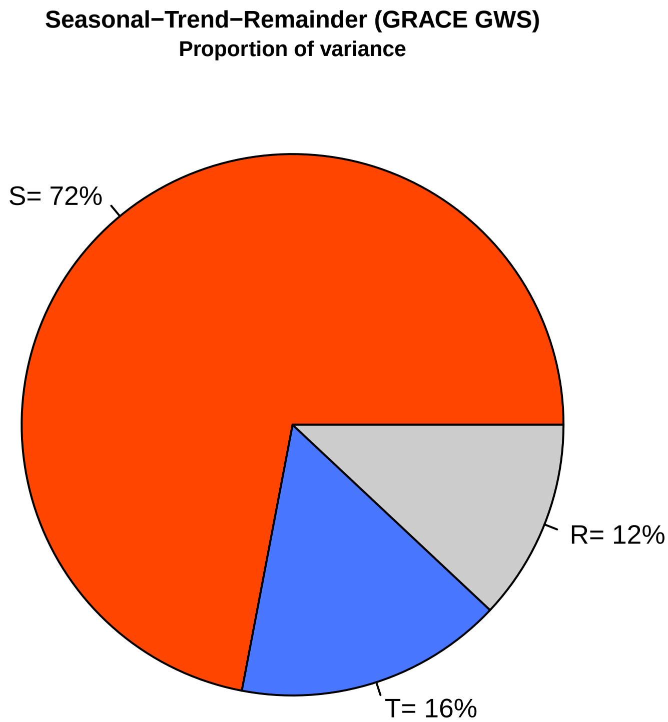

Fig. S60: Maranhao Basin (20)

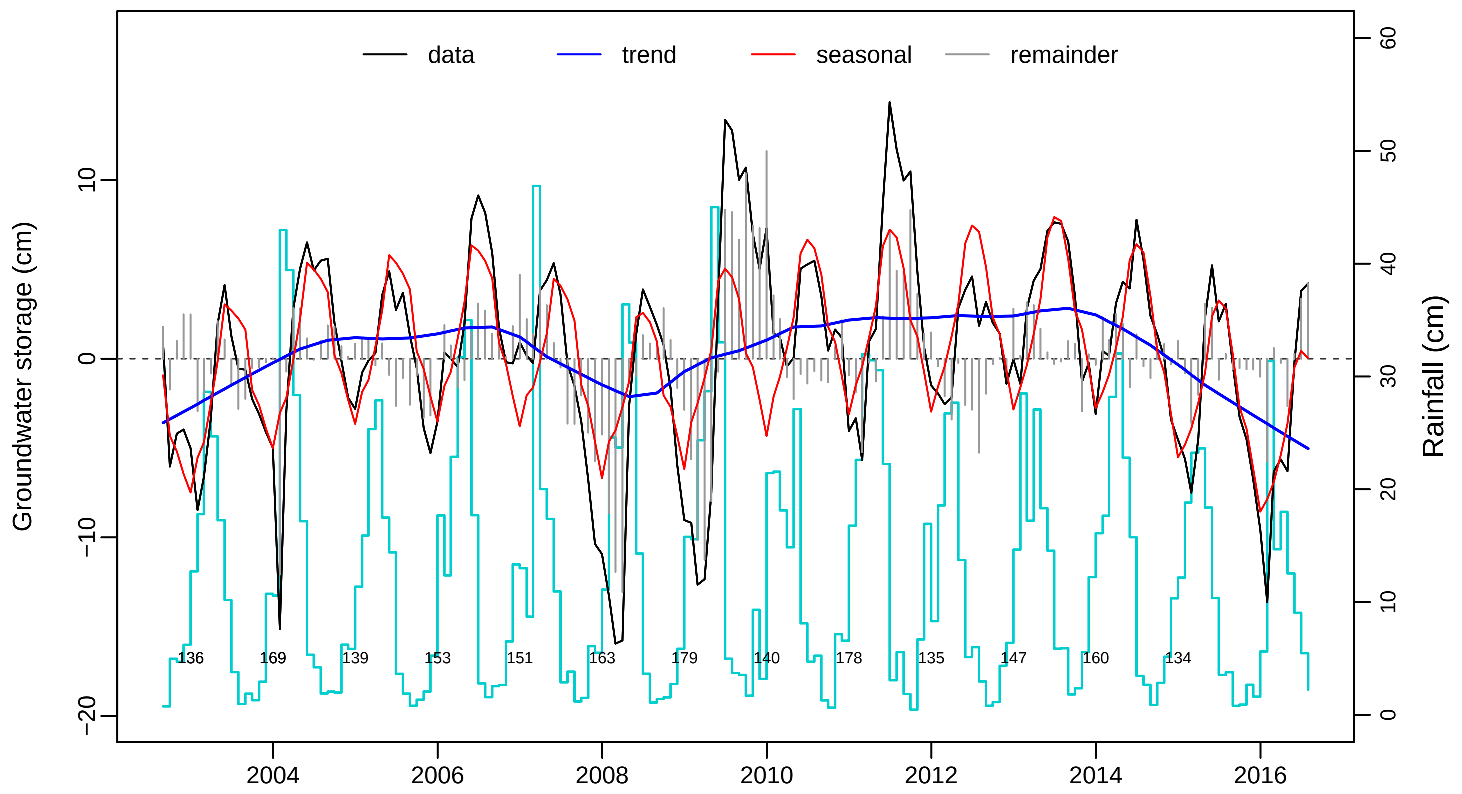

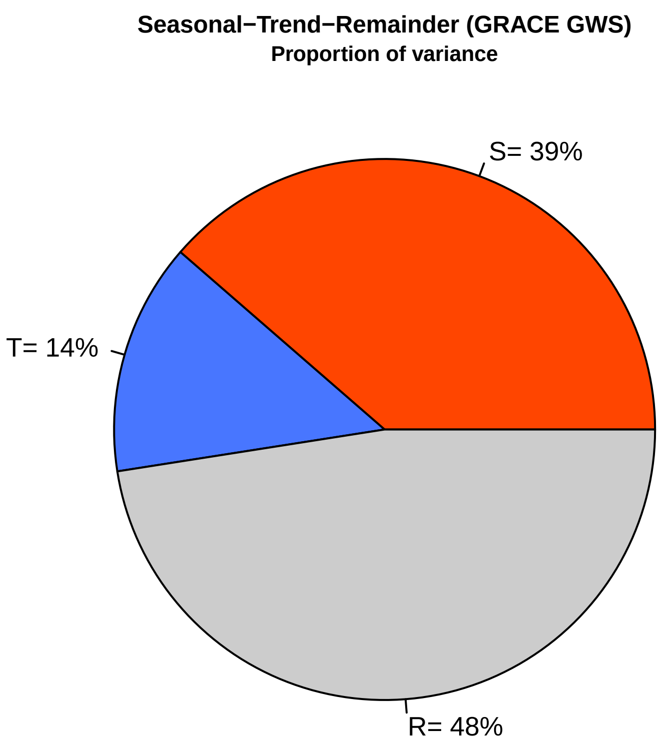

Fig. S61: Guarani Aquifer System (Parana Basin) (21)

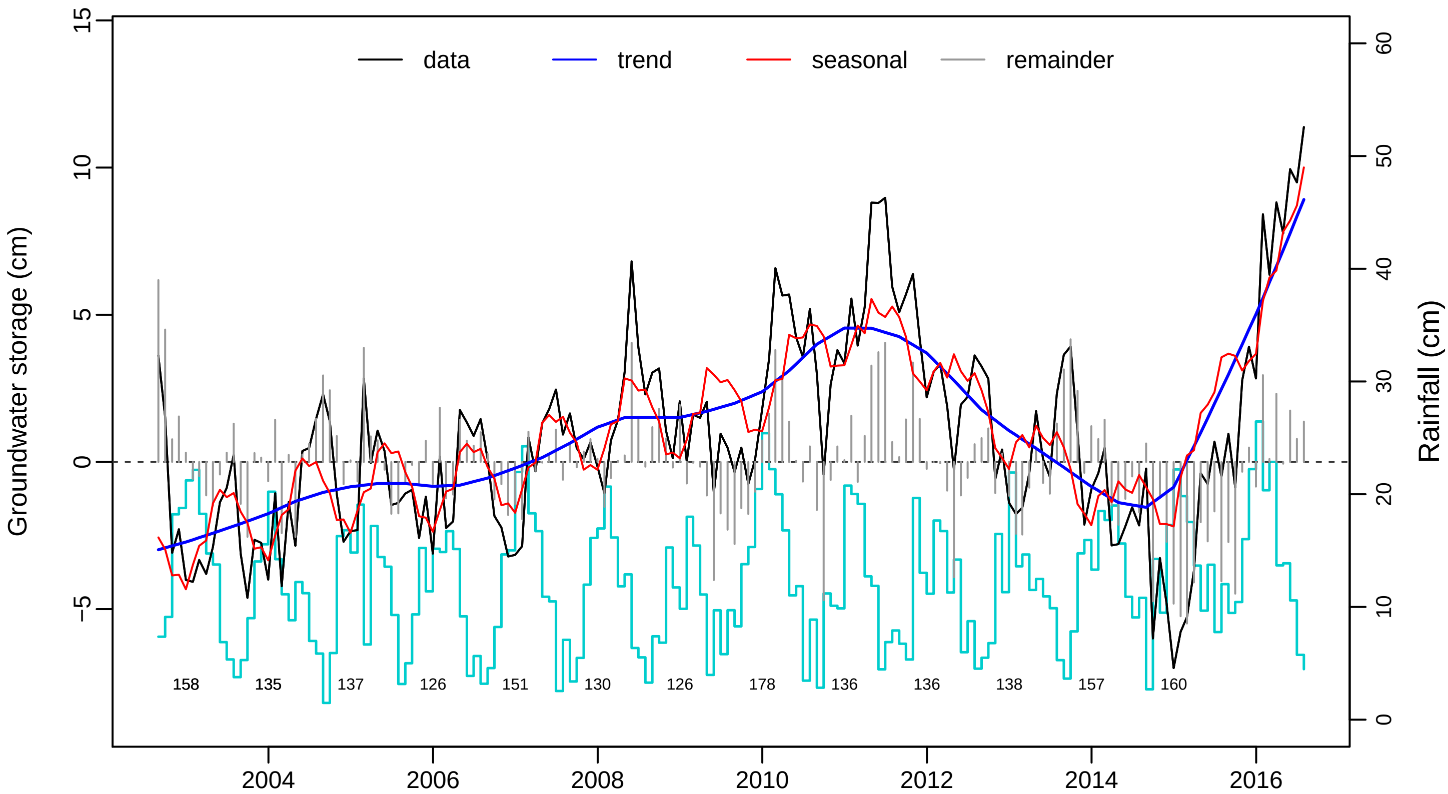

Seasonal−Trend−Remainder (GRACE GWS)
Proportion of variance

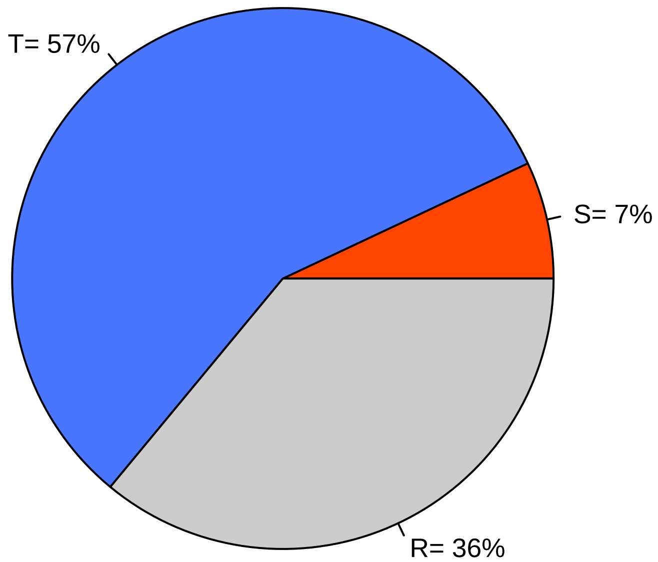

Fig. S62: Arabian Aquifer System (22)

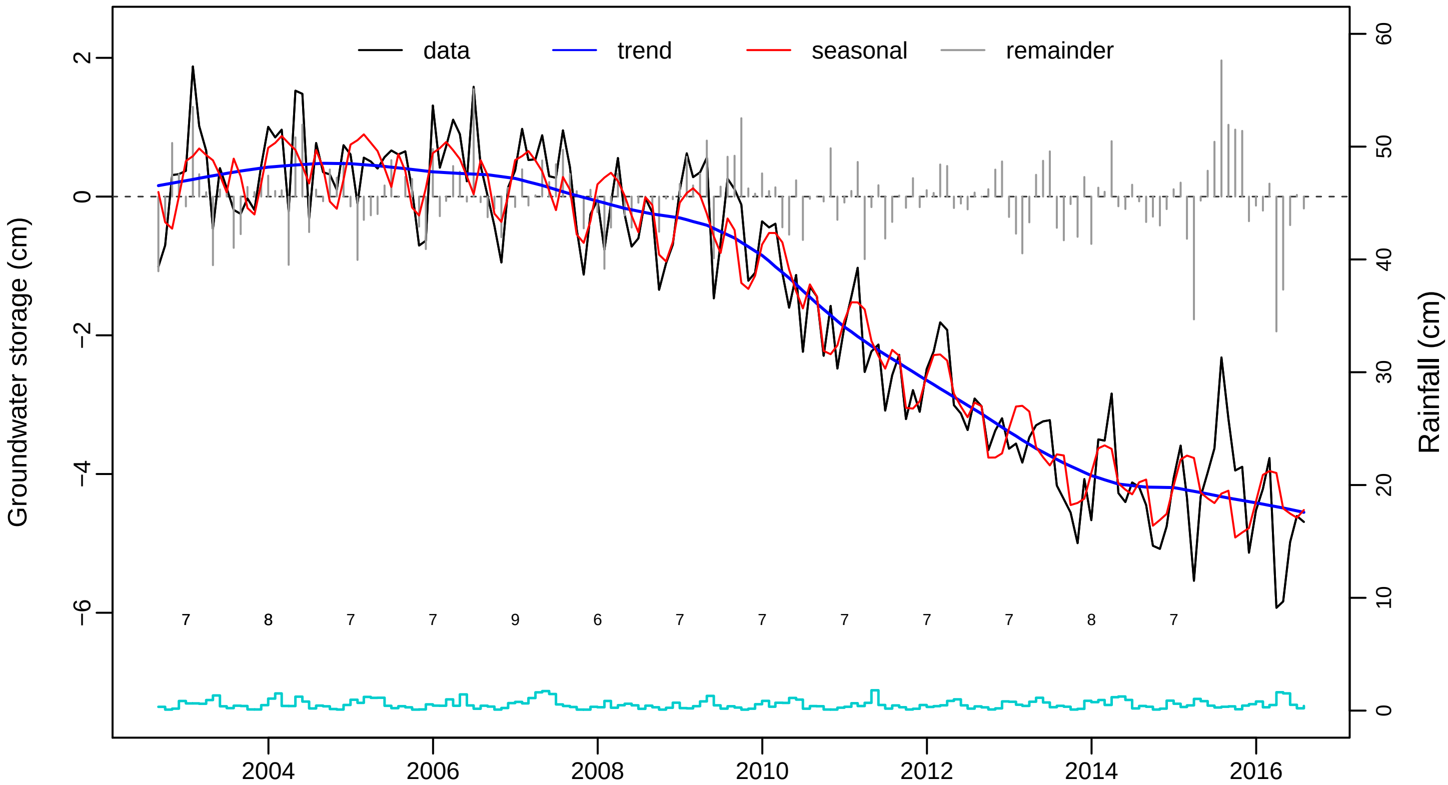

Seasonal−Trend−Remainder (GRACE GWS)
Proportion of variance

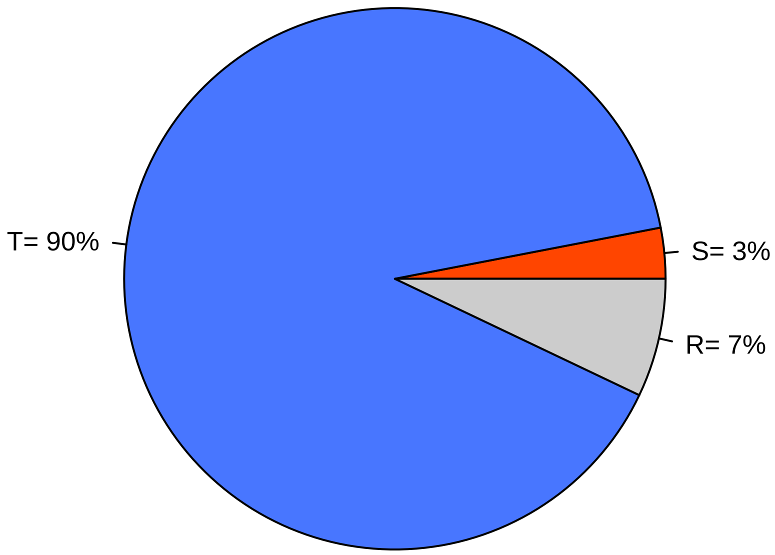

Fig. S63: Indus River Basin (23)

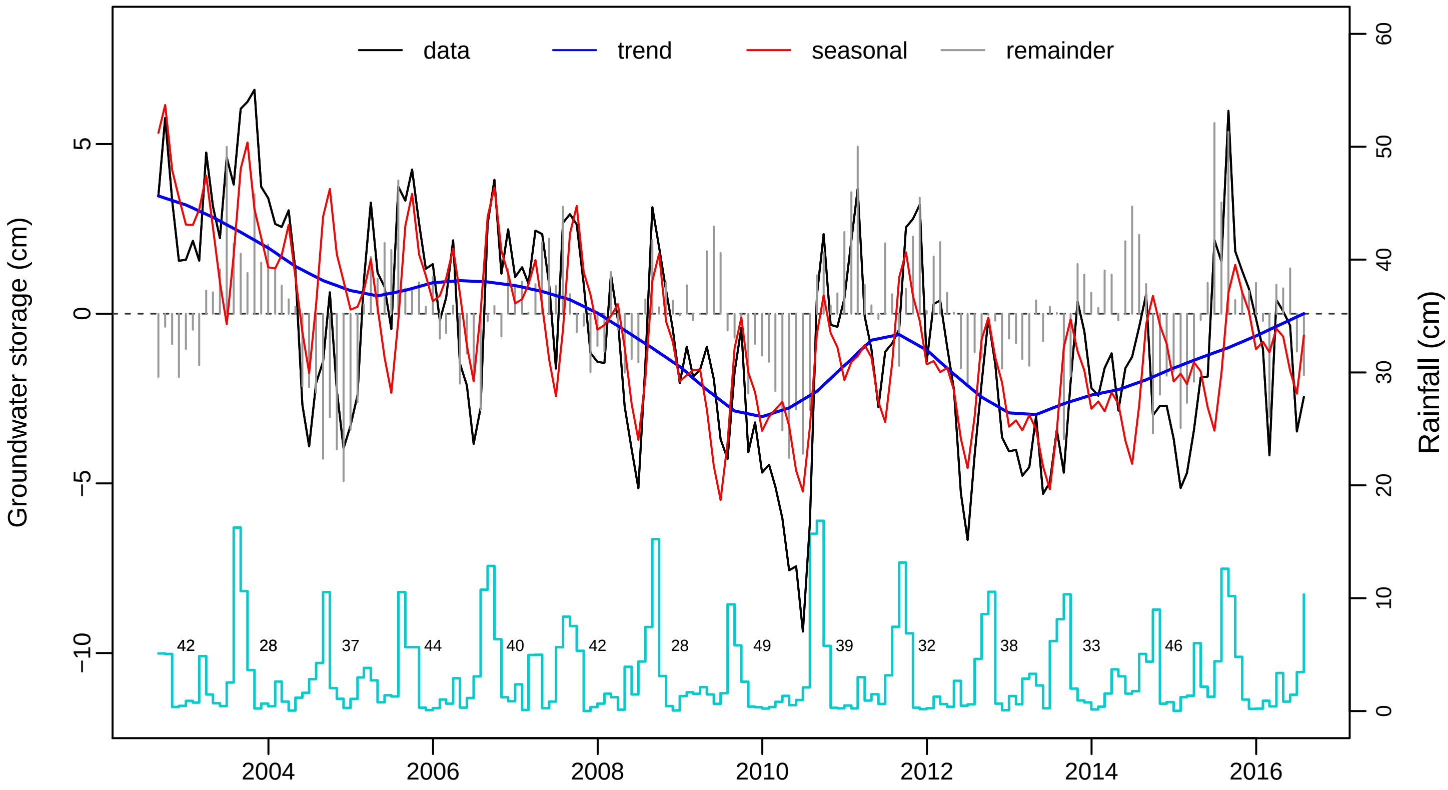

Seasonal−Trend−Remainder (GRACE GWS)
Proportion of variance

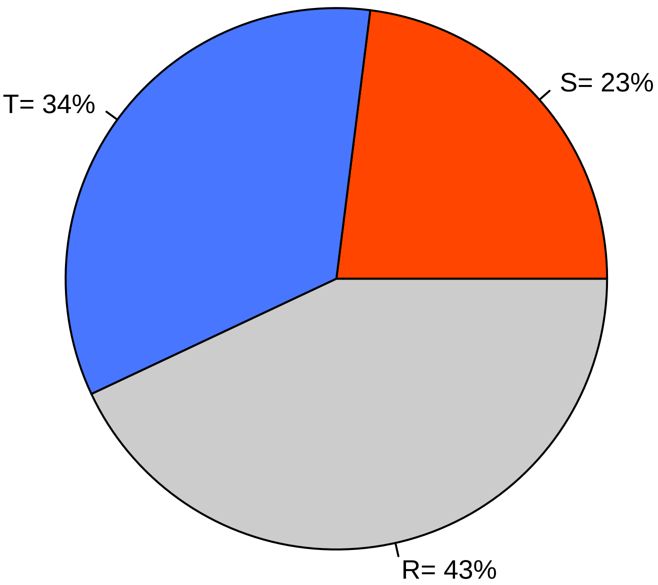

Fig. S64: Ganges−Brahmaputra River Basin (IGB) (24)

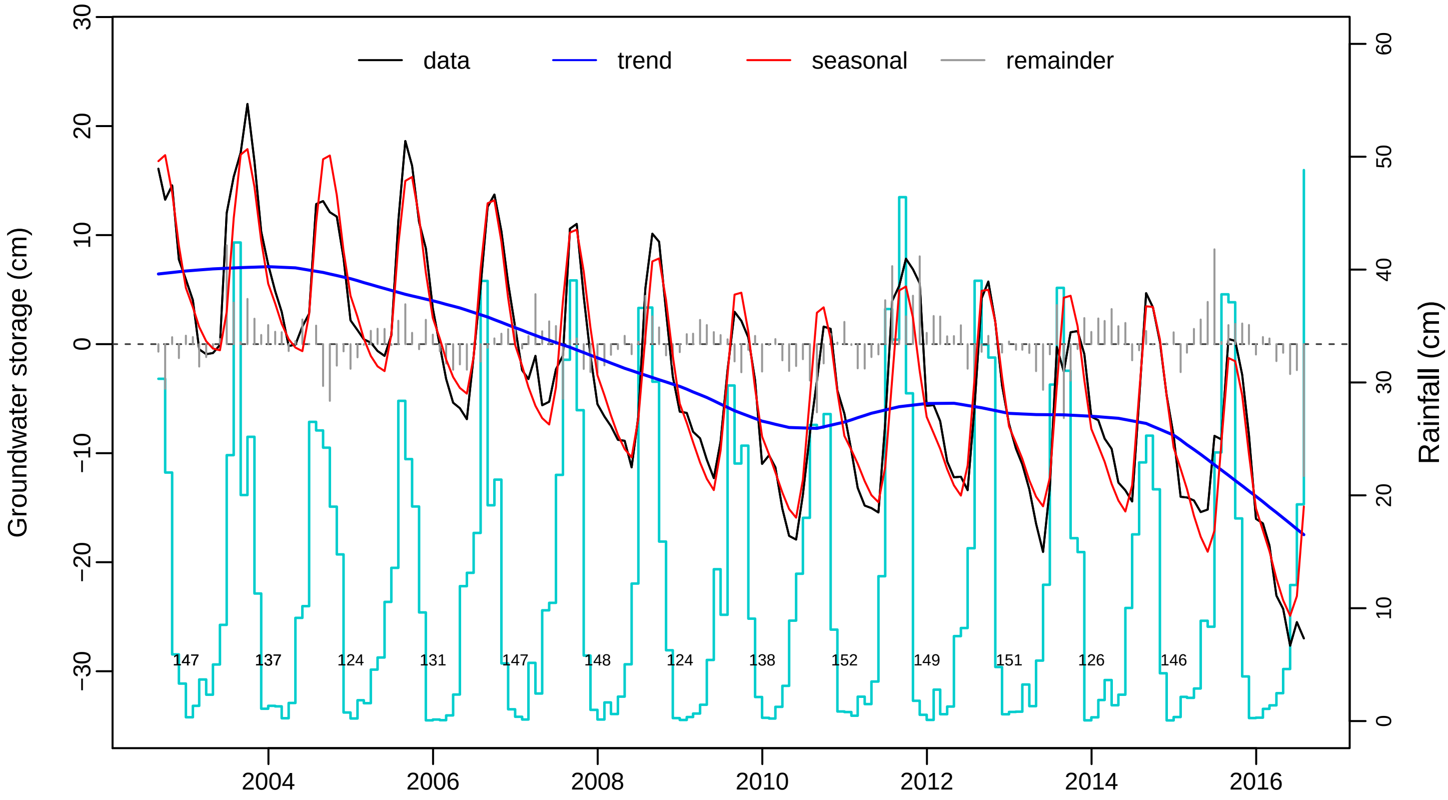

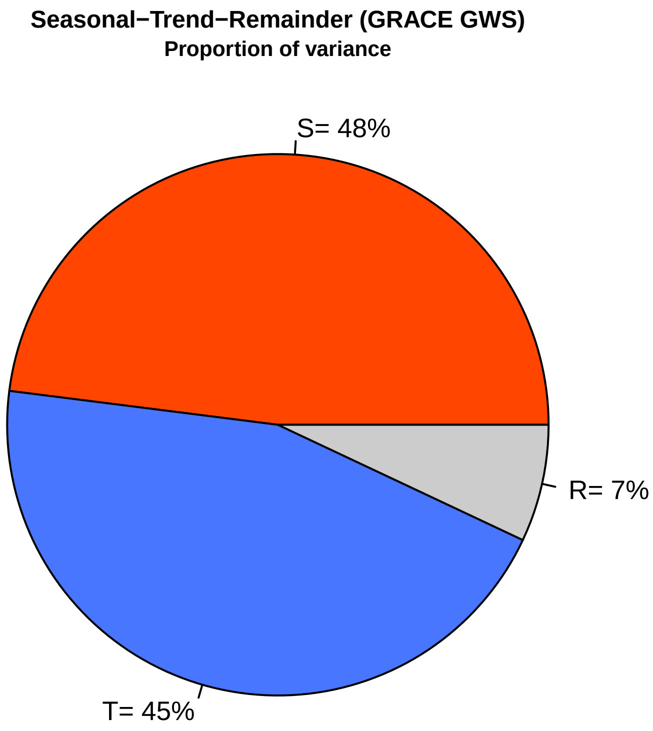

Fig. S65: West Siberian Artesian Basin (25)

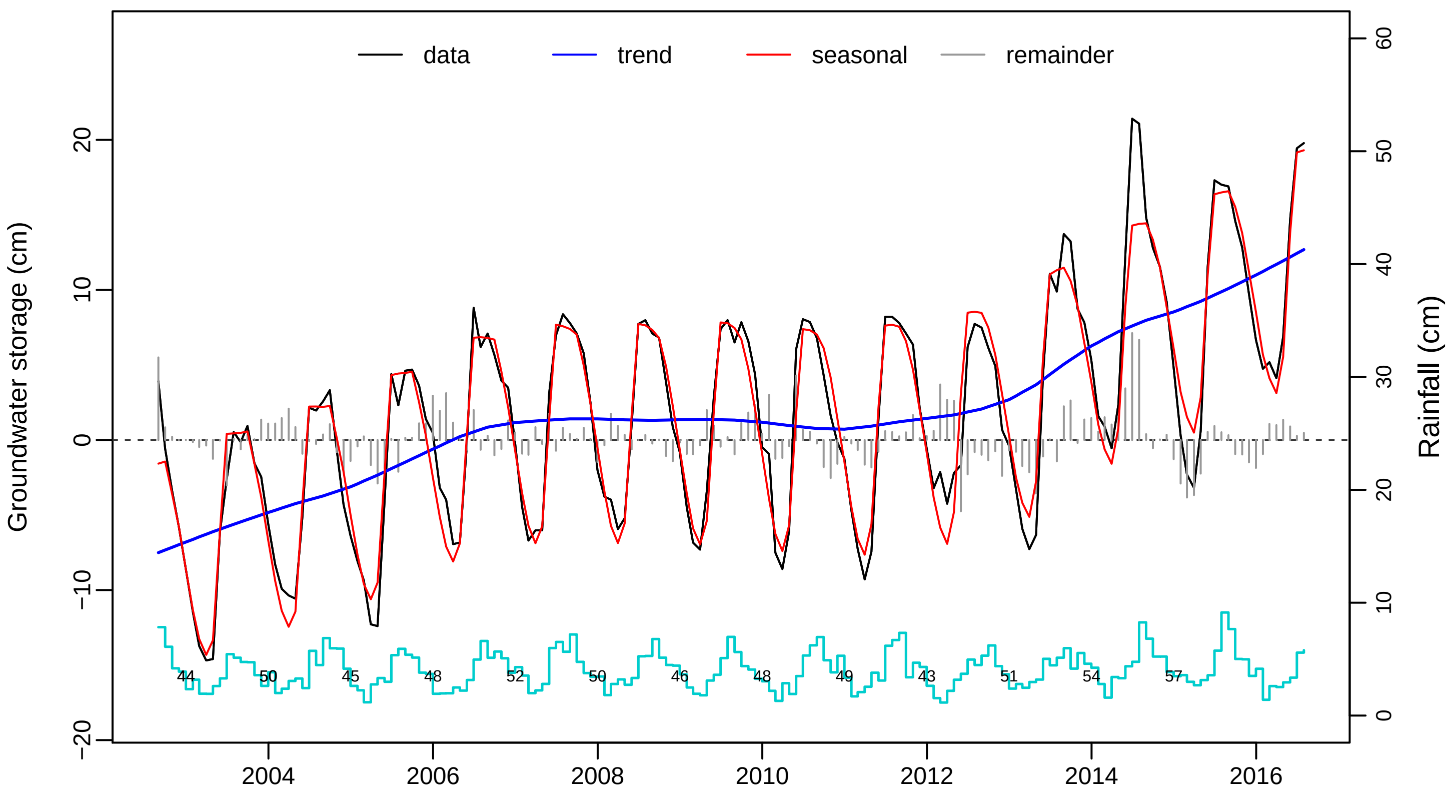

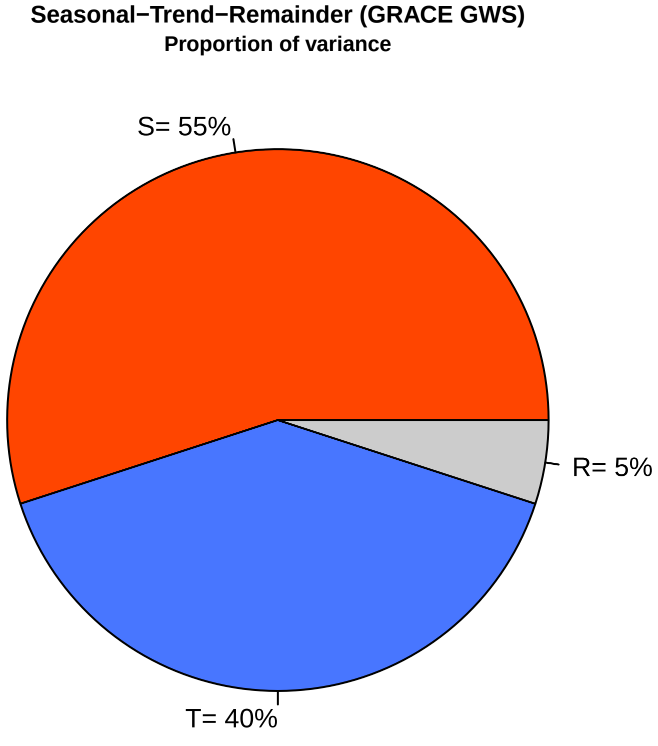

Fig. S66: Tunguss Basin (26)

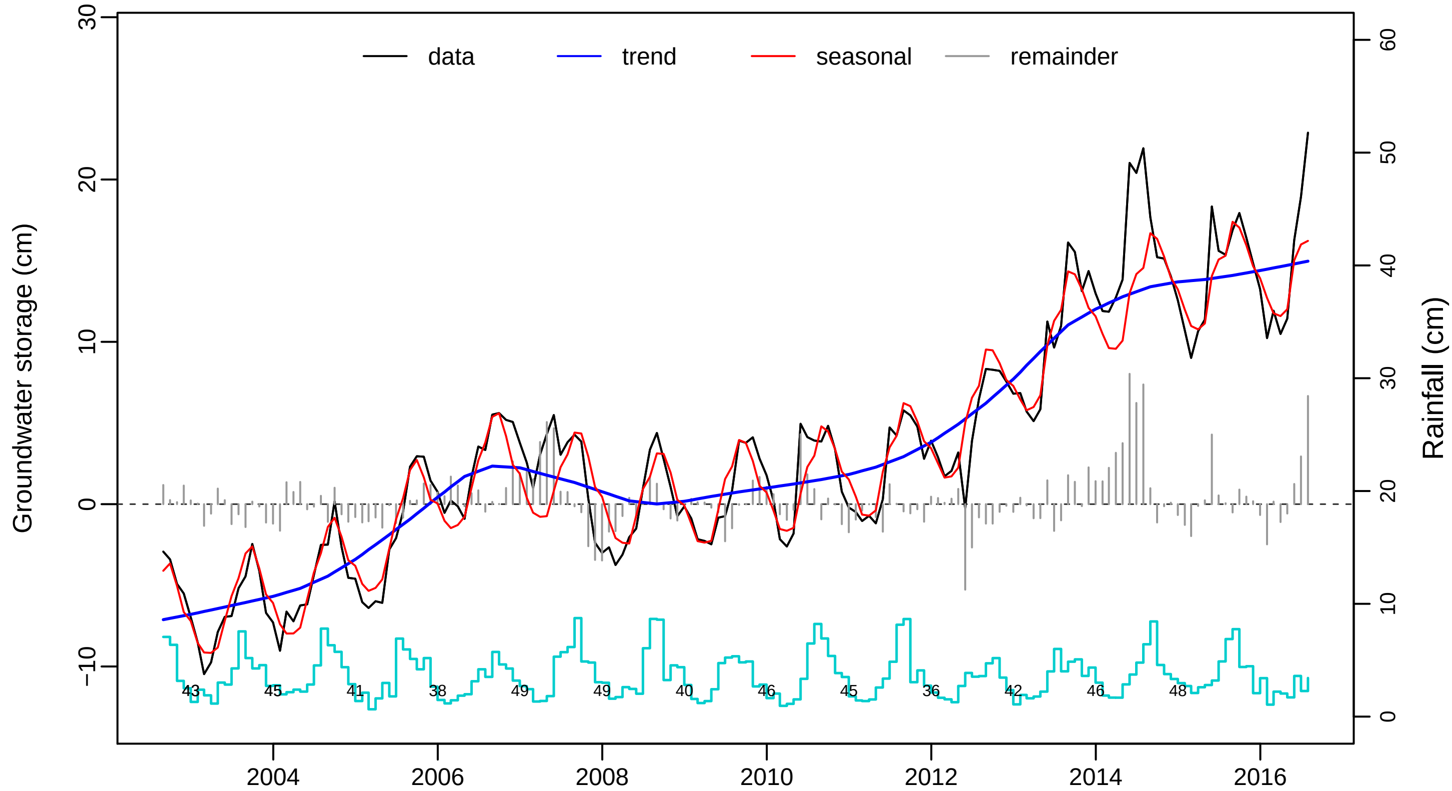

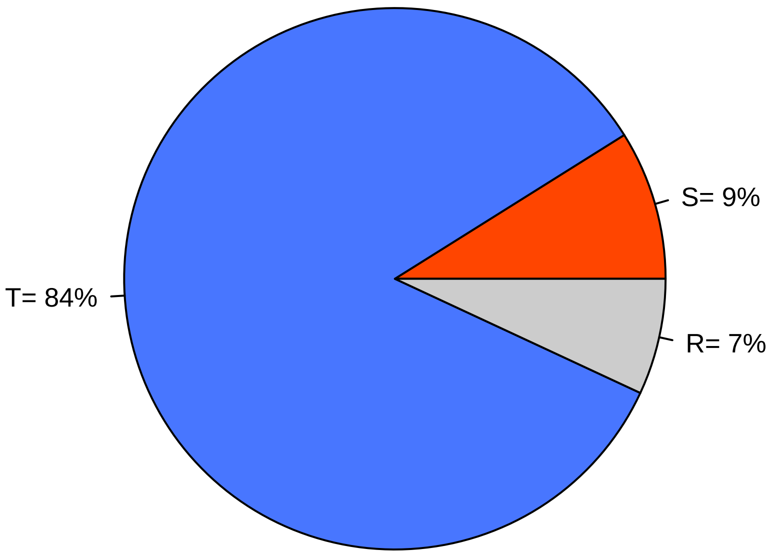

Fig. S67: Angara−Lena Basin (27)

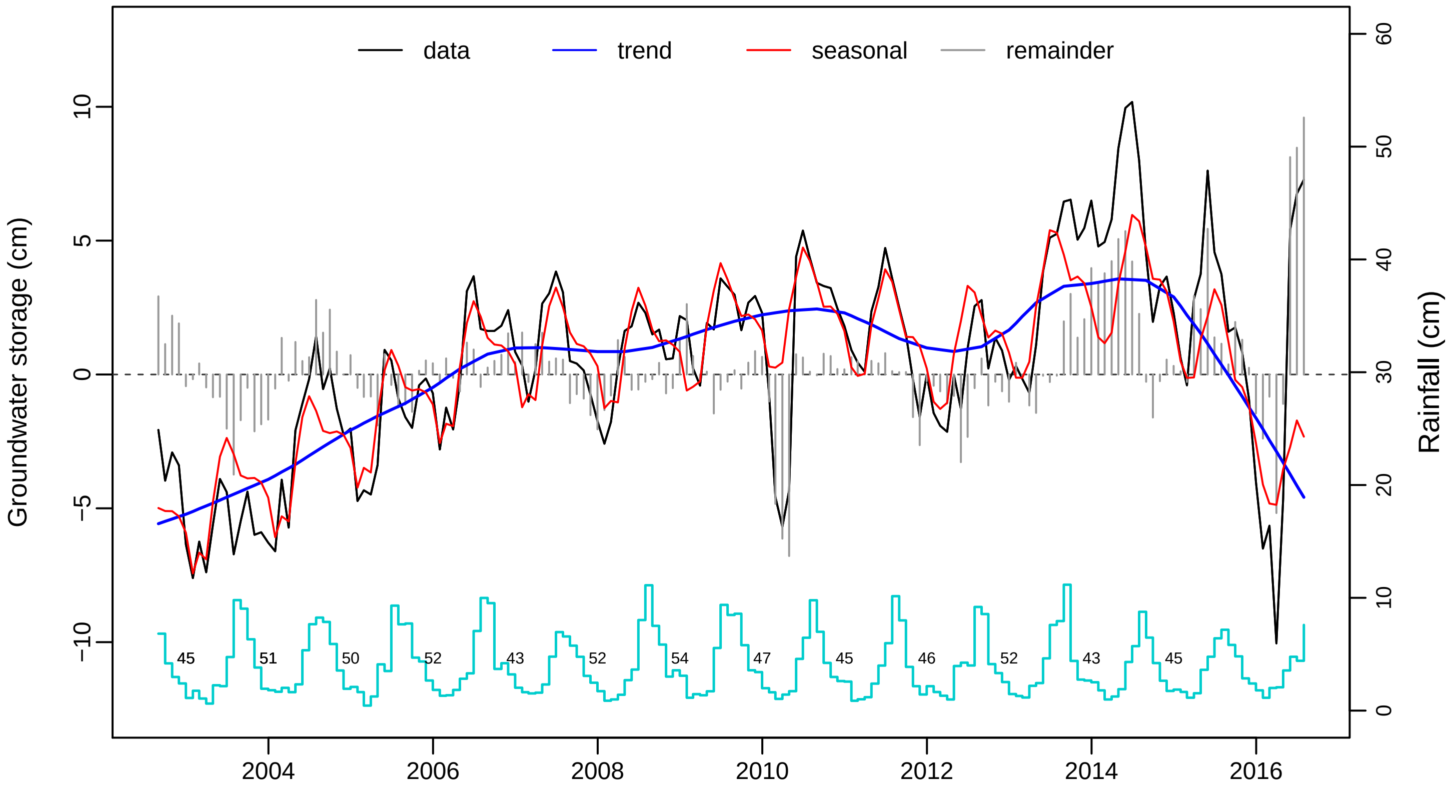

Seasonal−Trend−Remainder (GRACE GWS)
Proportion of variance

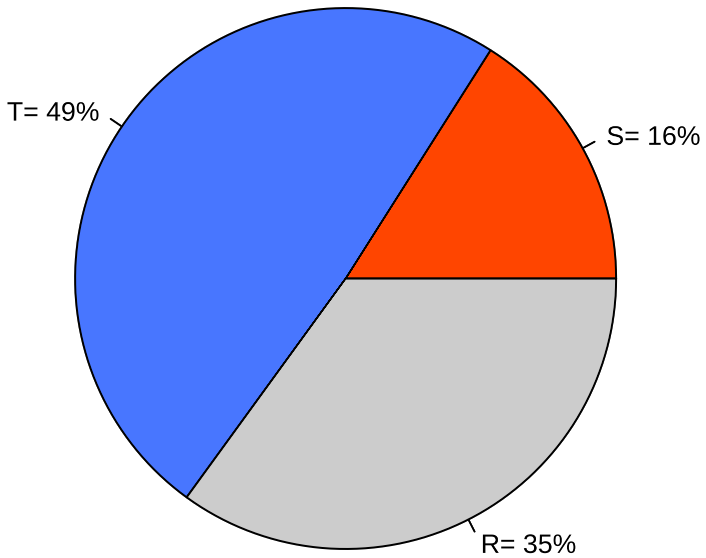

Fig. S68: Yakut Basin (28)

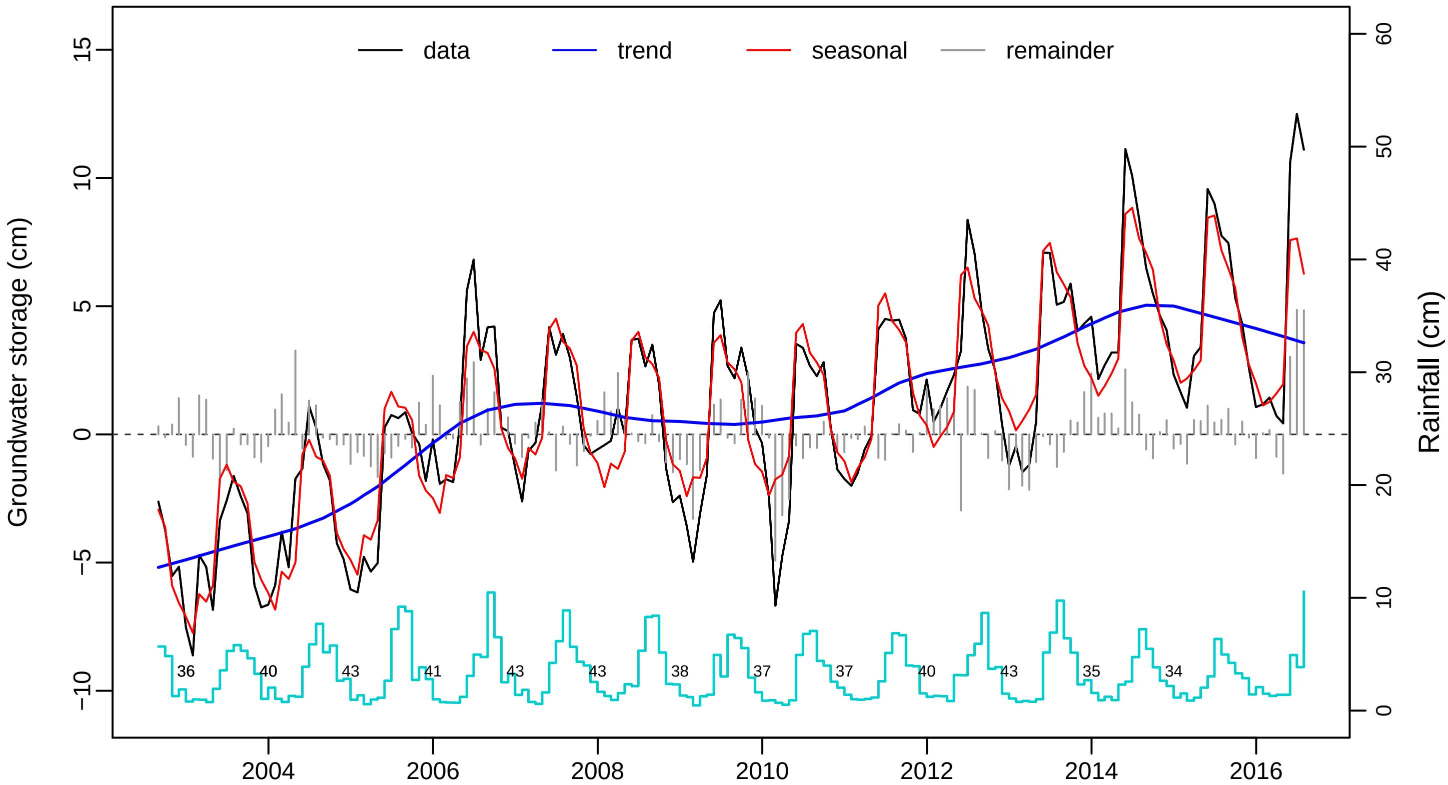

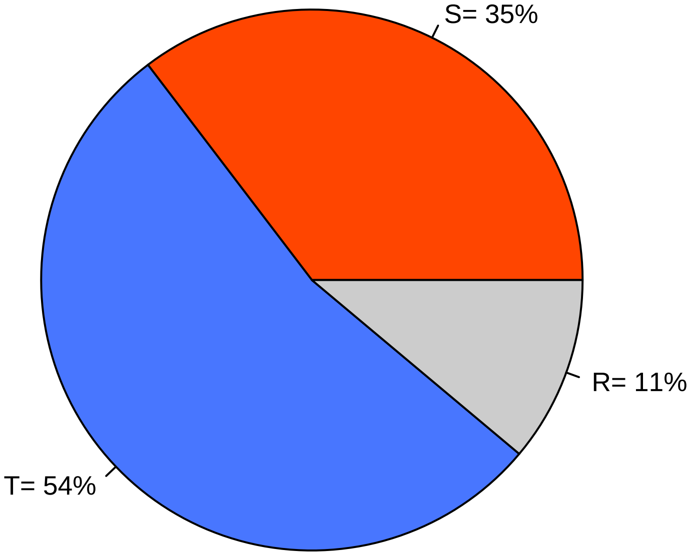

Fig. S69: North China Plains Aquifer System (29)

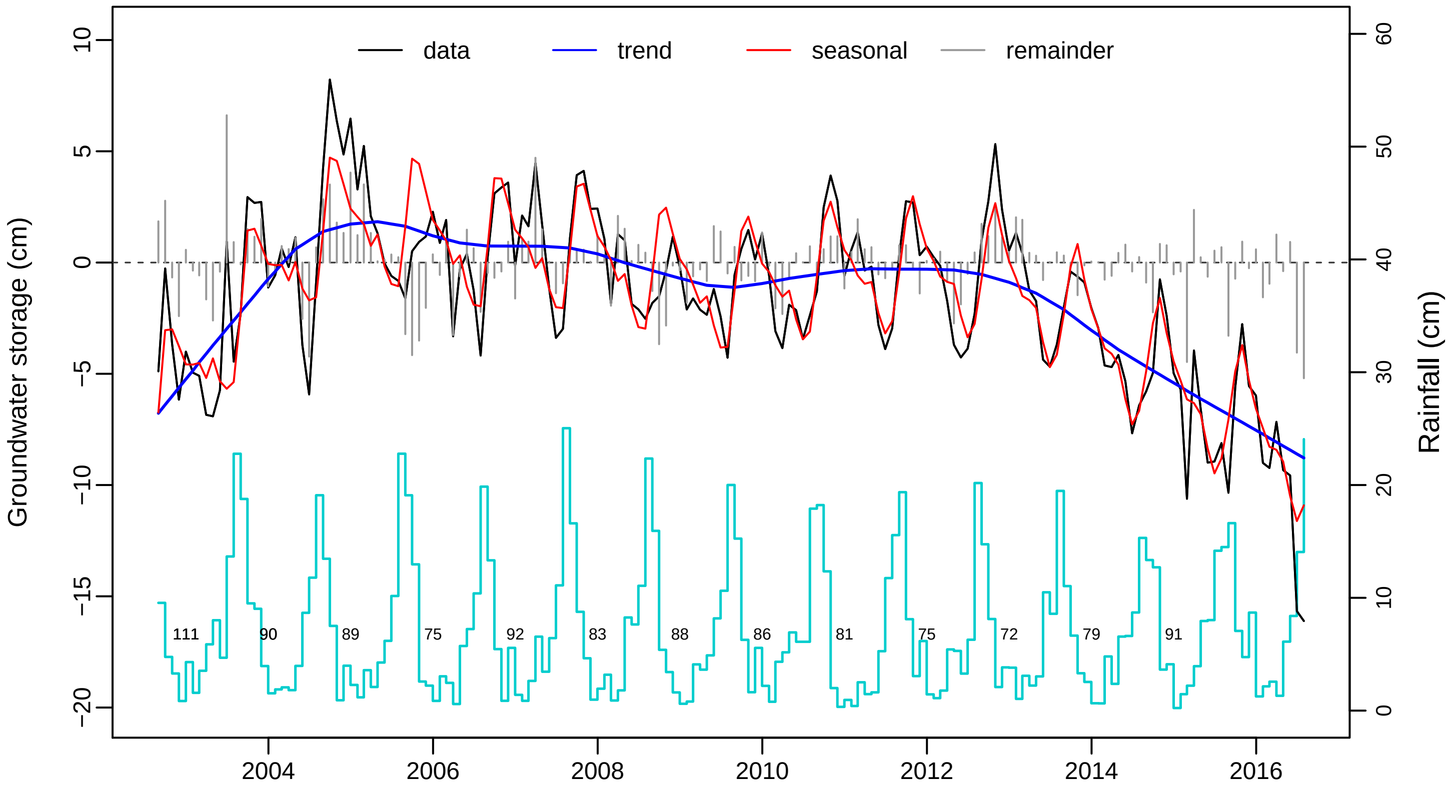

Seasonal−Trend−Remainder (GRACE GWS)
Proportion of variance

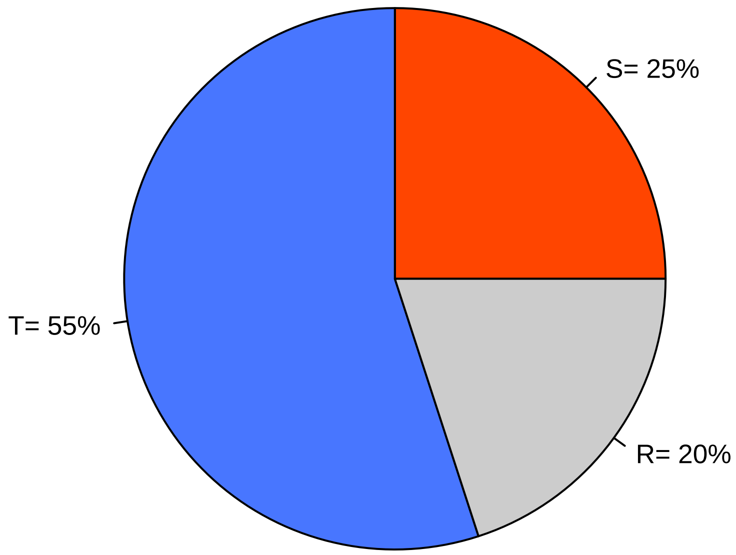

Fig. S70: Song−Liao Plain (30)

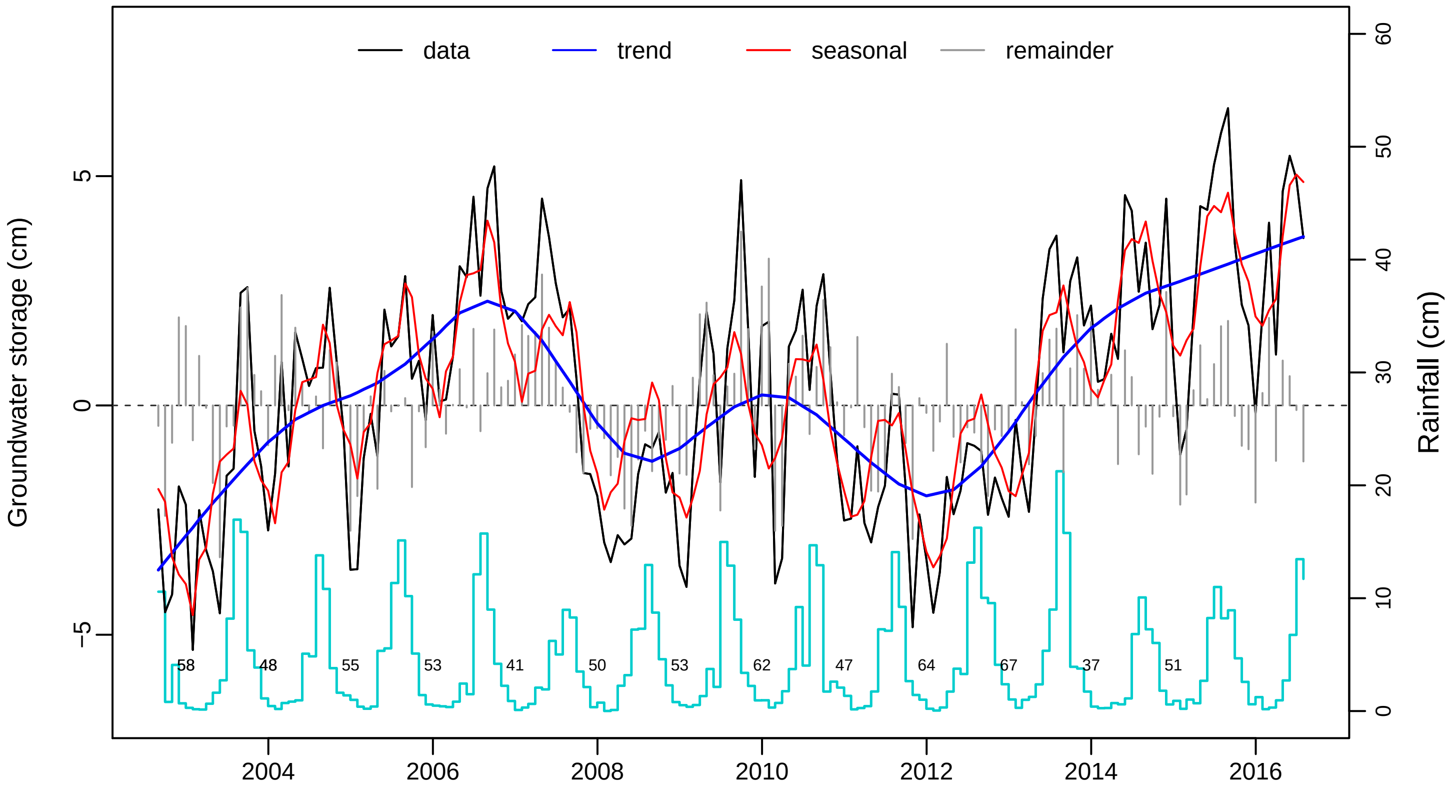

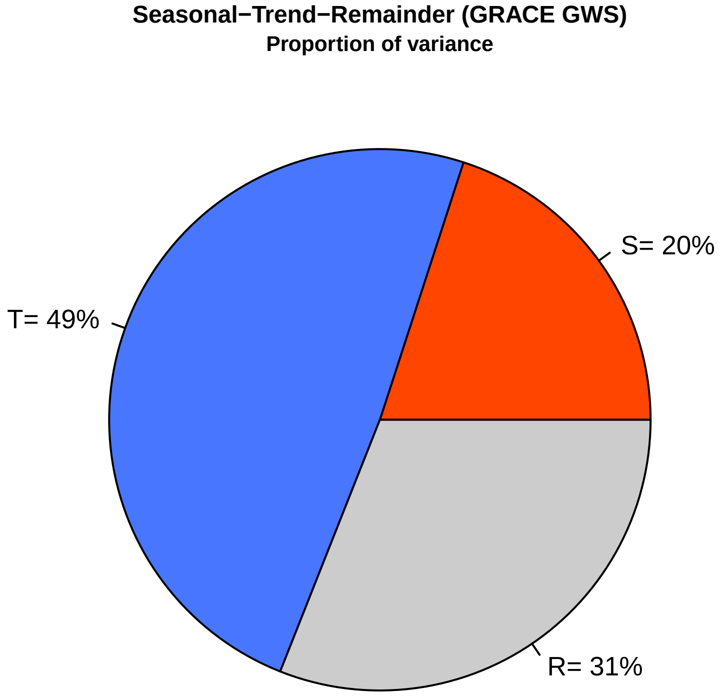

Fig. S71: Tarim Basin (31)

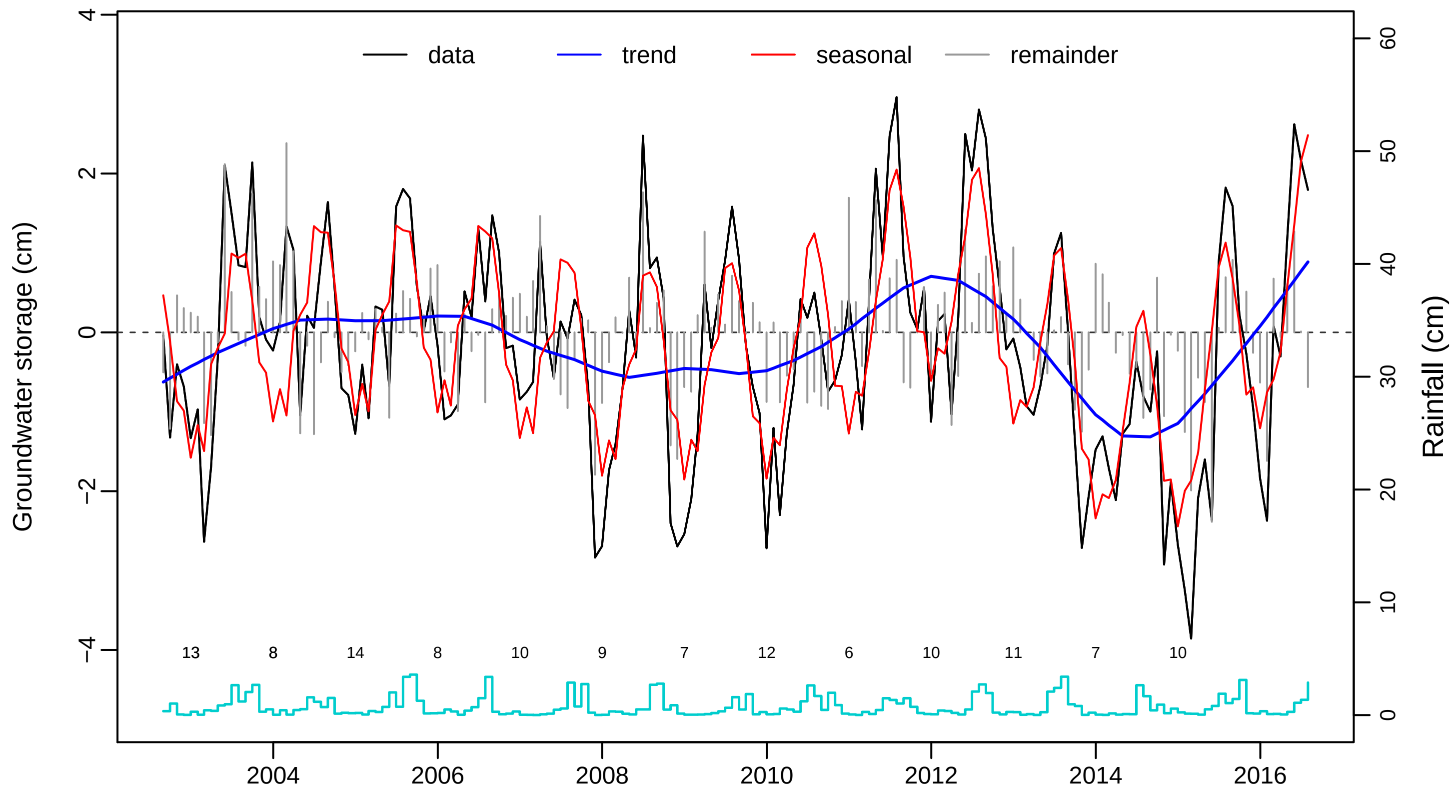

Seasonal−Trend−Remainder (GRACE GWS)
Proportion of variance

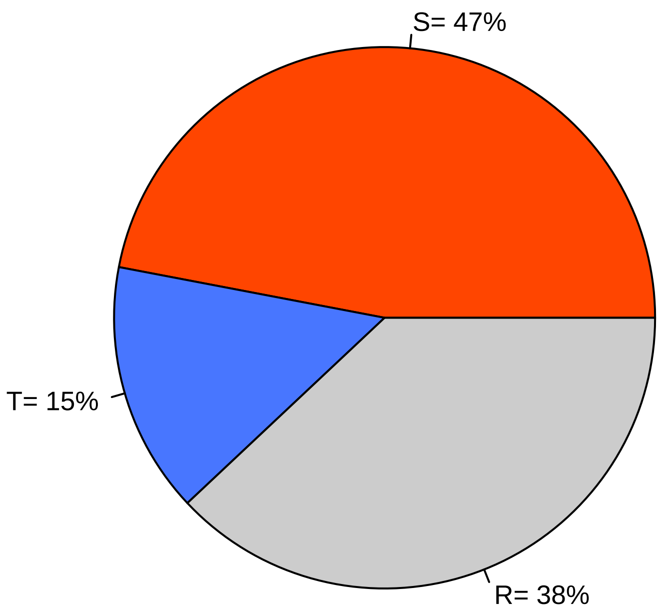

Fig. S72: Paris Basin (32)

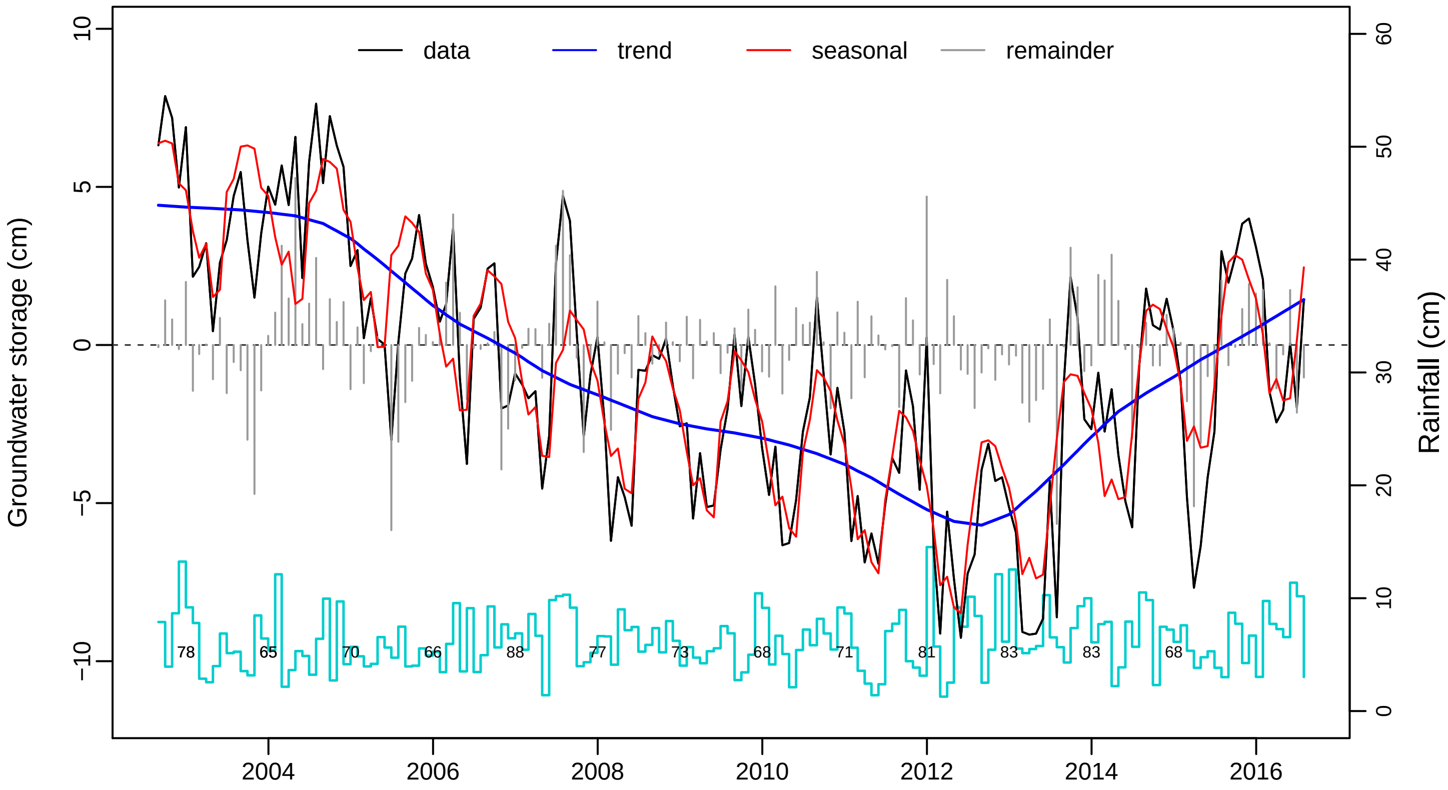

Seasonal−Trend−Remainder (GRACE GWS)
Proportion of variance

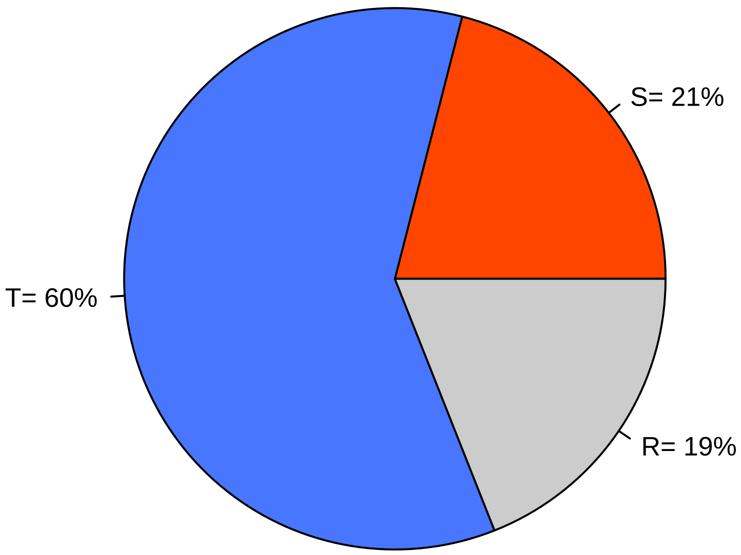

Fig. S73: East European Aquifer System (33)

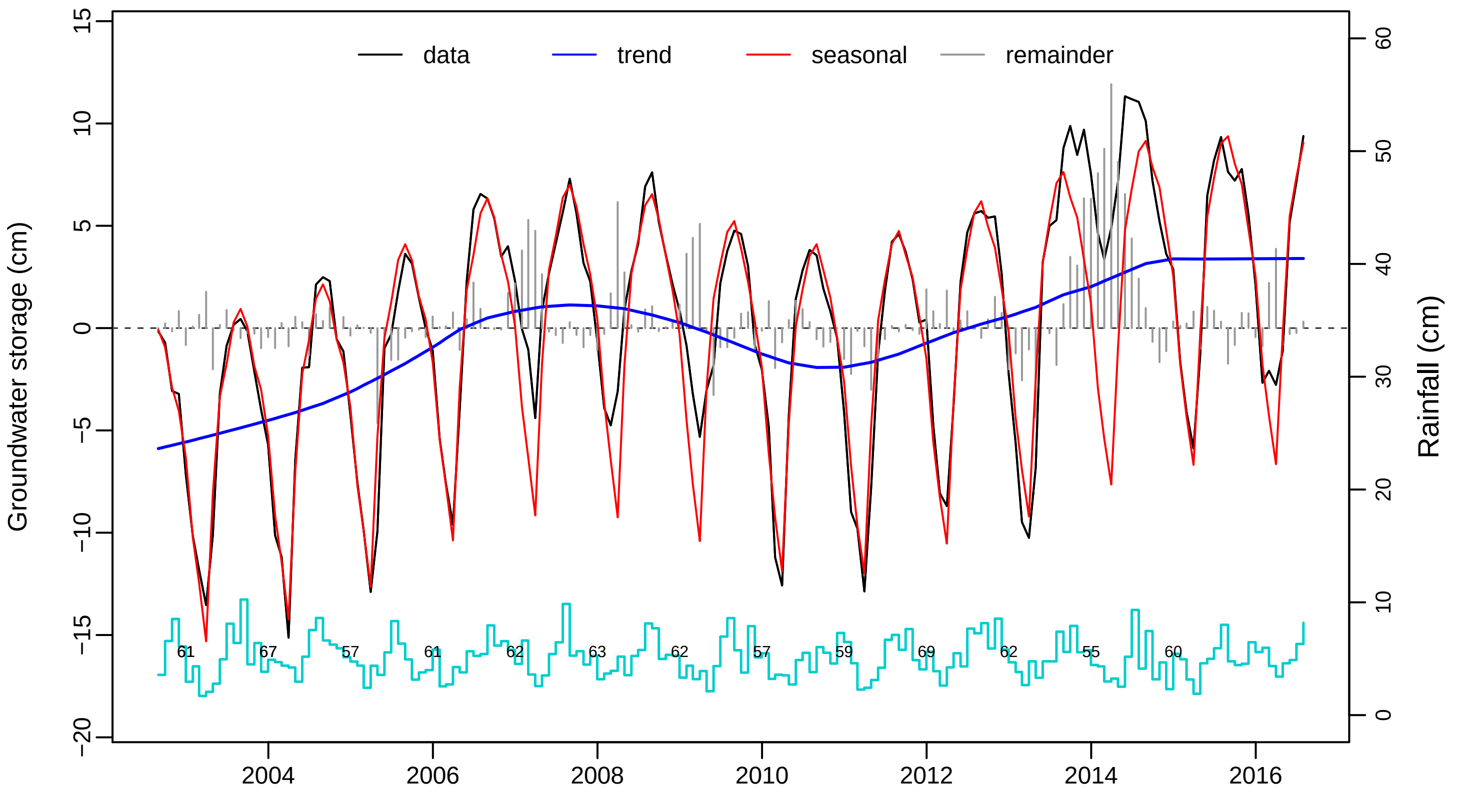

Seasonal−Trend−Remainder (GRACE GWS)
Proportion of variance

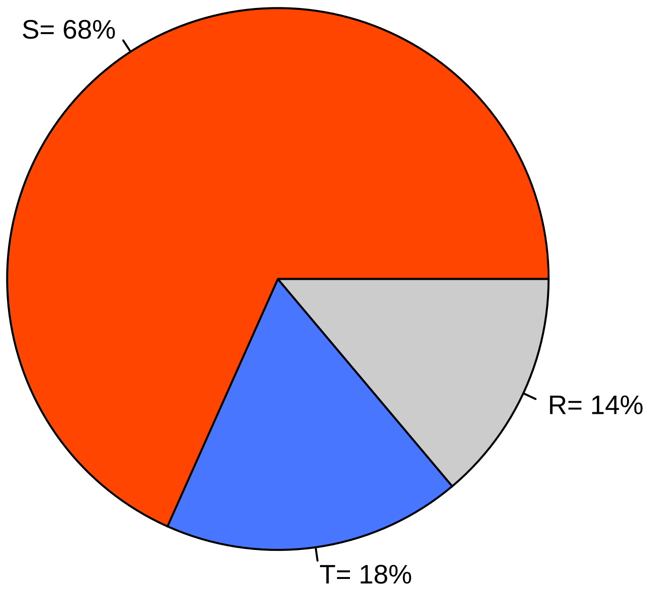

Fig. S74: North Caucasus Basin (34)

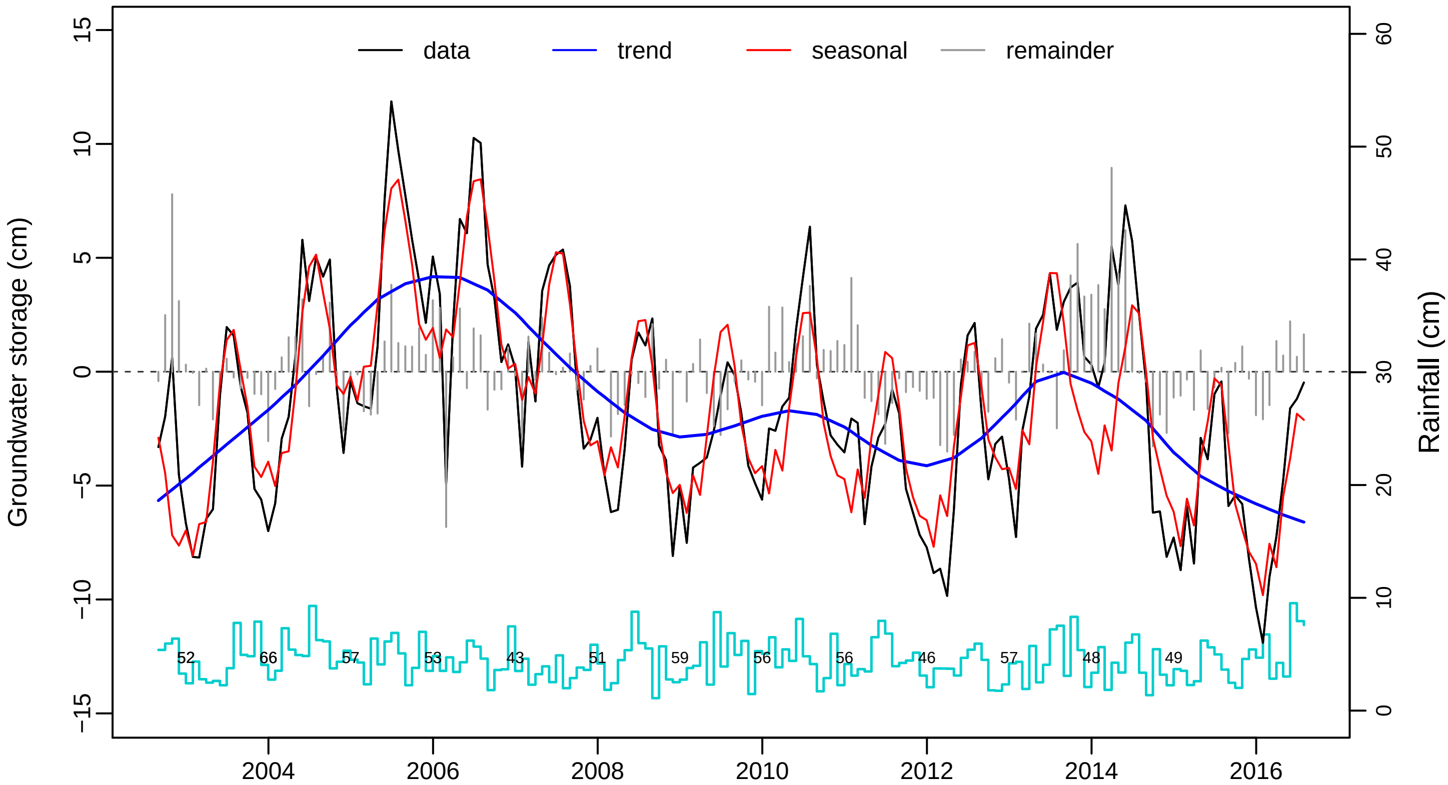

Seasonal−Trend−Remainder (GRACE GWS)
Proportion of variance

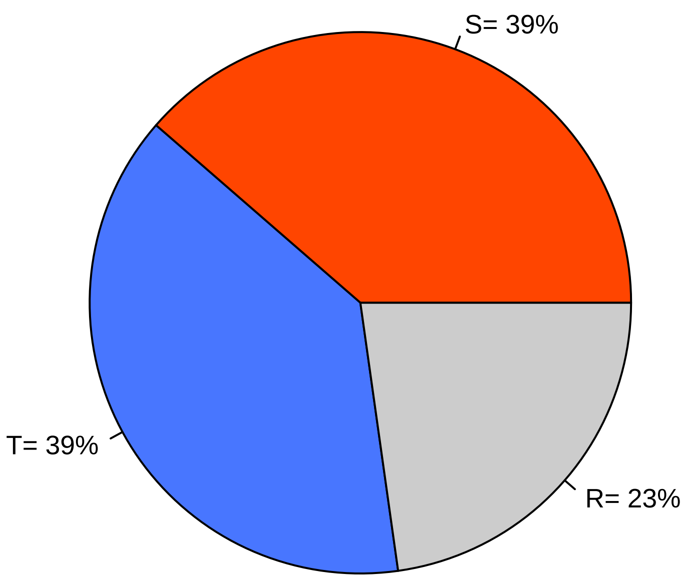

Fig. S75: Pechora Basin (35)

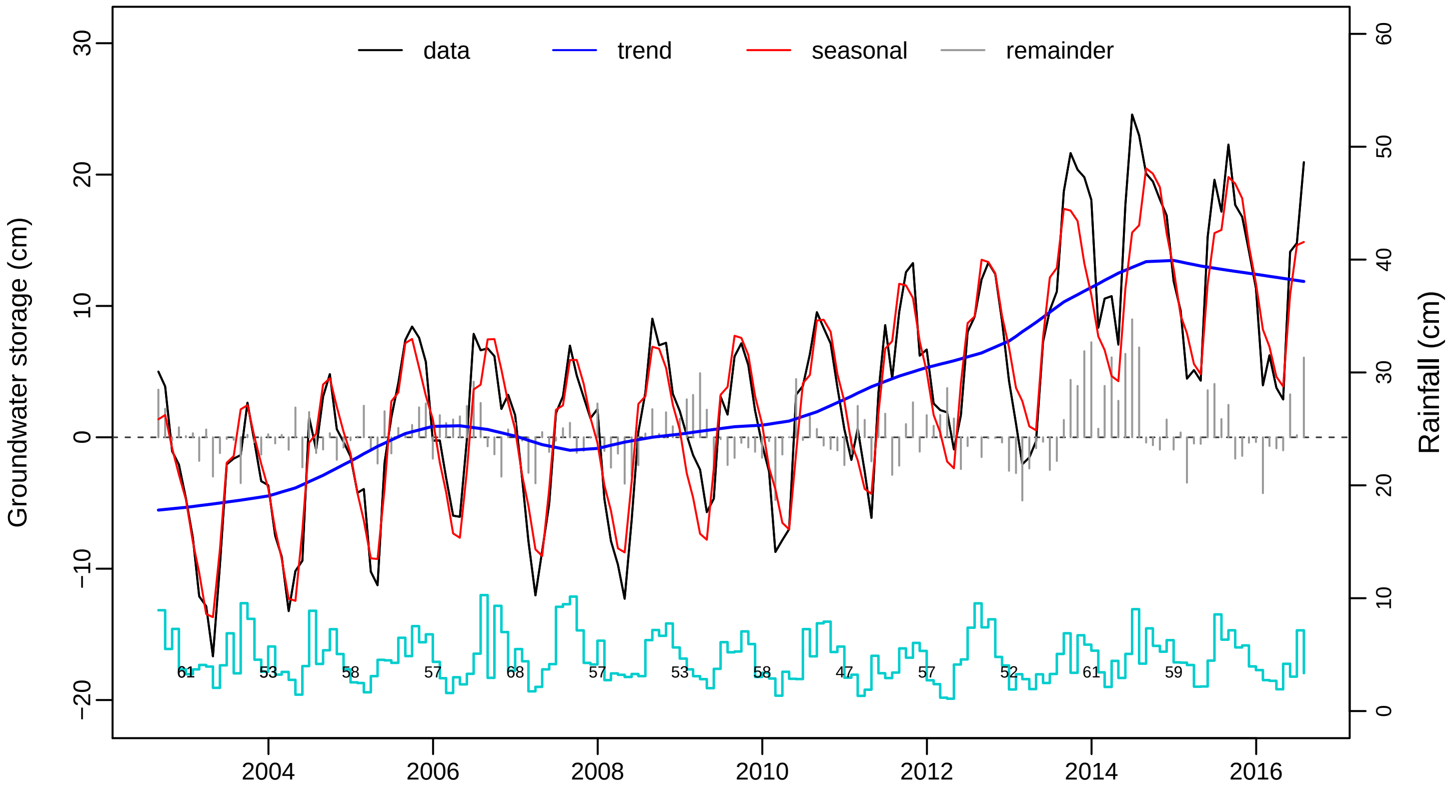

Seasonal−Trend−Remainder (GRACE GWS)
Proportion of variance

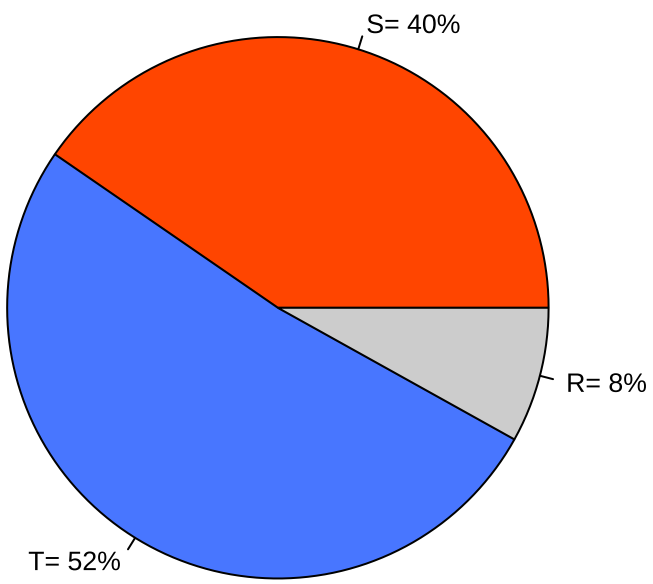

Fig. S76: Great Artesian Basin (36)

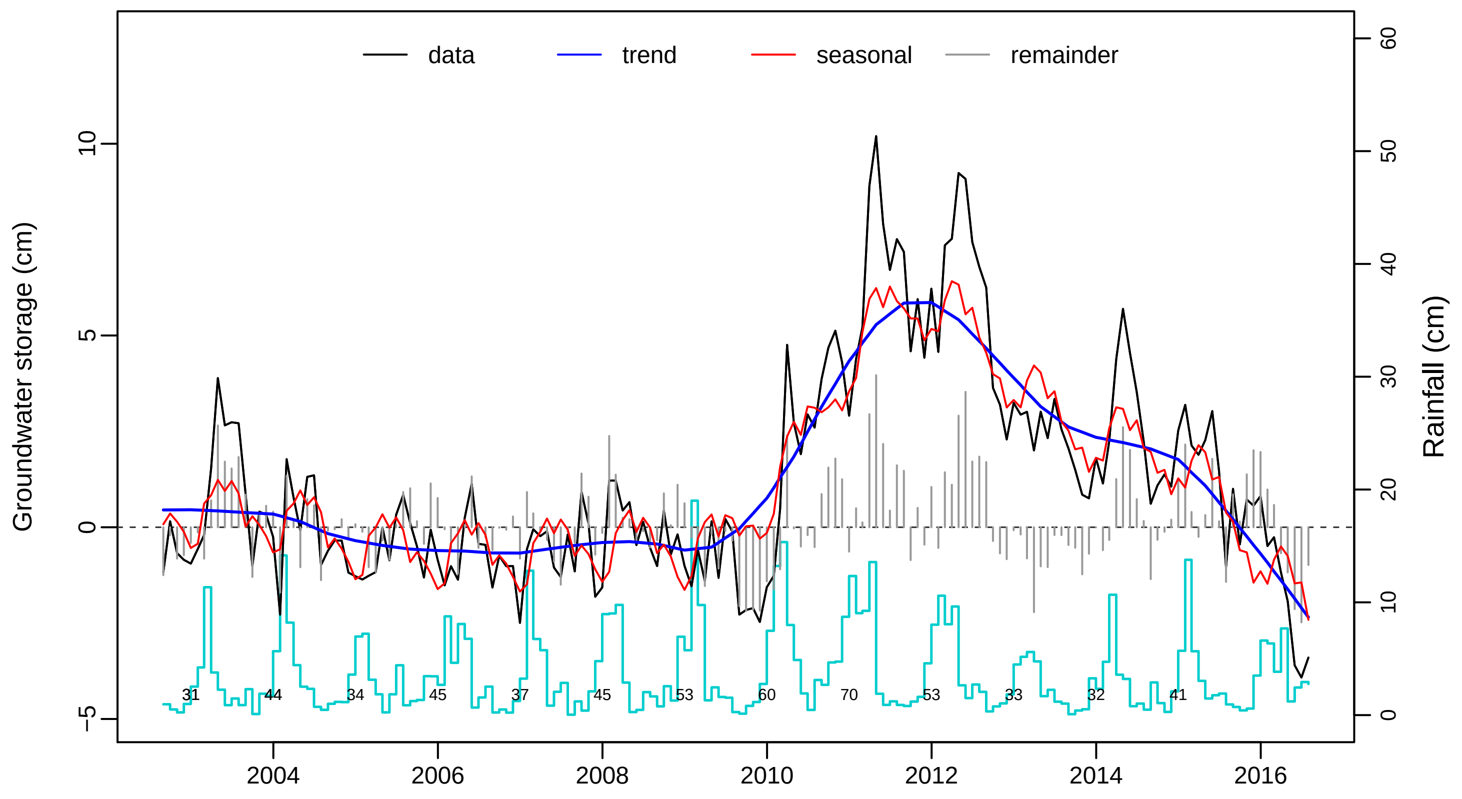

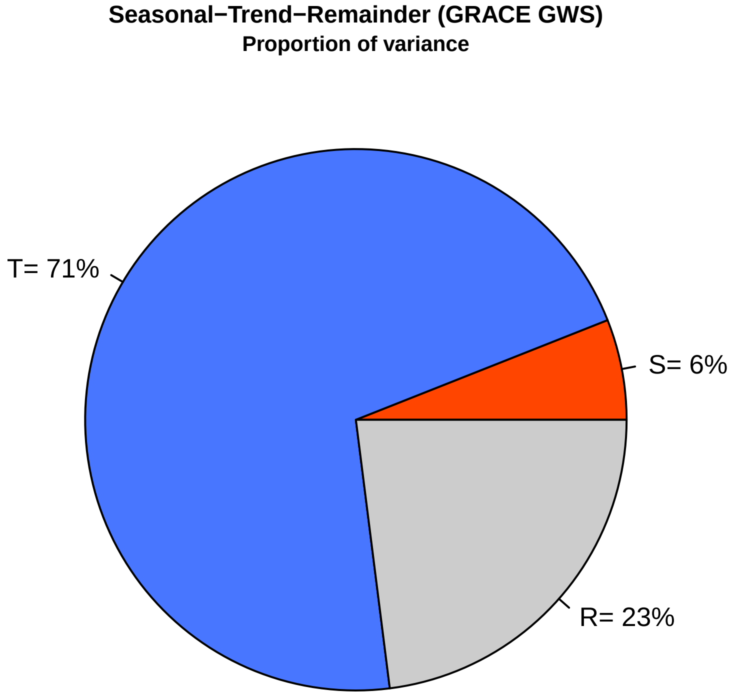

Fig. S77: Canning Basin (37)

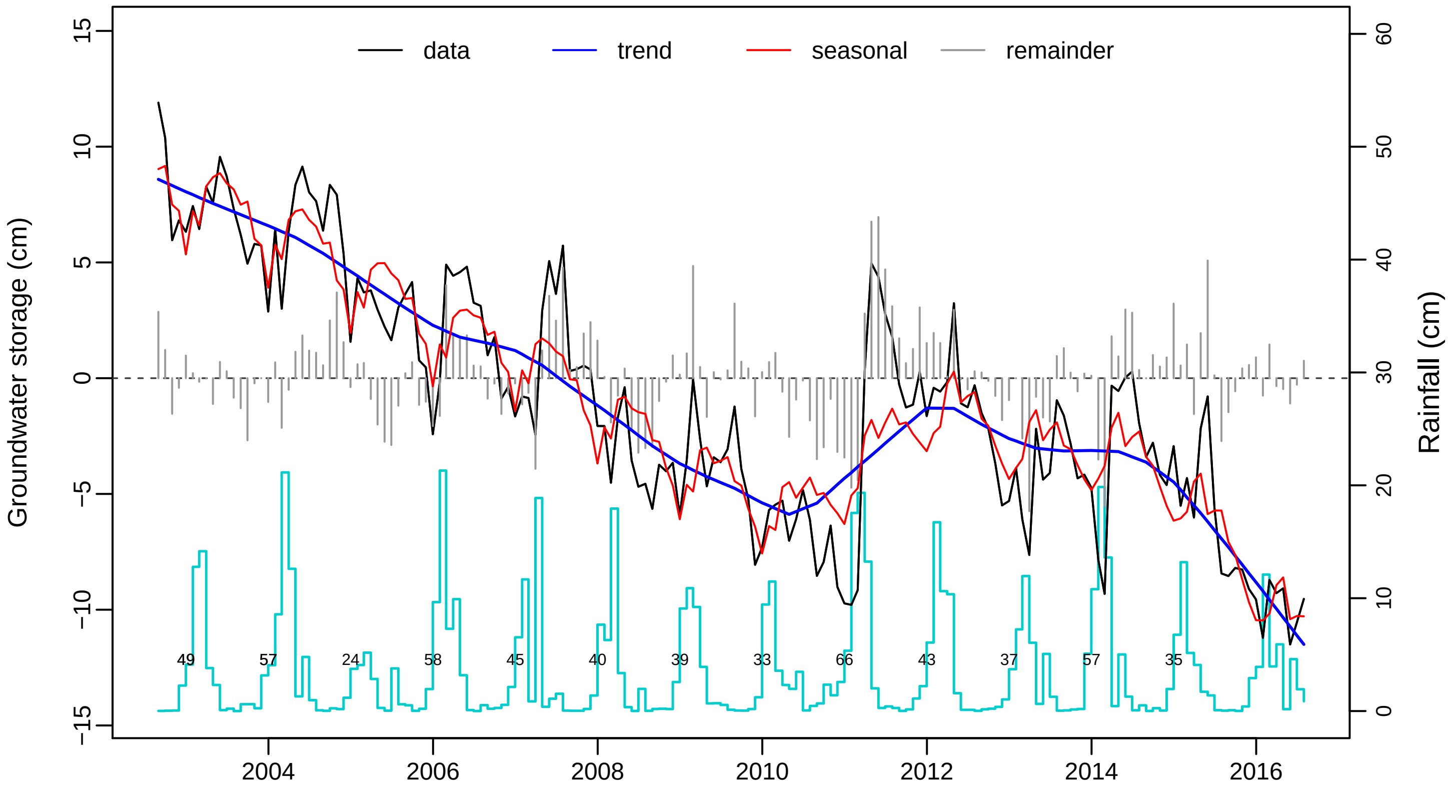

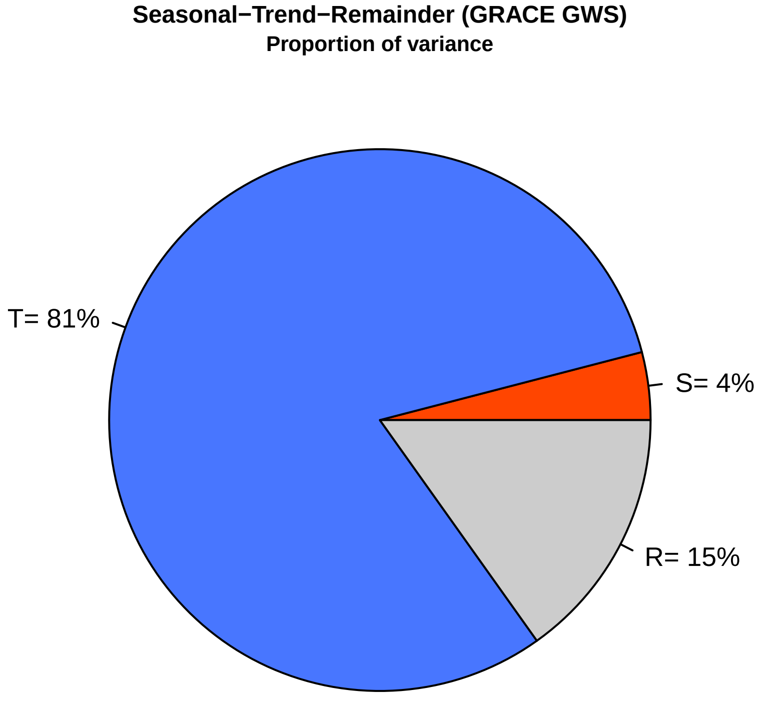

Fig. S78 Computational uncertainty in GRACE-GWS

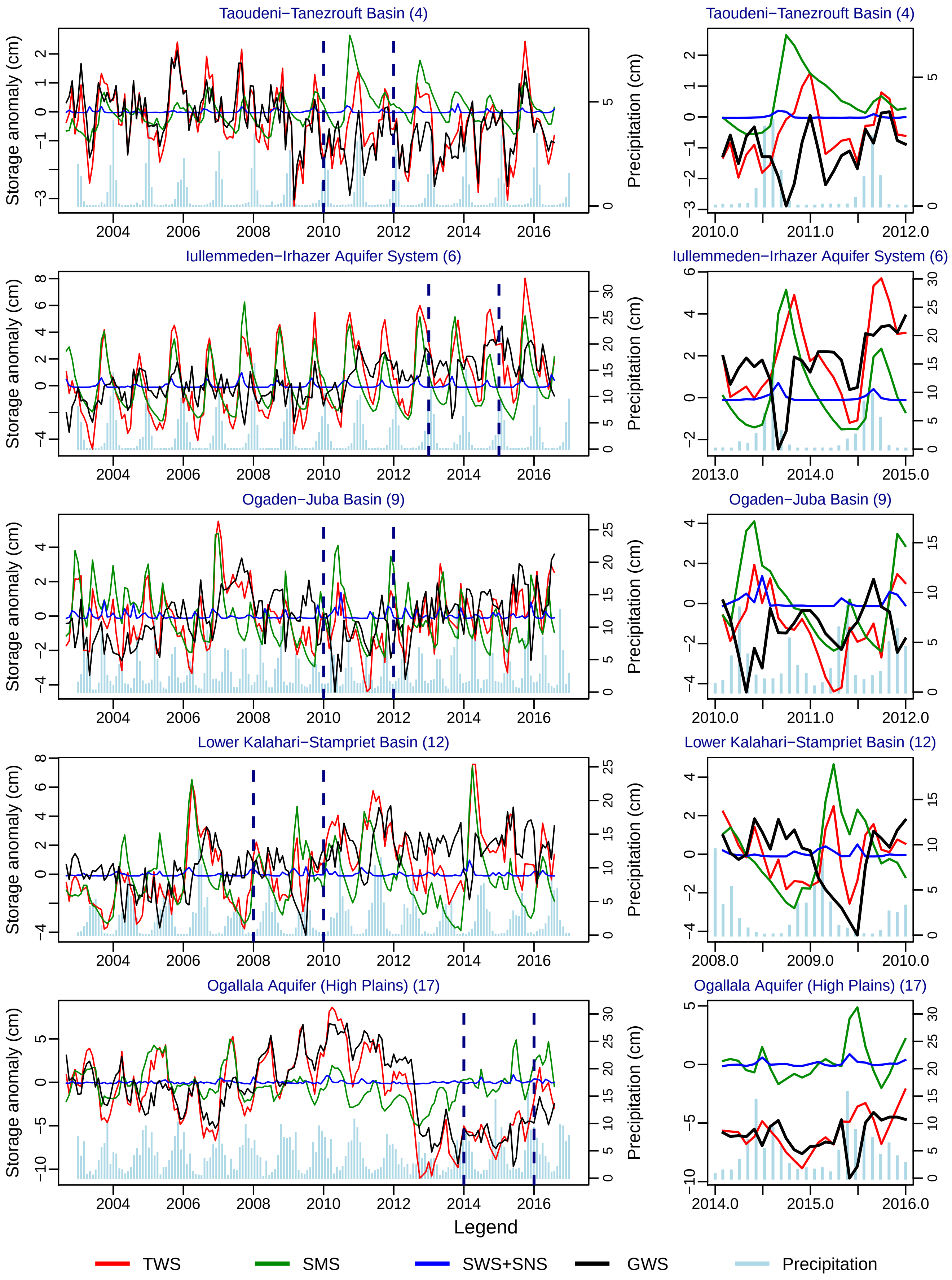

Fig. S79: Uncertainty in the estimates of GRACE-derived GWS from 20 realisations

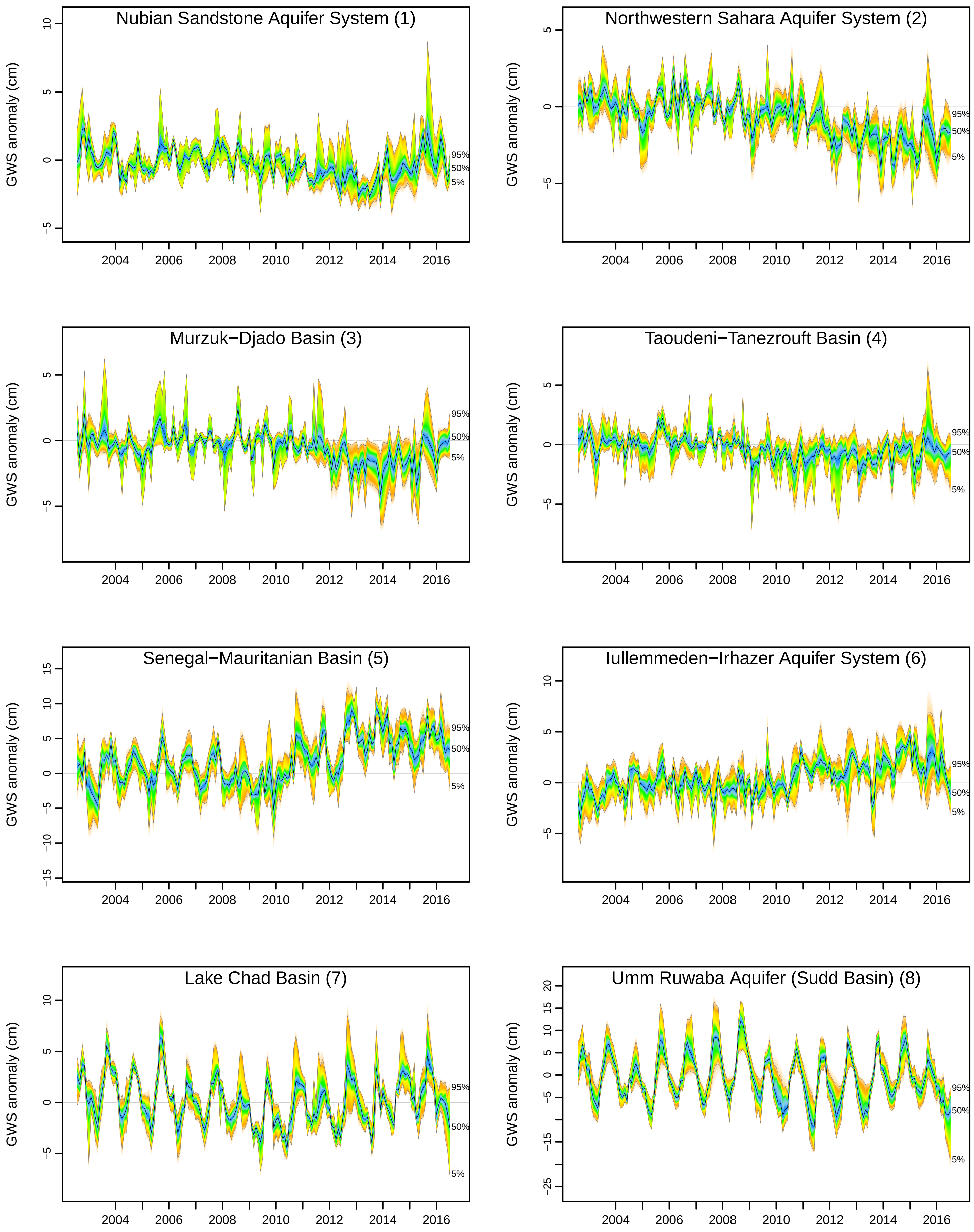

Fig. S79: Uncertainty in the estimates of GRACE-derived GWS from 20 realisations

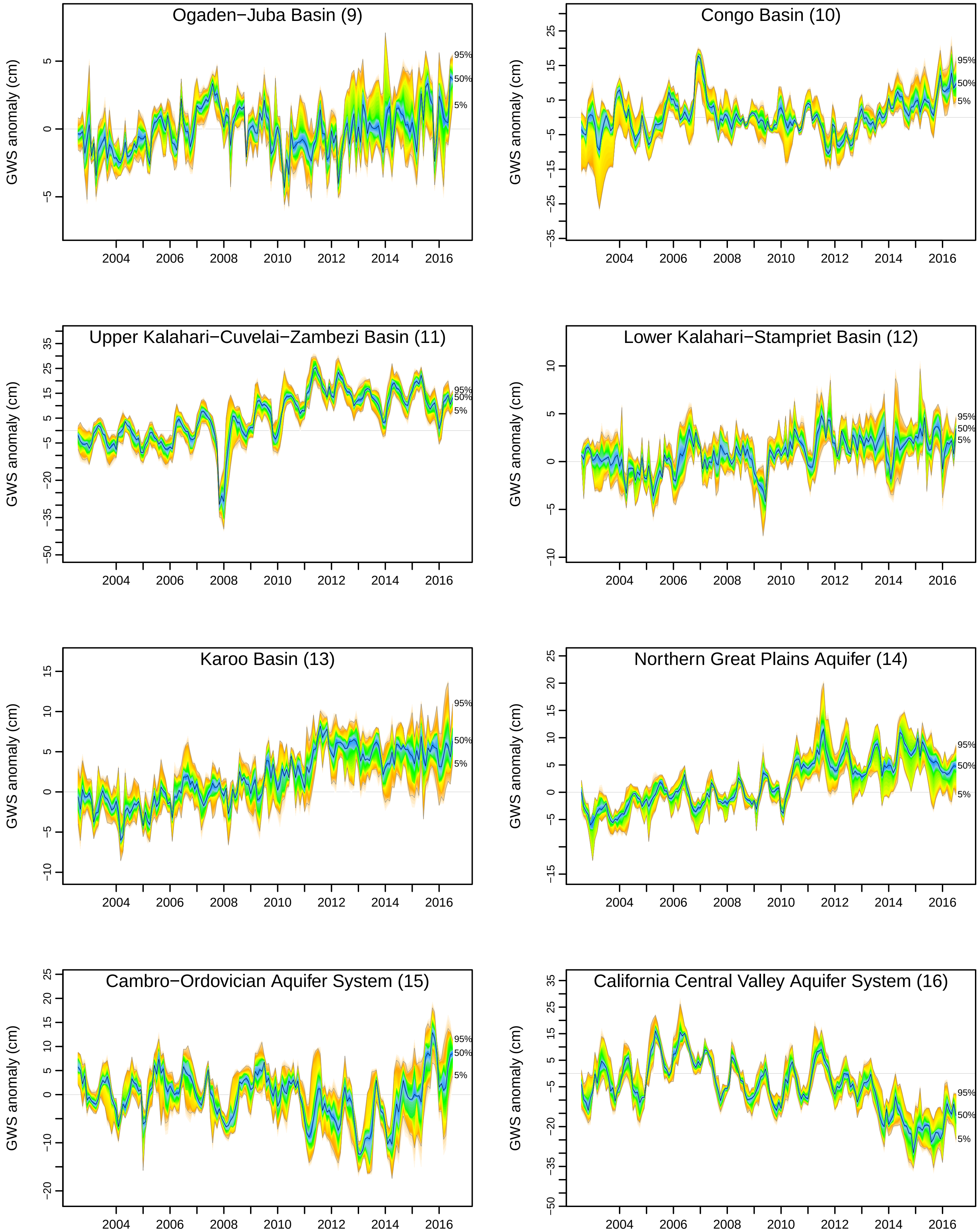

Fig. S79: Uncertainty in the estimates of GRACE-derived GWS from 20 realisations

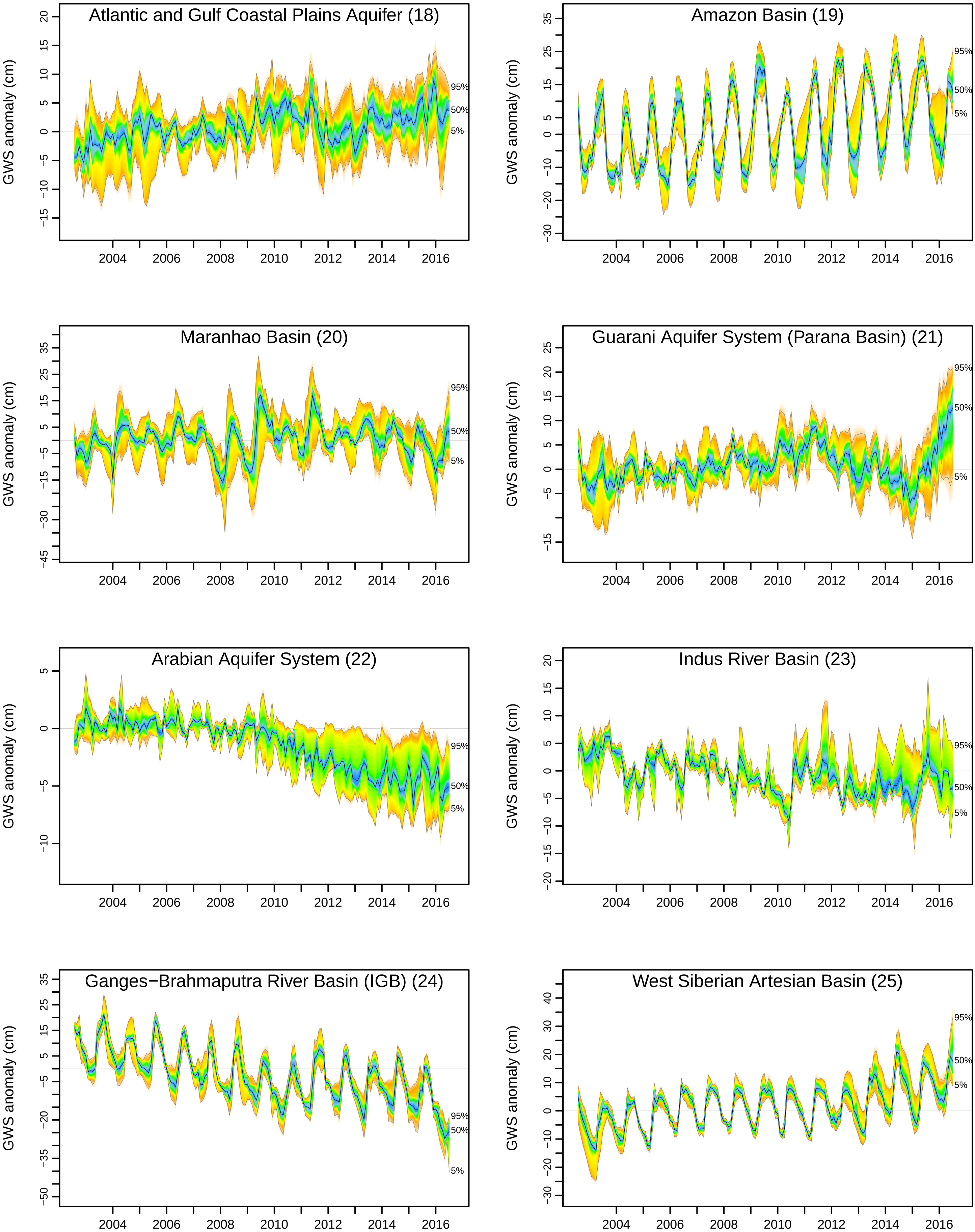

Fig. S79: Uncertainty in the estimates of GRACE-derived GWS from 20 realisations

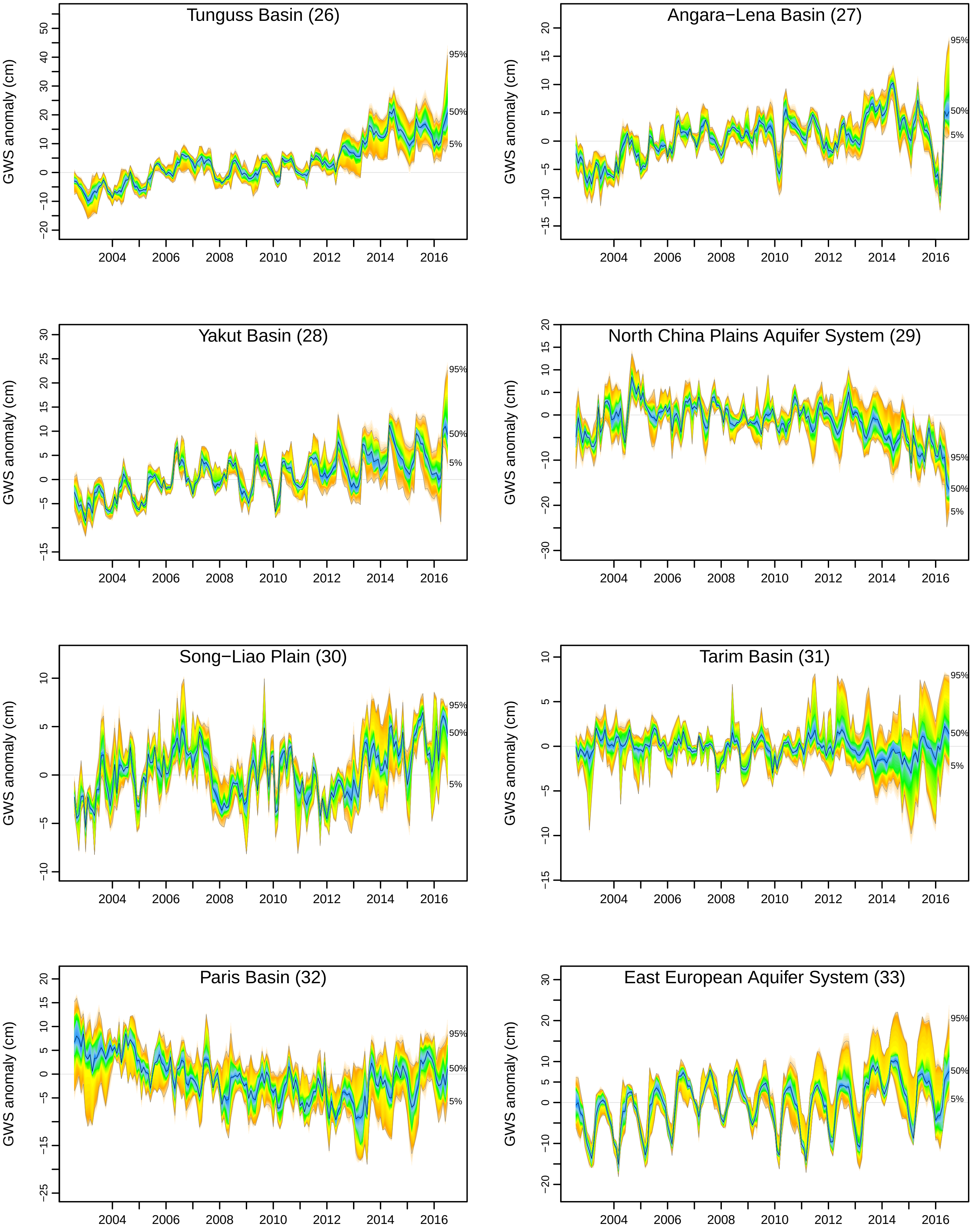

Fig. S79: Uncertainty in the estimates of GRACE-derived GWS from 20 realisations

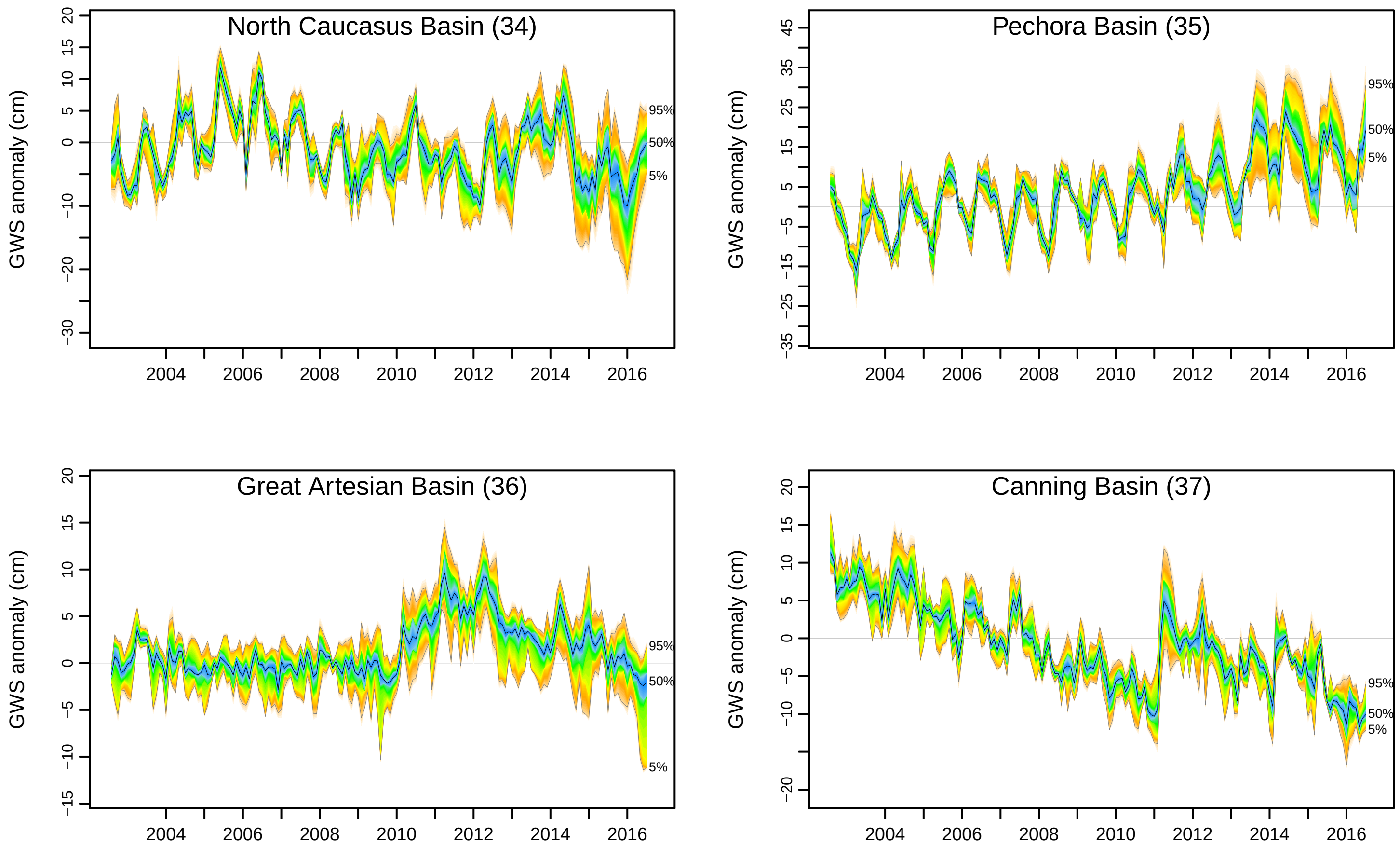

Fig. S80 (a) Makutapora Basin, Tanzania

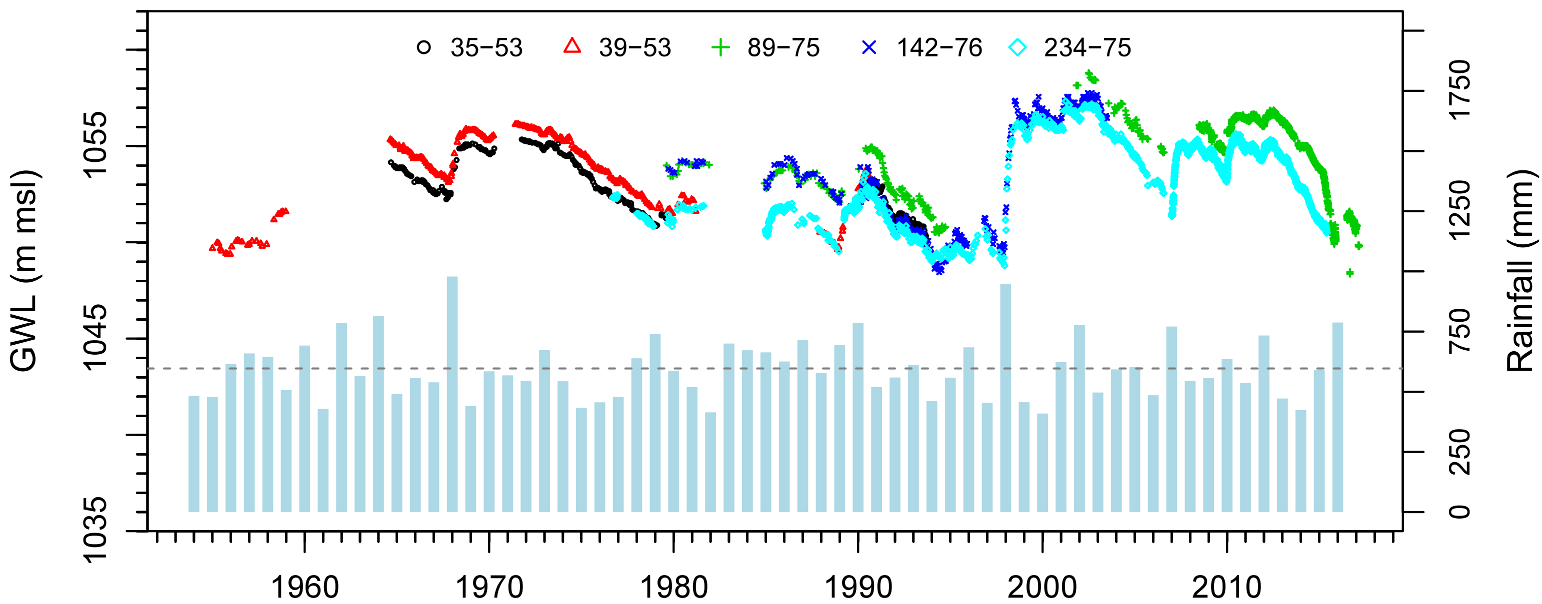

Fig. S80 (b) Limpopo Basin, South Africa